Internal in-service inspection of petrochemical storage tank floors to detect underside corrosion with Non-Destructive Testing Robot

by

N'Zebo Richard Anvo

London South Bank University

London
South Bank
University

August 2018

This thesis is submitted for the degree of Doctor of Philosophy

Acknowledgements

The research described in this thesis was carried out from September 2015 to August 2018 at London South Bank Innovation Center at TWI Cambridge.

I would like to thank Prof. Tariq Sattar my first academic supervisor without whom this work would have never been possible. Prof. Sattar remained a source of direction, motivation and inspiration for me. It was his confidence and guidance which allowed me to flourish my research capabilities.

I would like to thank my industrial supervisors Prof. Tat-Hean Gan and Dr Ivan Pinson who guide me during this work and provided me with knowledge of industrial requirement which was a great experience for me.

I also like to thank my second academic supervisor Dr Zhanfang Zhao who provided guide me and motivated me during this work.

I would like to thank my sponsors for The Welding Institute (TWI) Cambridge and London South Bank University for giving me the scholarship to support my study.

I would like to thank my family for their support through love and caring, most importantly, this effort is dedicated to my father and mother for investing all their lives into my studies and training. My mother prayers, motivation and guidance always keep me motivated.

Abstract

This research develops a new robotics technology for the in-service inspection of floor plates of the majority for the world's petrochemical storage tanks. The new robotic system aims to decrease inspection cost, reduce human inspector exposure to chemical and hazard environment during the inspection and eliminate tank outage entirely if the floor is found to contain no corrosion.

The research focus is on the design and development of a Non-Destructive Testing Robot (NDTBOT) prototype that uses active buoyancy control for its locomotion mechanism and uses NDT ultrasound to measure floor plate thickness as an indication of corrosion thinning. The NDTBOT hops from one location of the floor to another location to make ultrasound thickness measurements of a tank floor, thus avoiding issues of motion on a dirty tank floor (due to oil sludge). Also, a novel radio frequency (RF) data communication system is investigated and developed that can operate while submerged in oil. This system allows control commands to be sent to the NDTBOT by an operator outside the tank and NDT data to be recovered for analysis. To evaluate the performance of the NDTBOT making thickness measurement in the tank, three types of measurement techniques were used. First, the real thickness was measured using a Vernier caliper, the second method used a standard hand-held ultrasonic thickness measurement instrument and finally the in-service inspection thickness measurements were made with the NDTBOT operating in a water tank. The NDTBOT thickness measurements with an immersion ultrasound probe obtained more accurate results than hand-held contact ultrasonic testing.

Petrochemical storage tank size varies from 20 to 200 meters in diameter, rapid corrosion inspection in such tanks with a swarm of robots requires that a number of NDTBOTs be deployed inside the tank to perform the NDT. Such deployment needs coordination and control work between the robots to send the NDT data to the NDT inspector. Therefore, an investigation and experimental radio frequency wireless transmission is done in order to compare different radio frequency communication. Simulation with commercial software CADFEKO is used to perform simulation of RF wave transmission in petroleum and vegetable oil with selected radio frequencies of 200 MHz, 300 MHz, and 433 MHz. The experimental work and simulation results give confidence. The RF communication in petroleum medium is feasible for both control of NDTBOTs inside the tank and NDT data transmission back to a technician's console placed outside the tank.

Table of contents

List of figures

List of tables

Glossary of abbreviations

General	
$\boldsymbol{a}$	The acceleration
$\boldsymbol{\alpha}$	Attenuation constant
$\boldsymbol{\beta}$	Phase velocity
$\boldsymbol{\sigma}$	Conductivity
$\boldsymbol{\varepsilon}$	Permittivity
$\boldsymbol{\mu}$	Permeability
$\boldsymbol{A}$	The projected area
$\boldsymbol{AV}$	The average of reading thickness
$\boldsymbol{C_D}$	The drag coefficient
$\boldsymbol{f}$	Frequency
TOF	Time Of Flight
$\boldsymbol{F_B}$	Buoyancy force
$\boldsymbol{F_D}$	Drag force
$\boldsymbol{\rho_l}$	The density of the liquid
$\boldsymbol{m_a}$	The added mass
$\boldsymbol{m_0}$	Mass of the robot in air
$\boldsymbol{m_v(t)}$	Time varying mass flow
$\boldsymbol{M(t)}$	Time varying mass
$\boldsymbol{N_R}$	The Reynolds number
$\boldsymbol{v}$	The velocity
$\boldsymbol{\vartheta(t)}$	Displaced volume of liquid the time
$\boldsymbol{\vartheta}$	Kinematic viscosity
$\boldsymbol{W_0}$	Forces due to the mass of the robot
W	Watt
Acronyms	
API	American Petroleum Institute
ASME	American Society of Mechanical Engineers
AST	Aboveground Storage Tank
AUV	Autonomous Underwater Vehicle
BT	Buoyancy Tank
DC	Direct Current
EPA	Environmental Protection Agency
IDE	Integrated Development Environment
IMU	Inertial Measurement Unit
MFL	Magnetic flux leakage
NDTBOT	Non-Destructive Testing Robot
NDT	Non-Destructive Testing
EMW	Electromagnetic Wave
RF	Radio Frequency
ROV	Remotely Operated Vehicles
Rx	Receiver
Tx	Transmitter
UT	Ultrasonic Testing

ATEX	Atmospheres Explosives
VDC	Volts Direct Current
RHS	Right Hand Side
LHS	Left Hand Side
EMW	Electromagnetic Wave
HE	Housing Elecronics
GUI	Graphical User Interface
LMS	Local Mesh Setting

Chapter 1

Introduction

This research is directed at developing a new robotics technology for in-service inspection of floor plates for the majority of the world's petrochemical storage. This technology will be based on the deployment of mobile robots with non-destructive testing probe to carry out the in-service inspection. The new robotic system will decrease inspection cost currently, reduce human inspector exposure to chemical and hazard environment during the inspection and eliminate tank outage entirely if the floor is found to contain no corrosion. The research also investigates the design of a suitable radio frequency wireless communication method for NDTBOT to enable its remote control and to acquire NDT data and display at the operator's console. NDT is a method to look into materials with sensors to detect internal and hidden defects without cutting the material. The communication system is intended to speed up the inspection of a large tank with the deployment of a swarm of NDTBOTs.

1.1 Motivation of the research

Storage tanks are likely to degrade due to the storage materials, such as crude oil, oil products, petroleum, chemical and petrochemical raw materials. Most tanks are constructed of steel plates that are welded together to form the structure. The carbon steel is prone to attack by corrosion, and in some circumstances, cracks can build over time. Furthermore, damage to the tanks can lead to leakage of the contents, resulting in severe economic losses and environmental pollution. In order to avoid any damage to the environment, inspection, evaluation, and repair activities are performed periodically according to API safety regulations. Most of the storage tank welds and surfaces that are subjected to these elements are reachable from the outside, such as the walls and the dome.

However, only external corrosion and welds can be inspected from outside, while internal corrosion and corrosion on the floor can only be examined from the inside. Current inspection method requires the tank to be out of service for some weeks depending on the size of the tank. The inspection operation involves transportation of the product to other containers or location and cleaning of the tank before a human inspector can gain access into the tank and perform Non-Destructive Testing inspection. These factors pose several disadvantages such as the cost implication, time frame to get an inspection done and ultimately loss of revenue due to downtime. Also, high-risk exposure of workers to chemicals during the cleaning operation and inspection task is another limitation to using a human to carry out these tasks. Figure 1.1 shows the inspection with special protection.

Figure 1. 1: Aboveground storage tank inspection method (Silverwing, 2016)

In-service inspection robots have been used to inspect these tanks but still face some limitations in their application as follow:

- A tank with sludge deposits on the floor will pose a problem to the current crawler robots to perform an inspection due to their wheeled motion. The robots will only

work in a clean tank which has very low sludge and wax.

- An aboveground storage tank bottom floor is not free for movement; it contains some heating coils and roof support legs. Therefore, current robots have limitations when operating in these tanks because their control and NDT data transmission is done via an umbilical cable. This can become entangled in the tank furniture such legs to rest floating roofs, heating coil and draining pipes.

  Current tank inspection robots require high power (20-500W) for operation of NDT probes, servo drives and NDT flaw detectors which have to supplied via an umbilical cable.

1.1.1 Cost associated with the inspection and tank accident

Corrosion is one of the leading causes of aboveground storage tank failures. The US Environmental Protection Agency (EPA) NACE (2004) revealed that there are 8.5 million regulated and non-regulated Aboveground Storage Tank tanks in the United States with an inspection cost of $4.5 Billion. The causes of the accidents in a petrochemical plant are based on many factors such as leakage, lighting, maintenance error, sabotage, equipment failure, crack and rupture, static electricity and natural phenomena. Chang and Lin, (2006) reviewed some 242 accidents in 40 years that happened in petrochemical plants with 47.9% of the accidents occuring at petroleum refineries, terminals and pumping stations; 26.4% occurring in petroleum plants, 25.7% in other related facilities; 10.3% in gas plants and pipelines. Similar research done by (Zhou et al., 2016) found 435 recorded severe fire and explosion accidents at oil depots in China from 1951 to 2013 which are shown in Figure 1.2.

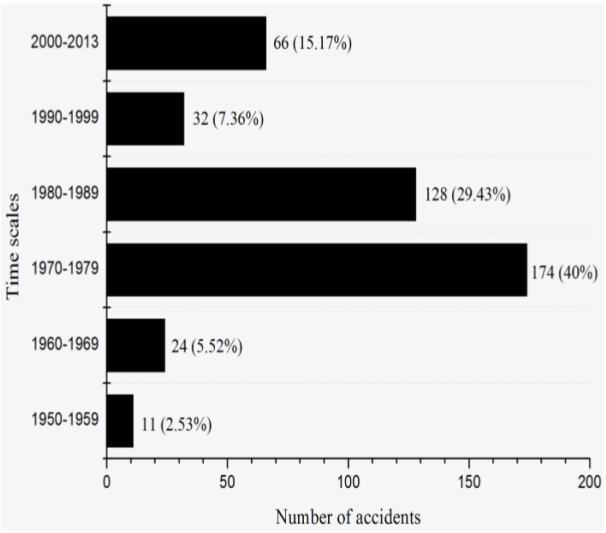

Figure 1. 2: Histogram of accidents during manual inspection of storage

tanks

The number of human casualties and area of accidents related to these years is reported in Tables 1.1 and 1.2. (Zhou *et al.*, 2016)

Table 1. 1: Number of deaths, serious and slight injuries. (Zhou *et al.*, 2016)

Personnel casualties	**Deaths**	**Seriously injured**	**Slightly injured**	**Total**
Number	390	175	775	1340

Table 1. 2: Area of accidents and number of accidents. (Zhou *et al.*, 2016)

Area of Accidents	**Oil storage area**	**Loading & unloading operation**	**Auxiliary operation**	**Others**	**Total**
Number of accidents	103	222	37	73	435

In-service inspection is a crucial aspect in tank inspection to determine corrosion early before leakage appears in which case it will be too late. Robots for in-service tank inspection can prevent loss of human life, environmental damage and could be an economical inspection method for tank owners.

1.2 Aims and Objectives

The aim of this research is to overcome the challenge set out by traditional inspection methods and in-service inspection robots. The research focuses on the design of a prototype of Non-Destructive Testing Robot that can operate safely in explosive and hazardous environments and measure the thickness of the storage tank floor plate using an ultrasound sensor. The design of NDTBOT will comply with American Petroleum Institute document API-653 that covers tank inspection, repair, alteration and reconstruction. NDTBOT will be inexpensive to reduce the cost of inspection and “hops” across the floor to make measurements, without any external moving parts. Investigation for proper communication with electromagnetic will make in future deployment a number of NDTBOTs as swarm robot for in-service storage tank floor inspection. Therefore, the control system and NDT ultrasonic data will be transmitted via RF wireless and the technique would enable the implementation of the robot localisation system. A variety of objectives can be intended for the design of a new robot

and investigation of proper communication in petroleum products to progress the technology further. The main objectives required to achieve the aims include:

- Perform a literature review and investigate the state-of-the-art of Aboveground Storage Tank and in-service robots for NDT inspection. This investigation aims to identify the research gap for in-service inspection robots for the petroleum industry.
- Develop small, inexpensive and expendable robots by investigating the most effective motion mechanisms to move an NDTBOT around a tank floor, methods to waterproof the robot and determine the optimum shape and size for small NDTBOT that can deploy an ultrasound probe and associated flaw detector with the simplest and most effective motion system.
- Design an active buoyancy control method to control the motion of the NDTBOT that could reduce the need for high power needed for robot locomotion.

- Develop and test a new robot prototype capable of initially working in water.
- Investigate the robot operation environment, to design the NDTBOT to be intrinsically safe for operation in flammable and explosive atmospheres.
- Investigate ultrasound NDT probes and electronics that can be easily integrated and encapsulated with the robot electronics and in case of deployment in zone 0 (environments in which ignitable concentration of flammable gases or vapours are present continuously and for long periods of time).
- Investigate and develop the optimum electromagnetic communication technology to use for oil and chemicals for the robot control system and NDT data transmission.

1.3 Intrinsic safety operation zone

Intrinsic safety utilises three levels of protection, zone 0, zone 1 and zone 2, illustrated in Figure 1. 3. In zone 0, ignitable concentrations of flammable gases or vapours are likely to exist under normal operating conditions. In zone 1, they may frequently exist because of repair, maintenance operations and leakage. In zone 2, ignitable concentrations of gases or vapours are not likely to occur in normal operation, only in case of accident or unusual operating conditions.

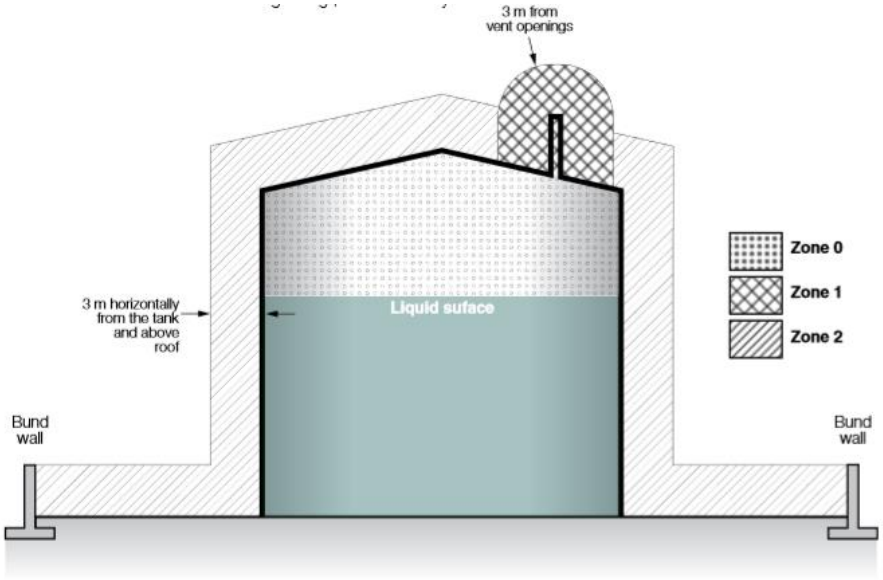

Figure 1. 3: Vertical storage tank, typical hazardous area and zone classification (Health and safety Executive, 2015)

1.4 Research contribution

The significant contribution of the current research arises from the development of a new robotic system that can be quickly deployed into operational storage tanks to perform ultrasonic NDT more cheaply. While a few robots for in-service inspection of petrochemical Aboveground Storage Tanks have been already developed, they are very large, heavy and expensive. The new robot is very small and inexpensive with a payload of 3.1kg; it uses very low voltage and power with an on-board rechargeable lithium battery of 12 volts. The NDTBOT does not use a crawler or propeller to move; it hops using a simple active buoyancy system which makes it suitable for any type of tank containing sludge, wax, heating coils and tank roof supports.

Another significant contribution is an investigation into the design and development of an electromagnetic radio frequency wireless communication system for in-tank use in oil/petroleum products. This has been performed with simulations and tested experimentally in petroleum products and vegetable oil medium using a very low power transceiver antenna to transmit and receive data via radio frequency wireless link. This breakthrough technology aims to replace the robot umbilical with an RF wireless link to acquire ultrasonic NDT data and control the robot. This will improve the in-service inspection operation and provide flexibility to operate in any tank and also provide the means to localise the robot within the tank.

All the significant contributions of this research have been reported in the publications

listed below:

1. Richard Anvo, Tariq P.Sattar, Tat-Hean Gan and Ivan Pinson, "Non-destructive Testing Robots (NDTBOTs) for In-Service Storage Tank Inspection", Journal of Mechanics Engineering and Automation 8 (2018) 103-109
2. Richard Anvo, Tariq P.Sattar, Tat-Hean Gan and Ivan Pinson, "Non-destructive Testing Robots (NDTBOTs) for In-Service Storage Tank Inspection", Proceedings of CLAWAR 2017: 20th International Conference on Climbing and Walking Robots and the Support Technologies for Mobile Machines, Porto, (2017), p:301

1.5 Research impact

The research has led to the winning of an InovateUK funded project, NAUTILUS, which is developing an inspection robot for the in-service NDT of petrochemical storage tanks.

1.6 Thesis outline

The thesis consists of six chapters including this introduction. The remainder layout of the thesis is as follow:

Chapter 2 presents a review of the state-of-the-art Aboveground Storage tank internal in-service inspection carried out with robots. It describes different techniques used by tank owners or operators to inspect their storage tanks and the wireless technology used in petroleum environments.

Chapter 3 describes the design of a prototype small size NDTBOT with a low payload that can be quickly deployed inside a storage tank for corrosion mapping (thickness measurement). The NDTBOT uses low power with an active buoyancy system that is able to move the robot around a storage tank.

Chapter 4 reviews NDT ultrasonic wave propagation in materials, types of wave, the acoustic impedance of tested object, and the refraction-diffraction effects that might occur during the test. It presents results of testing of the NDTBOT which was used to measure the thickness of different steel plates submerged in a water tank.

Chapter 5 presents investigations of radio frequency communication with the NDTBOT

Chapter 6 concludes this thesis with a summary of key achievements and future work.

1.7 Chapter summary

This chapter has briefly outlined the motivation of this research. The research rationale has been justified with an overview of current practice ranging from traditional manual inspection to in-service robotic inspection. It has identified the need for an in-service inspection robot for petrochemical storage tanks and has proposed the aims and objectives of the research that is required to find solutions to meet this need. Finally, this chapter lists contributions made to new knowledge and summarizes the scope and structure of this thesis.

Chapter 2

Literature review

A literature review is carried out to highlight gaps and limitation in the current research in the field of robots for in-service Aboveground Storage Tank inspection and their current communication systems. To understand the need for in-service inspection robots, a literature review is also carried out on current inspection methods.

2.1 Traditional Aboveground Storage Tank inspections

Traditional inspections of AST bottoms include a combination of several Non-Destructive Testing techniques, such as ultrasonic non-destructive testing, visual inspection, acoustic emission and magnetic flux leakage testing.

2.1.1 Ultrasonic non-destructive testing inspection

The Phased Array Ultrasonic Testing method can inspect any type of material and is the most widely used NDT method in industry. Started around the 1930s (OLYMPUS, 2018) it used very high frequency transmission into the material under inspection in order to detect the flaw. The advanced technology is able to use a single probe to contain a number of separate elements into a single housing known as a phased array. This configuration allows rapid scanning (Cochran, 2006) of a large area with flexibility in a change of angle and focus point. It can detect an external and internal defect and measure the thickness of the material under test. This technique of inspection requires the tank to be out of service for some weeks depending on the size of the tank. The inspection operation involves transportation of the product to other containers or location and cleaning of the tank before a human inspector can gain access into the tank and perform NDT inspection. Figure 2.1(a) shows inspectors performing inspections inside the tank floor when declared save to enter.

2.1.2 Visual inspection

Visual inspection is the oldest and probably the most important of all non-destructive methods. It is the process of examination and evaluation of different signs of distress in the structure which may include cracks, distortion and disintegration. It can be done using a camera, and it is easy to apply, and low cost compared to other techniques. Figure 2.1 (b) shows the instrument used in visual inspection.

(a) (b)

Figure 2. 1: (a) Ultrasonic flaw detector (NDTPI, 2018) and (b) camera inspections (Cornerstone, 2018).

2.1.3 Acoustic emission

Acoustic Emission testing is a non-destructive testing method that is based on the generation of the wave produced by a sudden redistribution of stress in the material. When a piece of equipment is subjected to an external stimulus, such as a change in pressure, load, or temperature, this triggers the release of energy in term of stress waves, which propagate to the surface and are recorded by the sensor. Detection and analysis of AE signals can provide information on the origin and importance of discontinuity in a material. Acoustic Emission testing is different from other NDT techniques because instead to supplying energy to the object under examination, Acoustic Emission testing listens for the energy released by the object naturally and also deals with a dynamic process in a material. Because of its versatility, Acoustic Emission testing has many applications within the industry.

Ireneusz et al. (2014) presented an Acoustic Emission monitoring system for the aboveground storage tank. Their research constructed a new monitoring system using the acoustic emission method. Laboratory tests and tests on a storage tank in a refinery by running the monitoring system for almost one year, enabled the detection of leakage and monitoring of their state in different conditions. However, the question of the accuracy of data collected from the acoustic emission sensor remains, due to the effect of signal noise and weather changes.

Liying et al. (2010) investigated the sensor array in a sizeable 20000 m^3 in-service vertical storage tank using Acoustic Emission. Four on-line defect detection methods were used that included the volumetric or mass method, acoustic emission, soil vapour monitoring and inventory control to find a defect in an aboveground storage tank containing fluid. The volumetric or mass method and soil vapour method was used to detect very low-level leakage but did not give the location of the defect. Furthermore, the inspection result is affected by movement of the floor, shell or roof and by a product temperature change. Figure 2.2 shows the application of acoustic emission sensors to inspect and monitor petroleum storage tanks. Figure 2.2(a) shows a set of several acoustic emission sensors in the range of 100 -200 kHz installed around the tank to detect and assess flaws in the structure including cracks and corrosion and Figure 2.2(b) corrosion and leaks on tank floor.

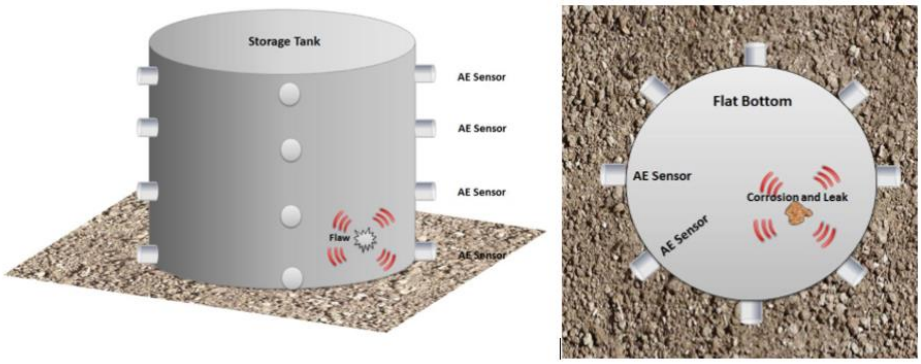

Figure 2. 2: Acoustic emission inspection and monitoring (Safety, 2018).

2.1.4 Magnetic Flux Leakage Testing

Magnetic flux leakage is a widely used approach to detect corrosion in applications where large areas are to be inspected in short timescales. Magnetic flux leakage has been used since 1980s as the primary internal inspection tool for the floor plate. The basic idea of magnetic flux leakage inspection is that the ferromagnetic material is magnetised close to saturation under the applied magnetic field and Hall effect sensors are then used to sense eddy currents. The basic principle is shown in Figure 2.3

Saunderson (1988) proposed the following approach: first screen the floor for defects with MFL followed by a detailed inspection of suspect locations using standard ultrasonic thickness measurement for validation, as to MFL signals received from adjacent defects can prove difficult to interpret. Moreover, (Ramírez et al., 2009) proposed that an MFL floor scanner should incorporate a combination of methods to detect the remaining floor thickness, determine the position of the flaw through linear scanning and identify the corrosion side of the plate.

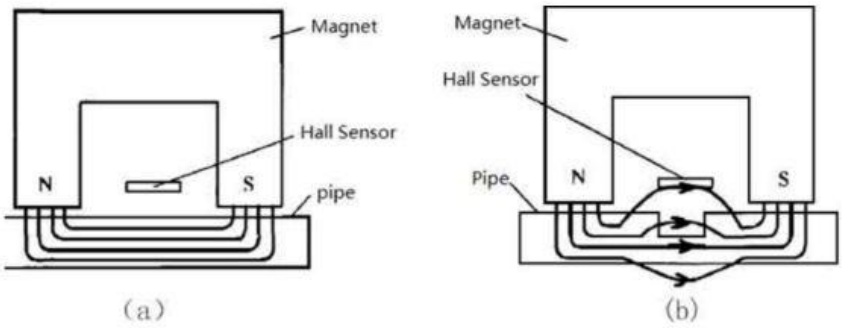

Figure 2. 3: Theory of magnetic flux leakage detection method (a) normal plate without flaw (b) plate with flaw/discontinuity Shi *et al.* (2015).

Floor coating is one of the main challenges that needs to be addressed especially with usage of composites coating instead of a conventional coating. Removal of the coating is often undesirable as it costs a lot to re-install, especially if there is no flaw detected after its removal. The confidence in an MFL floor scan is best for a bare metal plate and starts to decline with further additional protective coating application (Caruthers, 1996). Another challenge for MFL floor scanning is the presence of sludge sediment formed at the bottom of an oil tank. Proper surface cleaning and preparation is needed to remove the sludge as it may become an obstruction for the MFL scanner movement and even damage the MFL scanner wheel. Furthermore, a skilled operator is needed to operate the MFL floor scanner due to the complexity required to manoeuvre the scanning path while keeping the scanning speed constant at a speed sufficient to cover as much plate surface as possible to reduce the cost of inspection.

2.2 Robots for petrochemical storage tanks inspection

2.2.1 Wall climbing robot for in-service oil tank inspection

Mohammad et al. (2015) have reported a wall climbing mobile robot with permanent magnetic adhesion mechanism, which can be used for tank inspection. The robotic system consists of a mobile platform, a three-wheeled locomotion unit and adhesion mechanism that can move on a vertical wall. They have successfully tested in the real environment with a rough surface and welding seams of up to 14mm of height and 25mm of width. This mobile robot was not tested in the petrochemical storage tank, nor in-service inspection.

Andres (2015) proposed a similar design with a teleoperated wall climbing robot for oil tank inspection. He developed a robotic system consisting of wheeled locomotion which uses permanent magnets as the adhesion mechanism and a cordless teleoperated mobile platform that can move on vertical ferromagnetic walls. The proposed prototype was successfully tested under laboratory conditions proving its ability to move in any direction over a ferromagnetic surface. However, the robot was not tested in real environments such as storage tanks and the author did not mention NDT inspection.

An umbilical-free mobile NDT climbing robot for industrial application was developed by Sattar et al. (2012). This carries a single wheel probe operating between 1MHz and 10MHz to inspect defects, thickness or corrosion. The wall climbing robot is capable of inspecting oil tanks, petrochemical tanks, and bridges. However, the robot is only capable of inspecting the exterior wall of the tank, the tank floor which is most exposed to corrosion is still not covered.

Kalra et al. (2006) proposed a wall climbing robotic system for non-destructive inspection

of above ground floor tanks. The proposed robotic system consists of an autonomous mobile platform that can move on vertical walls of tanks carrying the test probes to detect corrosion or internal cracks in the tank walls. However, the inspection is limited to the outside walls of the storage tank. Furthermore, the robot is far from being able to detect underside corrosion of the tank floor.

Love et al. (2006) presented a wall-climbing robot for oil tank inspection with permanent magnet adhesion mechanism equipped with a non-destructive sensor. The system can be operated manually or autonomously to scan the external wall for possible faults using sensors. However, the inspection proposed in their paper is still external to the tank. Figure 2.4 illustrates the wall climbing robot for in-service inspection.

All the above developments are for external inspection while the internal in-service inspection is still challenging because none of these robots has the ability to inspect in-service storage tank floors.

Figure 2. 4 Wall climbing robot in-service inspection (ENVIROPRO, 2018).

2.2.2 Internal in-service inspection of petrochemical storage tank floors

The tank floor scanning robots for in-service inspection are smaller in number because of the sophisticated design requirement. This is due to the need for proper insulation and waterproofing of the whole robot and the connecting instrument while it's submerged in the contained liquid. Sattar et al. (2003) presented the design of floor and wall-climbing robot, called RobTank to inspect the internal walls and floors of oil and petrochemical storage tanks. The surface changing mobile robot was successfully tested in a water tank and a fire fighting

training tank in the Sines refinery, Portugal. Figure 2.5 shows the first RobTank deployment in a manhole of the aboveground storage tank Figure 2.5(a) and petroleum product Figure 2.5 (b).

Further research by Sattar et al. (2003) led to the design and development of an amphibious and mobile robotic inspection system to test welds located inside floating production storage offloading (FPSO) tanks. The new model has added a variable buoyancy tank that controls buoyancy around the neutral buoyancy of the robot. The robot was successfully tested in a 7meter deep-water tank.

(a) (b)

Figure 2. 5: in-service inspection robot RobTank (2003).

The robot was designed to operate in the air as well as submerged in water. However, the moving parts such as thrusters and wheels make it difficult to make the robot intrinsically safe for operation in an explosive environment such as petroleum products. Also, motion of the robot on a tank floor is difficult due to the deposit of sludge.

The Solex Environmental System in conjunction with the Texas Natural Conservation Commission demonstrated the operation of Maverick (1998), a remote-controlled robot system for inspecting in-service, aboveground petroleum and petrochemical storage tanks. Maverick performs floor inspections from inside the tank while submerged in refined products including gasoline, diesel and fuel oil. It uses a multi-channel ultrasonic sensor, an onboard video system to record inspections and a sonar-based tracking system. The robot was certified for safe operation in Class 1 Division 1 Group 1, Figure 2.3 (a) and (b) shows the robot and its deployment for a demonstration test.

(a) (b)

Figure 2. 6: MAVERICK for in-service inspection, Solar Environmental (2010).

Similarly, a robot system for above-ground storage tank inspection Neptune (1994; 1995) shown in Figure 2.4 was developed by the Robotics Institute and the Field Robotics Centre at the Carnegie Mellon University. The complete system is comprised of a robot crawler vehicle, which carries visual and ultrasonic sensors for aboveground storage tank inspection. The control system and ultrasonic data transmission is done via a fibre-optic telemetry system. The robot actuation system and sensors require 500W of power. The robot has been used in explosive petrochemical products for in-service inspection.

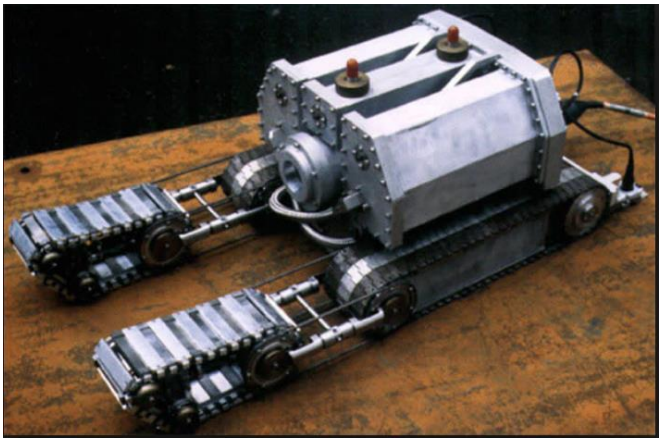

Figure 2. 7: In-service inspection, Neptune (1994; 1995).

Another online tank inspection robot from TCR Arabia, the OTIS robot has been designed to clean and inspect the steel floor of oil tank while still in operation. The robot uses UT sensors to detect any variation in the thickness of the bottom plate while the tank remains in service. The Figure 2.8 (a) shows OTIS robot and Figure 2.8 (b) upgrade version.

(a) (b)

Figure 2. 8: Online tank inspection robots,
(a) OTIS (2002) and (b) upgrade version.

The upgraded version is represented in Figure 2.8(b). Both robots utilise a triangulation navigation system to continuously locate the robot and track the ultrasonic readings and use an on-board 360 degrees sonar sensor for obstacle avoidance.

Another, in-service inspection robot design by PETROBOT (2016) for AST was tested with the tank filled with water. The complete robot is comprised of a robot crawler vehicle, localisation system, and UT for floor thickness measurement. However, the storage tank used for the demonstration was free of any obstacle. The robot control commands and UT data acquisition is done via an umbilical cable. Figure 2.9 (a) shows the robot and Figure 2.9(b) deployment in a storage tank with a massive deployment system.

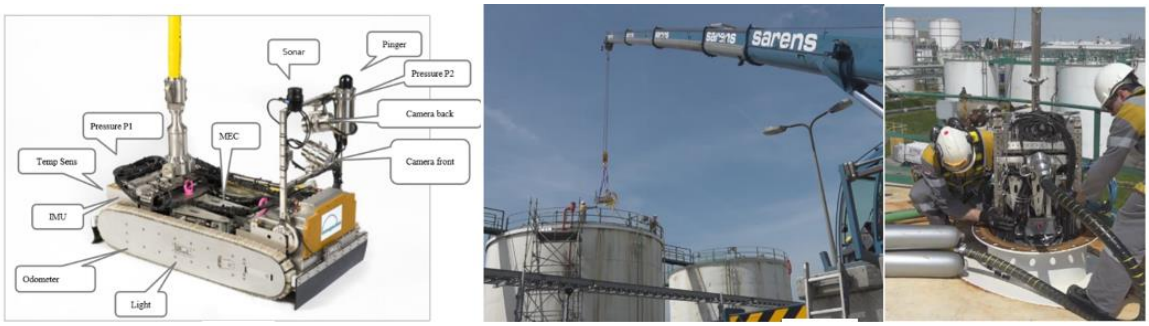

(a) (b)

Figure 2. 9 Online tank inspection robots, PETROBOT (2016).

Mantar Robotics has designed a robot for in-service inspection which safely goes into fuel storage tanks to perform visual inspection inside the tank and inspect the tank floor. The visual inspection and the tank thickness UT data is retrieved via cable and the locomotion system is based on a crawler design. Figure 2.10 shows the deployment of the robot into the manhole of a tank.

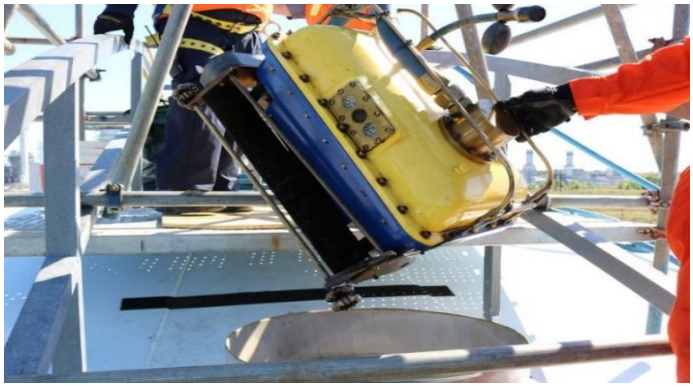

Figure 2. 10: Online tank inspection robots, PETROBOT (2016).

Stingray robot for online storage tank floor inspection was proposed by DIAKONT (2017). The robot performs NDT using onboard magnetic flux leakage and an array of ultrasonic testing sensors for the floor thickness measurement. The crawler robot suitable for complete API 653 inspections was equipped with a jet system to clean the sludge and sediment to allow the inspection to be done. Figure 2.11 (a) shows the robot and Figure 2.11 (b) the deployment test. The supply voltage and ultrasonic testing data are done via cable.

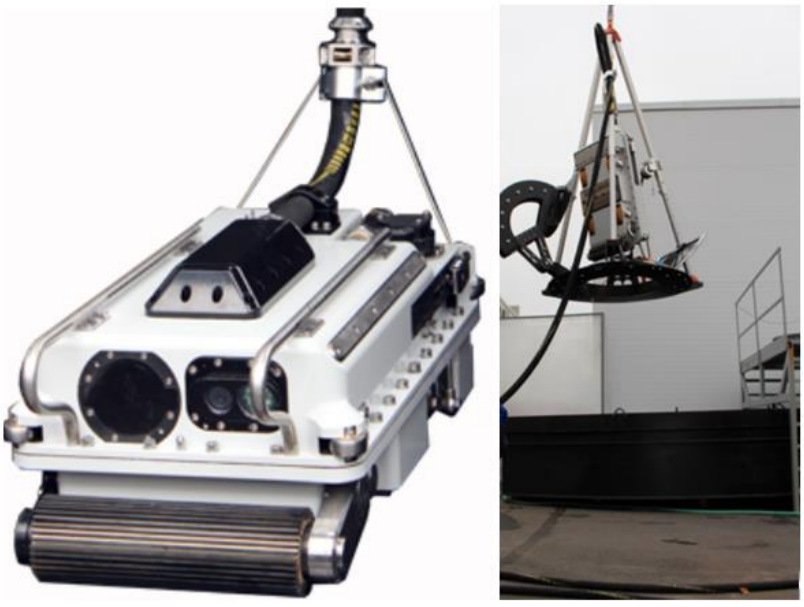

(a) (b)

Figure 2. 11: Online tank inspection Stingray (Diakont, 2017).

Similarly, the Inspector robot from Newtonlabs (2017) is designed for water tank inspection and dry petrochemical storage tanks. The robot receives power and communicates with its control console and NDT ultrasonic system via an umbilical cable. The navigation system is based on a camera to track the robot position in the tank and to locate the position of the flaw. Figure 2.12 (a) shows the older version and Figure 2.12 (a) the new version.

Figure 2. 12: Online tank inspection Newtonlabs (2017).

All the above robots are designed for entry through manhole openings in the roof of a tank. Power and NDT signal acquisition umbilical cables (about 100 m lengths), are difficult to manage. Also because of their moving parts, the crawlers are difficult to move in a specific amount of sludge and require high power to operate in such an environment. The need for long and heavy umbilical cables is a significant disadvantage and tank farm operator acceptance of these robots is very difficult to achieve because of the very stringent safety requirements imposed by the operators and regulations. Table 2.1 shows a comparison of in-service and out-of-service storage tank floor inspection.

Table 2. 1: Comparison of in-service and out-of-service tank floor inspection.

Conventional In-Service API 653 Floor Inspection	**In-Service Robotic API 653 Floor Inspection**
Tank needs to be put out of service. It includes draining, purging, and cleaning (takes months before actual inspection)	Tanks can remain in full operation inside contained product. Inspection can be done immediately with minimum preparation.
Human inspectors need to enter the tank with supervision and safety instruments continuously monitoring confined space hazards such as toxic gases.	Confined space work is eliminated. Entry of human inspector is only when necessary. This method reduces the health and Safety risk.
Proper planning is needed as tank outage costs a lot of money (transportation, cleaning, and stop of production).	Inspection can be done on-demand because it does not interfere with the production process.
Visual inspection, MFL Scanning, and UT inspection take a significant amount of time.	Usage of the robot with automated scanning provides reliable data with higher efficiency.
Inspection focuses primarily on data acquisition as limited time is provided due to health and safety reason while working in a confined space.	Data acquisition and analysis can be done thoroughly at the same time. Reading can easily be repeated if needed at any time.
Commissioning and refill are required.	No refill required.

2.3 Electromagnetic communication for data transmission in petroleum

All in-service inspection for petrochemical storage tank robot explored so far have used cables for robot control and NDT data transmission. Using very low power (1to 2W) with low-frequency RF communication in this environment would be a critical forward step to widespread uptake of in-service inspection robots because it would eliminate the inspection challenges associated with heating coils and tank roof supports as well as data transmission and for robot localisation. Currently no work on Radio Frequency communication for in-service inspection robots in petrochemical storage tanks has been published. Research on underwater wireless communication is reported in (Lloret et al.,2012), (Che et al.,2009) and (Centelles et al., 2015). Wireless applications for the oil and gas industry past and present methods of communication in oil and gas have included satellite communication (on a limited basis), cellular and specialised mobile radio, fibre-optics, and general offshore telephone service using radio frequencies (Rydl and Simpson, 2004).

The communication systems cited above allow communication between any offshore oil platform and land-based telephone networks via a team of employees working on the site to monitor and report to management on a continuing daily basis. Wireless technologies and applications could provide a solution to some operational problems in the oil and gas industry by providing the ability to access real-time information and rapidly react to problems and eliminate or reduce the monitoring team. Also, research focused on wireless communication in the case of oil and gas wells has recently increased. Franconi et al. (2014) report the use of electromagnetic telemetry in offshore drilling platforms as well as during well production to increase the efficiency.

Current wireless communication in the oil industry is used for pipe monitoring and reservoir level management in real time. These include SCADA systems which typically include the master stations, application software, remote terminal units and all associated communication equipment to interface the devices. There are many industries using SCADA systems for data acquisition that vary from simple to complex applications such as temperature and humidity of a climate-controlled building to traffic light system monitoring, power grid systems, storage tank liquid level and pressure. Figure 2.13 shows plant monitoring using SCADA systems.

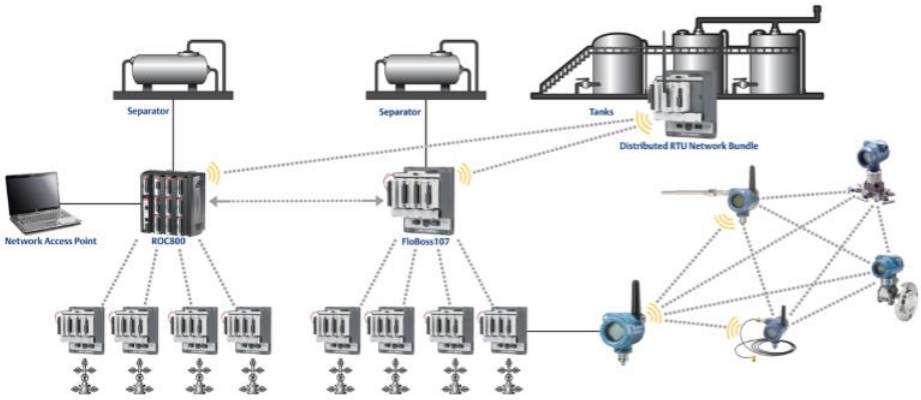

Figure 2. 13: SCADA system implementation in the oil industry (Remote and Controller, 2018).

Advanced satellite remote monitoring: A Texas-based oil company has used wireless communication with satellites for remote monitoring widely dispersed oil wellheads (Rydl and Simpson, 2004). SIEMENS supplies RUGGEDCOM and SCALANCE (SIEMENS, 2018) wireless communication systems that could be deployed in the oil industry for monitoring pipes. Figure 2.14 shows the idea of the wireless system mounted on an oil pipe to monitor the pressure and send the information to the operator. When a difference appears in the pressure data, the operator will know the location area of leakage.

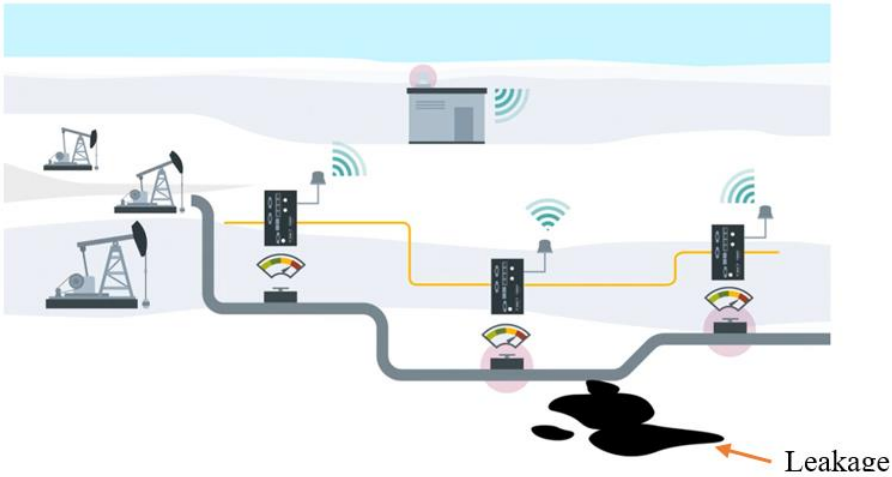

Figure 2. 14: wireless pipe leak detection. (SIEMENS, 2018)

2.4 Research gaps in current in-service storage tank inspection

This literature review has identified most of the petrochemical inspection that is performed with traditional methods in which most of the tanks are empty and cleaned before the inspection can be done by a human inspector. Petrochemical storage tank robots for in-service inspection are few and less well reported while the reported developments have several limitations for in-service inspection application in petroleum environments. Some

aboveground storage tank robots reported for in-service inspection have used locomotion methods such as wheels, crawlers and propellers. Also, the deployment of the robot requires heavy equipment such as crane because of their size and weight. The ultrasonic data collection and robot control movement is done via a heavy umbilical cable. Moreover, the adopted locomotion actuators to drive the robot and the ultrasonic techniques used to inspect the tank floor require high voltages to supply the higher power needed. For example, a power of 500 W was required for the sensors and locomotors in (Neptune, (1994; 1995) which far exceeded the established regulation safety limits for operation in the storage tank.

The petrochemical environment is hazardous where flammable gas mixes are present all the time. Therefore, using a robot with moving parts such as crawlers, propellers and pneumatics with drive shafts in this environment have a high risk of igniting a spark with friction during the inspection or the deployment. Moreover, the high power used by these robots becomes a hazard to the environment the in case of electrical short circuits and failure. Also, certification and acceptance of these types of robot to be used in the petroleum field becomes very difficult.

The NDTBOT will overcome all the above-mentioned difficulties. The robot is lightweight, easily deployable, does not require a crane for deployment, is small size and thus is easily inserted into storage tank manholes. Moreover, the NDTBOT locomotion mechanism is based on a buoyancy system which is operated with a micro-pump to move the robot to a different location around the tank. The NDTBOT total power requirement in fully operational mode with all electronics and ultrasonic NDT hardware on-board is less than 2 Watts with power supplied by board batteries of a maximum of 12 volts which last for 1h30 minutes after test. The robot electronics are easily encapsulated into flameproof epoxy, therefore, can meet the zone 0 requirements, and the low power robot makes it acceptable for ATEX certification.

Current research literature does not report the use of radio frequency communication for in-service inspection robots for use inside petrochemical storage tanks. Indeed most of the research focuses on underwater wireless communication. Therefore, an investigation of a suitable RF communication system for data transmission inside petroleum storage tanks for in-service inspection with robots reported in this thesis is novel. Due to the unusual structure inside a petrochemical storage tank, where robots are not free to move due to internal heating coils and legs to support floating roofs. This development offers the possibility in the future to deploy several NDTBOT robots as a swam to reduce the inspection time with the RF system

enabling communication between the NDTBOTs. It also could be the technology to develop a localisation system for the NDTBOT.

2.5 Chapter summary

This chapter has highlighted the inspection methods used for petrochemical storage tank inspection and identified current in-service robot developments for internal inspection of floors and walls. The main limitations found in robot designs for locomotion as well as communication systems are making the robot comply to zone 0 environment protections. This research targets the design of very low power robots using buoyancy systems for locomotion and where the flaw detector electronics can be encapsulated in antiflammable epoxy for deployment in zone 0. It also proposes a suitable communication technique for operation inside oil tanks. The novel NDTBOT could be the next breakthrough robot for economic in-service petrochemical storage tank inspection, environment protection and life protection.

Chapter 3

NDTBOT Prototype Design

Storage tank in-service inspection is very challenging due to the explosive environment. Therefore, a prototype robot has to be developed that is low power (1to 2 W) and avoids any moving parts that can create a spark in a tank. The idea of buoyancy control to move the robot randomly inside the tank using low voltage (6 to 12 V) with robot battery on board is a novelty and is a research contribution to petrochemical storage tank inspection. This chapter describes the development of a prototype small size NDTBOT with a low payload that can be easily deployed inside a storage tank for corrosion mapping.

3.1 NDTBOT Inspection environment

3.1.1 Types of tanks

The most fundamental classification of storage tanks is based upon whether they are above or below ground. Robotic inspection is limited to aboveground storage tank, which has most of its structure above ground. The bottom of the tank is usually directly placed on an earthen or concrete foundation. Aboveground storage tanks are used to store chemicals and petroleum products. They are usually easier to construct, cost less, and can be built with far larger capacities than underground storage tanks and they are constructed with steel plates welded together. Most ASTs range from 3 to 100 m in diameter and 2 to 14 m high. The roof of the tank can be used to classify types of tank designs (Myers, 1997).

- **Fixed roof tank**

  It can be vertical or horizontal; the vertical tank is cylindrical with a fixed roof. The roof shape varies which can be conical, dome shaped or flat. The drawback of this type is that they are not suitable for high vapour pressure storage unless vapour recovery is used which means that it allows evaporation of the stored liquid. Unlike the vertical tank, the horizontal shape is elliptical; it is found in both above-ground and underground tanks.

- **External Floating roof tank**

  Consists of an open topped cylindrical steel shell with a floating roof that moves relative to the change of liquid level. There are two main types of roof: the pontoon roof is typical for floating roofs and is formed with a diameter approximately 10 to 30 m. The other type is the double-deck roof consisting of two layers which is built for very small tanks with a diameter of 10 m. The purpose of the external floating roof tank is to reduce the volatility of stored material. The main problem with floating roof is that the rain water can accumulate on the roof.

- **Internal floating roof tank**

  These tanks are vertical with cylindrical shells just as fixed root tank but with a cover that floats on the surface of the liquid. The floating interior cover has sufficient buoyancy to ensure that the roof will float under all conditions, the floating roof and the tank shell have a gap of between 20 to 30 cm.

- **Domed roof tank**

  This type of tank comes with a heavier deck to block the wind, it is similar to an internal

floating roof tank and has a welded deck and self-supporting fixed roof.

The NDTBOT is designed to be inserted into storage tanks with a fixed roof or floating roof through minimum manhole sizes of 300 mm for underside corrosion inspection of tank floors, Figure 3. 1 and Figure 3. 2 shows aboveground storage tank.

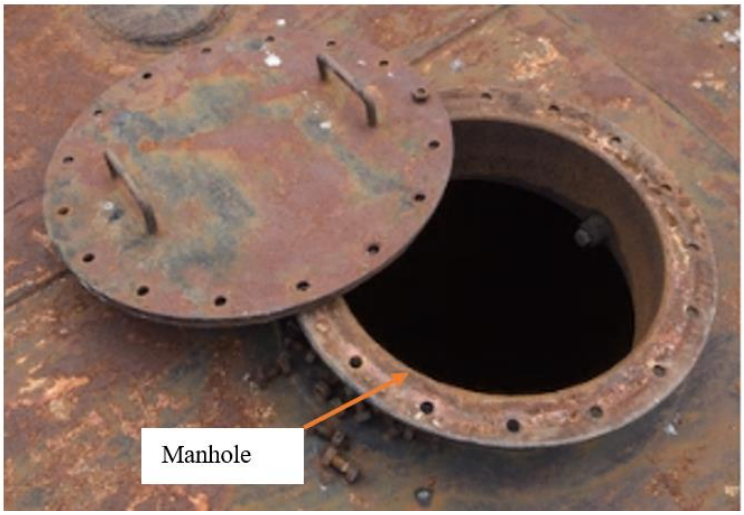

Figure 3. 1: Aboveground storage tank manhole (Georgia, 2017)

Figure 3. 2: Aboveground storage tank (Georgia, 2017)

3.1.2 Corrosion of tanks

Exposure of storage tanks to the environment results in corrosion in different areas of a tank such as an external surface wall, the external surface under the tank bottom, and the vapour space between liquid level and the roof of a tank. The NDTBOT is designed to inspect the tank bottom underside to which access from the outside is not possible. The corrosion is usually caused by salinity in the groundwater and other factors such as ground chemistry. The tank underside corrosion varies significantly based upon the site, design, foundation, drainage condition and other factors. Figure 3. 3 shows the corrosion locations in the storage tank.

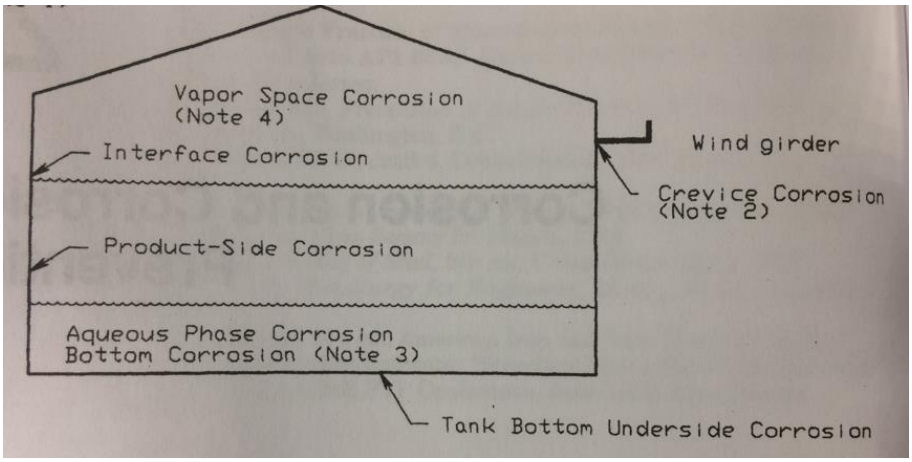

Figure 3. 3: Tank corrosion modes (Myers, 1997).

3.1.3 Explosion in storage tanks

Storage tanks in refineries and chemical plants contain large volumes of flammable and hazardous chemicals. A small accident may lead to a million-dollar property loss and a many days of production interruption. In the last 50 years, trade organizations and engineering societies such as the American Petroleum Institute, American Institute of Chemical Engineers, American Society of Mechanical Engineers, and the National Fire Protection Association have published strict engineering guidelines and standards for the construction, material selection, design and safe management of storage tanks and their accessories. (James and Cheng-Chung, 2005) reported that 242 tank accidents occurred in the last 40 years due to static electricity, equipment failure and operational error. The three main ignition sources presenting high risk when working in a hazardous area are specified with some examples in Table: 3.1

Table 3. 1: Classification of sources of ignition

Ignition Sources	Examples
Hot Surfaces	Surfaces heated by coils, resistors, lamps, brakes, or hot bearings. Hot surface ignition can occur at the Auto-Ignition Temperature (AIT) or spontaneous ignition temperature at which a hazardous substance will spontaneously ignite without further energy.
Electrical Sparks	Occur when circuits are broken, or static discharge takes place. In low voltage circuits, arcs are often created through the making and breaking of electrical contacts
Friction and Impact Sparks	When casings or enclosures strike other tank surfaces

3.1.4 Intrinsic safety protection of NDTBOT

The robot operates in a non-defined zone when submerge in liquid. However, before getting to the liquid, the NDTBOT goes through zone 0, therefore, it needs to meet the requirement for zone 0 environments. The required protection for the region method and standard are shown in Table 3.2.

Table 3. 2: Zone definition (Victor, 2003)

	PROTECTION TYPE	STANDARDS	PROTECTION METHOD
Zone 0	Intrinsic Safety	EN 60079-11	Where the design limits the ignition spark energy to below that which, will ignite the explosive gas. Safe even with two simultaneous faults.
	Special protection	EN 60079-26	Special construction normally based on the use of two independent types of protection both individually.
	Encapsulation	EN 60079-18	Integral components which can potentially ignite an explosive gas are encapsulated allowing the isolation of these components from the explosive atmosphere surrounding them. This allows the strict control of surface temperatures under normal and fault conditions.

3.2 Design of NDTBOT for operation in a hazardous environment

The NDTBOT has been designed to travel through Zone 0 when it is inserted into a tank through the vapour zone and then operate while immersed in a liquid which is a non-defined zone. The components of the NDTBOT required for motion and ultrasonic NDT are described in Appendix A-1.

The NDTBOT is powered with an on board 12 VDC battery with a lifetime of 1h30 minutes after lab test. Temperature sensor to monitor the robot internal temperature, a water detection sensor to detect leakage in the robot. Inertial measurement unit to maintain the NDTBOT at an

angle of 90 ± 5 degrees to the inspection surface because of the UT zero-degree probe integrated into the robot. The IMU is used to maintain the correct angle when the robot lands on a weld or other discontinuities. The robot is level when it lands on discontinuity so that a measurement can be made in that area.

All selected component for NDTBOT are low voltage with a maximum required voltage of 5 to 12VDC which is good in terms of intrinsic safety which required the nominal voltage 24VDC. It is the first robot which will operated intrinsically safe because the robot is built with the concept of zone 0 environment protection (Table 3.2). The NDTBOT use buoyancy system for locomotion therefore no moving part as early in the literature review all robot use crawlers or pneumatics for locomotion.

3.3 NDTBOT first design and prototype

The first design Figure 3.4 and prototype of the NDTBOT, see Figure 3.5, was developed to test its motion and inspection capability in a water tank. It comprises of two sealed boxes, Buoyancy Tank mounted on top of a box called the Housing Electronics that houses all the electronics. An external control switch is used to control the up and down and stop movement of the NDTBOT.

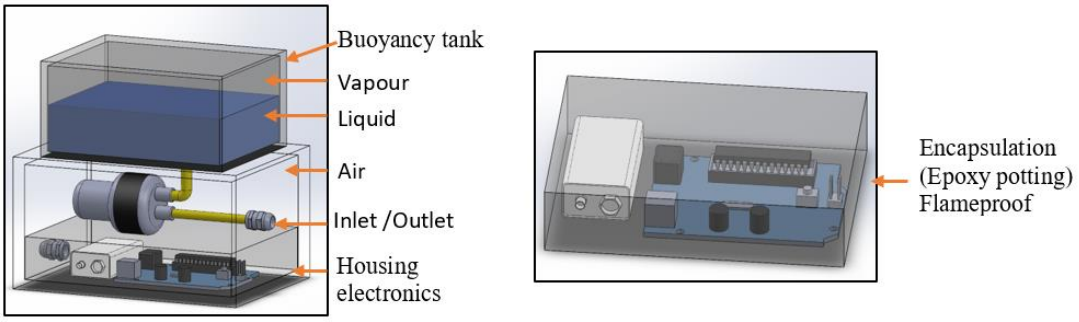

Figure 3. 4: NDTBOT first design.

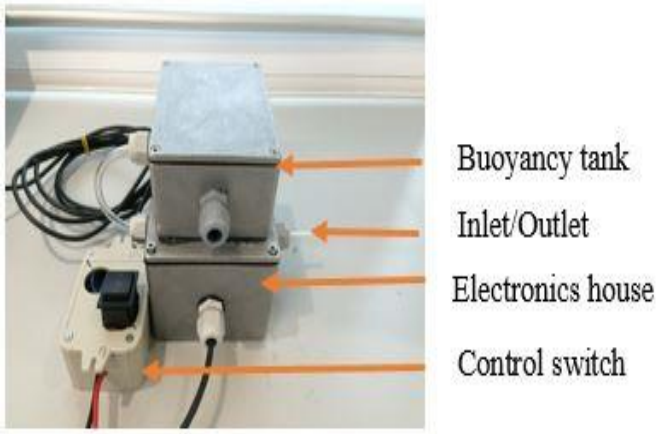

Figure 3. 5: NDTBOT first design.

Dimensions of the rectangular box-shaped BT are 114x89x56 mm while HE is 140x102x77 mm. The mass of the whole system is 1.67 kg.

3.3.1 Buoyancy control system for NDTBOT

Different buoyancy systems have been developed for autonomous underwater vehicles and remotely operated vehicles to save power when performing exploration operations. By definition, an autonomous underwater vehicle is a robot which travels underwater without requiring input from an operator. It constitutes part of a larger group of marine systems know as unmanned underwater vehicles. A remotely operated underwater vehicle is controlled and powered from the surface by an operator via an umbilical. Buoyancy systems are used in most submarines and submersible equipment. Research (Ibrahim et al.,2015) proposed buoyancy control for a spherical underwater robot vehicle. The proposed buoyancy control was based on a ballast tank with a DC motor to pump water in and out for the robot to be neutrally buoyant or positively buoyant. The prototype was successfully tested. However, the system used a variable ballast tank with a complicated setup, which is far from the simple waterproof micro-pump used in this research.

Further work Stephan et al. (2015) presented a similar approach to develop an automated buoyancy control system for a remotely operated underwater crawler. The system consisted of hydraulic, electric and control subsystems. It allowed the operator to navigate the robot to any desired depth by controlling the amount of air within each chamber which is supplied by compressed air cylinders using sensors and microcontrollers. Again, this control system was designed for sea operation with a complex controller compared to the simple design proposed in the current development which is suitable for the internal storage tank environment.

Similar research Masmitja et al. (2014) developed buoyancy with an engine piston. The piston was made of stainless steel with a plunger of a radius 100mm and path length of 200mm. It was able to collect and eject 1.5 litres per minute of water. The system was successfully laboratory and field tested. However, the buoyancy system needs more power to operate with 9A as operating current and is designed to work in the ocean. Anthony et al. (2014) in their research proposed variable buoyancy control for a bottom-skimming autonomous underwater vehicle. Their method was based on feedback control to actively change the volume of the ballast chamber based on a load cell measurement. However, this system was designed to operate with heavy weights and is not suitable for a small device due to the size of the ballast tank.

Energy storage is limited for the submersible robot. To provide energy, the robot is supplied power via a heavy umbilical cable which also transmits data such as video and chemical data over extended periods of time. For vehicle motion, thrusters may be used. However, there are two disadvantages to this method: high energy consumption and the risk of ignition in a flammable environment due to the moving parts (thrusters). The proposed buoyancy system in this research has many advantages such as low cost and low energy consumption. Therefore, on-board batteries can be used to power up all NDTBOT systems and reduce the size of the umbilical cable. It is simple to operate and will not provoke perturbations in the inspection environment which is an essential condition for ultrasonic zero-degree probe thickness measurement. The NDTBOT, see Figure 3.6, uses a variable buoyancy system to perform up/down movement It is made negatively buoyant by pumping in surrounding liquid to dive to the tank floor, see Figure 3. 6 (b) and positively buoyant by pumping it out to move up, see Figure 3. 6 (a). The latter condition lifts the robot off the floor while simultaneously providing a force to displace it sideways using a pump as a thruster.

In this way, the robot is made to “hop” across the tank floor to inspect the floor with the ultrasonic testing probe randomly since sideways motion is not controlled.

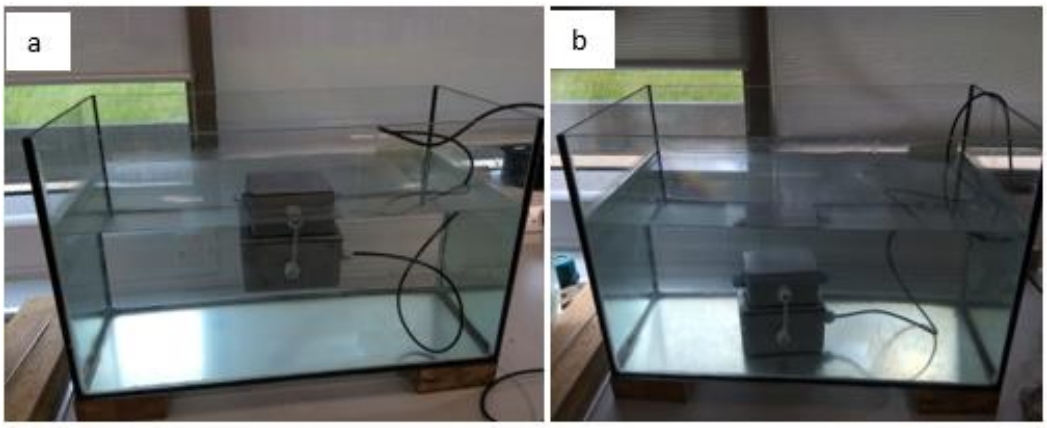

Figure 3. 6: NDTBOT in a water tank.

3.3.2 Thickness measurement test

The goal of this experiment was to measure the thickness of different steel plates using the submerged NDTBOT in a water tank. The analysis was based on using a conventional immersion ultrasound transducer to determine the thickness of steel plates. The UT probe was mounted on the side of the NDTBOT. Figure 3.7 shows an experiment with steel plates submerged in the water tank. The Omniscan flaw detector, power supply and the switch to control the robot were placed outside the tank and connected to the NDTBOT. The micro-pump and circuit board were integrated into the NDTBOT and an ultrasound probe mounted on the side. The probe used in the experiment was a conventional submersible ultrasonic transducer, single element, diameter 12.75 mm and frequency 2.25MHz. The test was successful. The NDTBOT was able to move randomly on the floor to measure the thickness of the steel plate submerged in the water tank. Preliminary results were used to get better understanding of the new concept robotic system, its functionality and limitations in order to improve in the final version of NDTBOT.

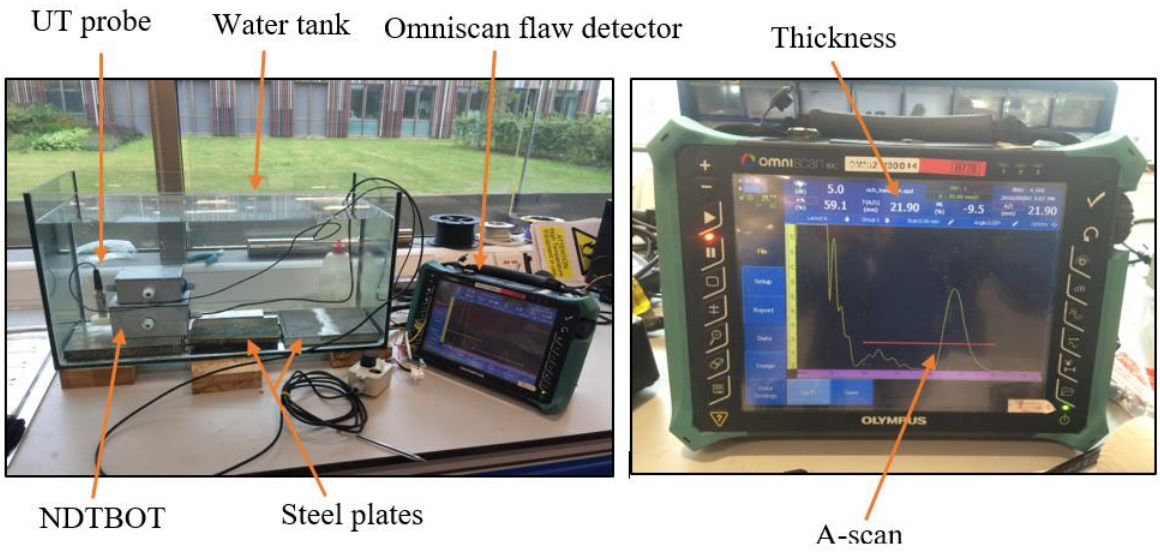

Figure 3. 7 NDTBOT A-scan test.

3.4 NDTBOT advanced design and prototype

The final design of the NDTBOT was made to meet specific requirements to be able to operate in petroleum storage tanks. The body was designed to move freely in the operating environment with a cylindrical enclosure for the electronics and a dome shape for the buoyancy tank. All electronics, batteries and ultrasonic probe were embedded into a single cylindrical enclosure where they can be encapsulated in an unflammable epoxy. The idea from the first design is still unchanged. It comprises of two parts, a dome shaped BT mounted on top of a cylindrical HE. The NDTBOT is made negatively buoyant by pumping in surrounding liquid and positively buoyant by pumping it out. The latter condition lifts the robot off the floor while simultaneously providing a force to displace it sideways using a pump. In this way, the robot is made to “hop” across the tank floor. A zero-degree ultrasound immersion probe mounted in the centre of the bottom tank is used to measure floor plate thickness. Figure 3.8 shows NDTBOT design and Figure 3. 9 (a, b, c) shows the final prototype of the NDTBOT with 3.1 kg maximum weight in air.

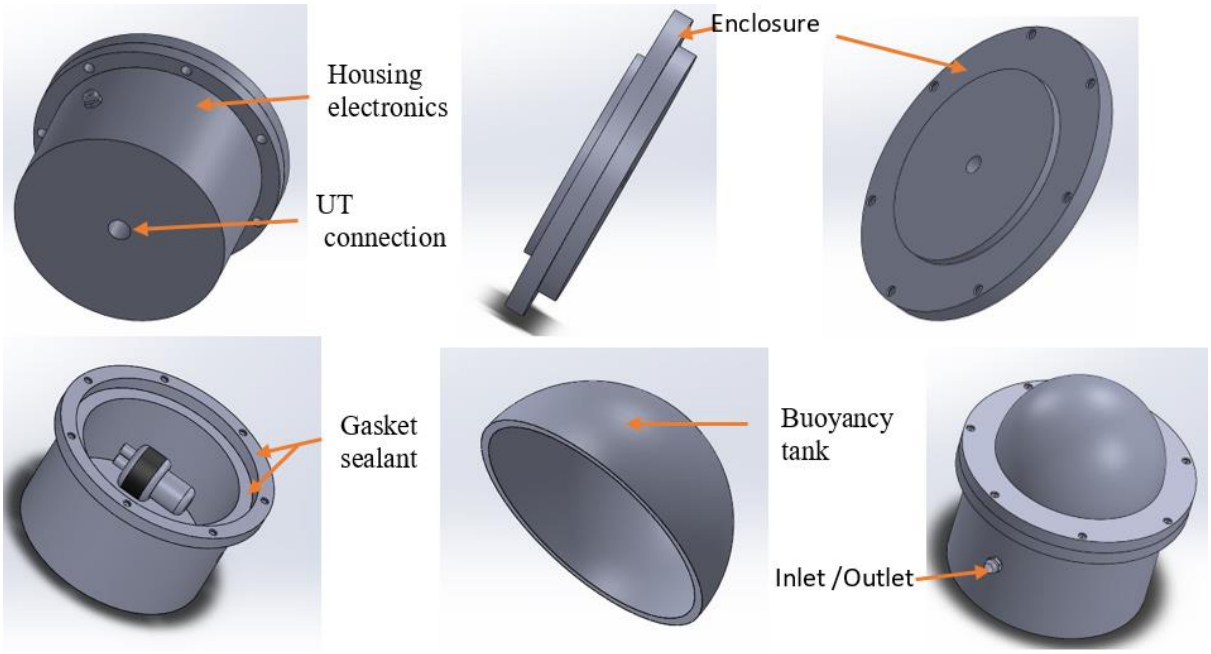

Figure 3. 8: NDTBOT design.

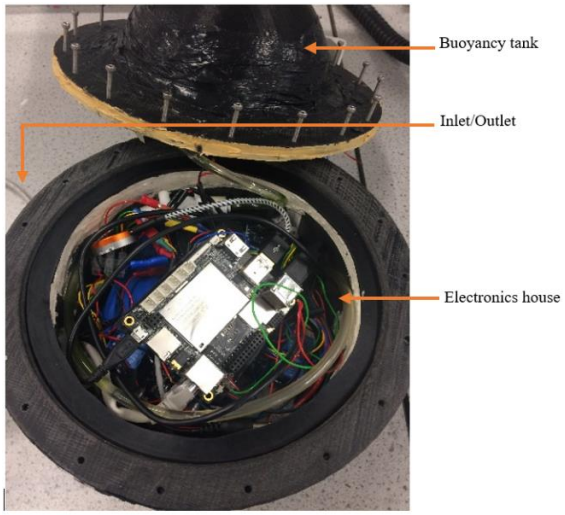

(a)

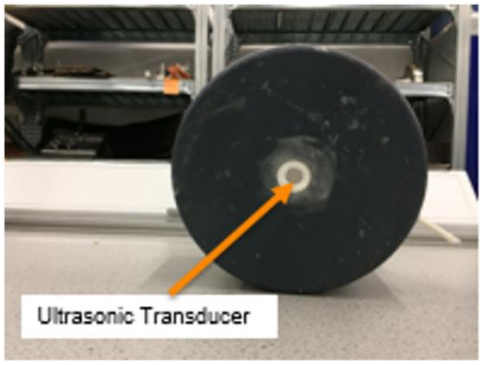

(b)

(c)

Figure 3. 9: Assembled NDTBOT prototype.

In order for the robot to perform inspection in an explosive and flammable environment such as in aboveground storage tanks, the robot operation must avoid creating a spark which can ignite an explosion in the tank due to heat and the presence of a vapour mixture. Therefore, the BT will contain only flammable liquid and vapour, but no heat or ignition sources and hence needs no protection. The bottom box housing contains all the electronics (battery, micro-pump, microcontroller, flaw, microcomputer and ultrasound probe), will be hermetically encapsulated in flameproof epoxy. The micro-pump is made of flame-proof material and will not get hot as it will be operated only for short periods to move the robot. Cable glands used on the first prototype are designed for underwater IP68. Therefore, with no moving parts, a sealed watertight box, and all electronics epoxy potted, the overall robot is likely to obtain ATEX approval for operation in flammable and explosive environments and be used in a storage tank for in-service inspection.

3.5 NDTBOT system

The robot control system is composed of a user control interface where the user enters a command and views the state of the robot. The central processing unit is a microcontroller where all commands are processed and displayed to the user. It is connected to sensors to monitor the internal state such as temperature, humidity, leakage and an Inertial Measurement Unit to know the orientation of the NDTBOT. The micropump is connected to the microcontroller to enable the system to move up and down using the buoyancy system. A solenoidal valve is used to assist the pump to cope with pressure by closing the liquid path when required. The NDT computation unit processes the pulser/receiver signal from the UT probe and sends it to the central processing unit.

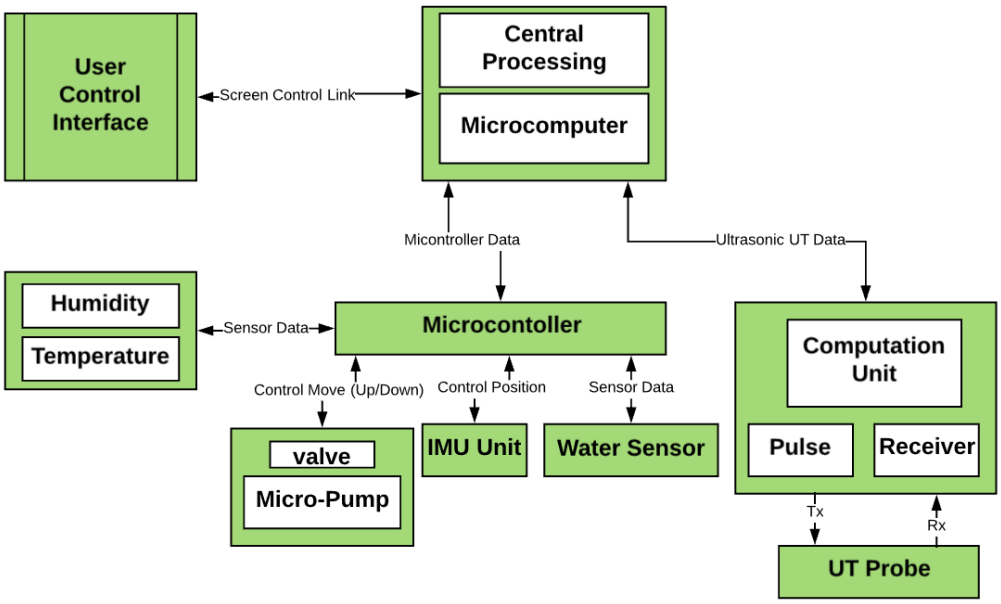

Figure 3. 10 NDBOT control diagram.

3.5.1 NDTBOT User control

The NDTBOT USER INTERFACE is standalone software built with an integrated development environment using Microsoft Visual Studio. The language used to build the NDTBOT USER INTERFACE is Visual C# (Appendix A-2) which is an object-oriented language. Figure 3.11 shows the design of the robot user interface which is divided into four windows commands and each of the commands are explained (1 to 4).

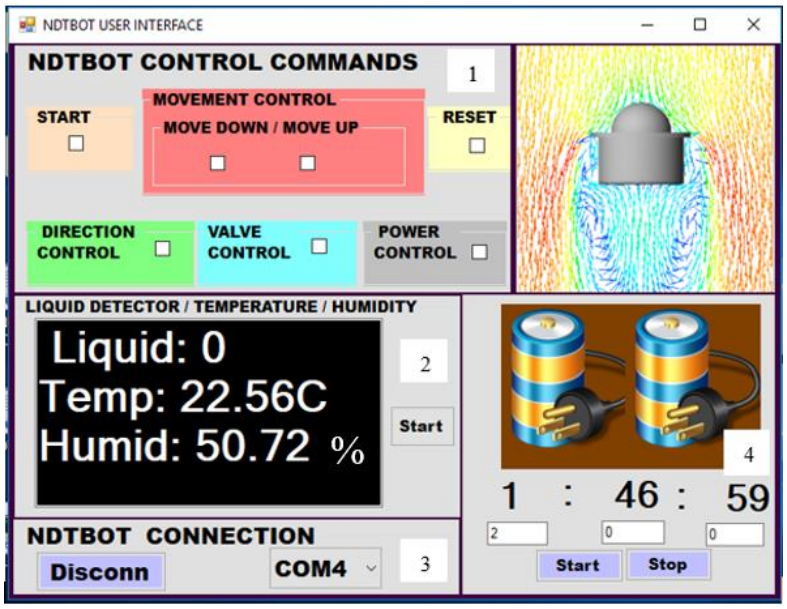

Figure 3. 11: NDTBOT user interface.

1. **NDTBOT CONTROL COMMANDS**
    - START, RESET enable a user to switch on or reset the NDTBOT system.
    - MOVEMENT CONTROL with sub-commands MOVE DOWN/MOVE UP which control the movement of the robot with DIRECTION CONTROL (up/down).
    - VALVE CONTROL is used with the micro-pump to control the internal buoyancy tank by shutting the valve so that no liquid flows.

      POWER CONTROL is used to cut off power in case of leakage into the NDTBOT electronic tank or any other eventuality
2. **LIQUID DETECTOR/TEMPERATURE/HUMIDITY WINDOW**
    - The SCREEN displays the state of the robot by monitoring a fluid sensor to sense any leakage, a temperature sensor to display the temperature and humidity inside the NDTBOT enclosure.
3. **NDTBOT COMMUNICATION**
    - COM is used to select the communication port and establish communication between the robot and the computer for control.
4. **BATTERY**
    - The batteries window is used to monitor the battery life by displaying remaining working time which enables the robot to be recovered from the tank before the battery runs out.
5. **IMU READER**
    - The IMU Reader shown in Figure 3.12 is used to correctly position the NDTBOT on the tank floor. It is used to make sure that the robot is in a vertical position on the floor because the NDT probe correctly measures the floor plate thickness if the probe angle is $90 \pm 5°$ The system is used to assist the reading of the ultrasonic zero degree probe placed underside the NDTBOT to read the thickness of the bottom plate.

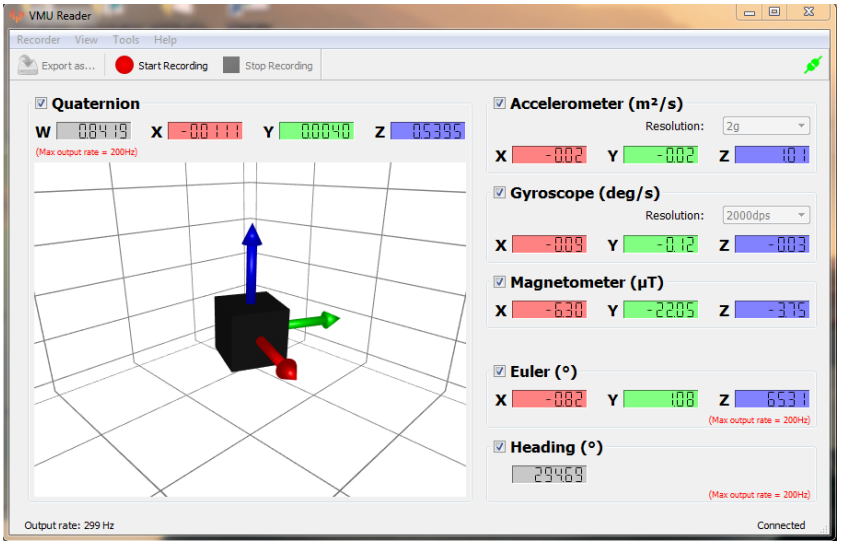

Figure 3. 12: IMU reader.

3.5.2 NDTBOT buoyancy tank

The NDTBOT utilised the same buoyancy control system (up/down) used in the first prototype to control the robot movement randomly inside the tank. The robot buoyancy tank has a maximum capacity of 600 ml with an initial volume of the liquid in the tank being 200 ml. Therefore the NDTBOT uses 400 ml to vary its buoyancy to sink or to float. For safe operation of the micropump to avoid overheating and to control the internal buoyancy tank pressure, minimum liquid was added into the buoyancy tank in air.

3.6 Calculating the forces applied to the NDTBOT

3.6.1 NDTBOT at neutral buoyancy

Using the assumption that friction force is negligible this experiment performed in a water tank. The system is subjected to forces due to the mass of the robot acting downward W_0 and the reaction buoyancy force F_B applied by the liquid acting upward. Figure 3. 13 shows the robot at the surface.

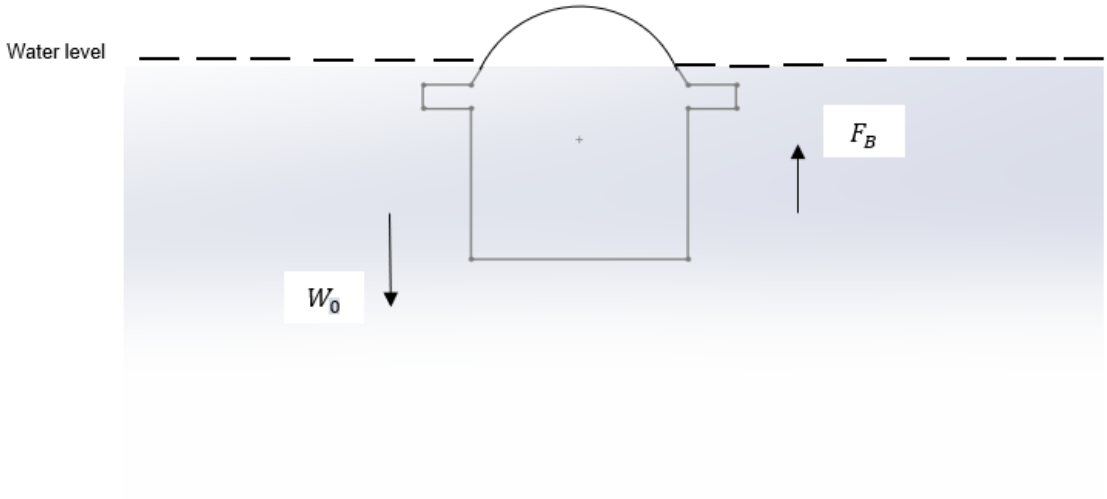

Figure 3. 13: NDTBOT initial position.

The weight of the robot in air is:

$$W_0 = m_0 g \tag{3.1}$$

Where m_0 is the mass of the NDTBOT in air and g is the acceleration due to gravity.

The buoyancy force for a submerged object is equal to the weight of displaced water. At the surface, the NDTBOT body is not fully immersed therefore the buoyancy force could be expressed as a function of time as follows:

$$F_B = \rho_w \vartheta g \tag{3.2}$$

Where ρ_w is the density of the liquid, ϑ is displaced volume of liquid for a submerged robot. The submerged weight W of the object is defined as:

$$W = W_0 - F_B = [m_0 - \rho_l \vartheta] g \tag{3.3}$$

At neutral buoyancy, the weight of the NDTBOT in liquid is zero.

3.6.2 NDTBOT moved from the equilibrium position

When the NDTBOT starts to descend by operating the pump, the mass M of the robot changes and is the sum of the mass of liquid $m_v(t)$ added to the buoyancy tank. $m_v(t)$ is time varying mass flow. The total mass of the NDTBOT is now the mass of the robot in air (m_0) plus the added mass $m_v(t)$. For a totally submerged robot, the buoyancy force does not change because the total volume of the robot is submerged in static fluid in a storage tank. Thus, the new time varying mass is expressed as follow:

$$M(t) = m_0 + m_v(t) \tag{3.4}$$

Figure 3.14 shows the different forces applied to the robot during vertical descent motion.

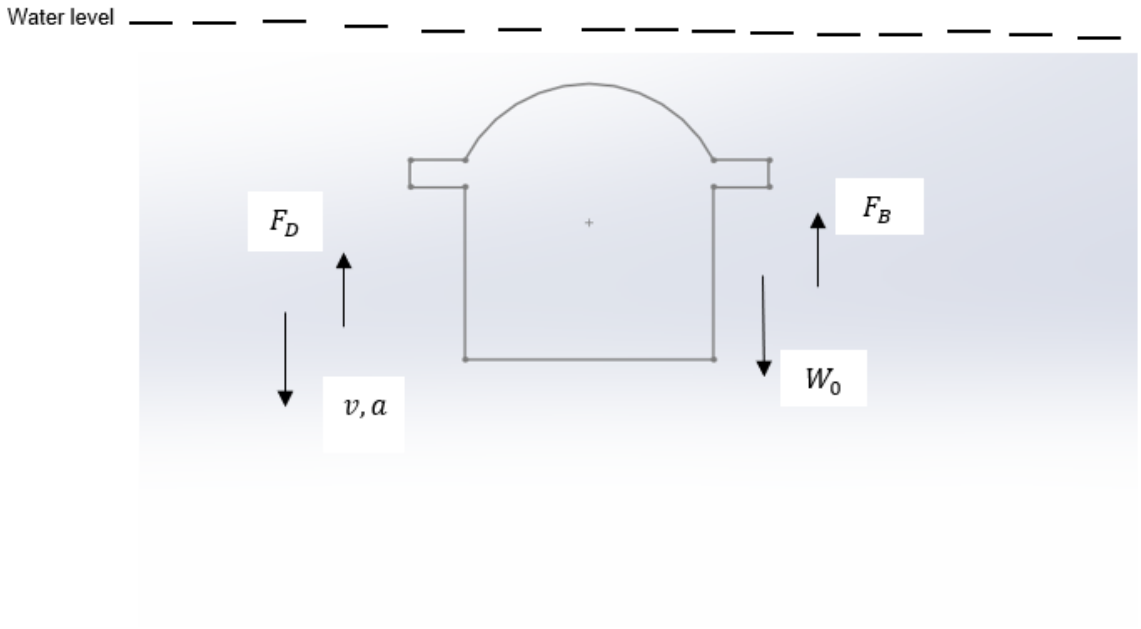

Figure 3. 14: NDTBOT moves from initial position

The total drag force F_D on the NDTBOT body is due to the sum of two drags forces. The first drag, pressure drag, is due to the disturbance of the stream as it passes the body, creating a turbulent wake. In a storage tank, the robot moves in static fluid and creates a disturbance flow. The second drag is the friction drag due to shearing stresses in the thin layer of the fluid near the surface of the body called the boundary layer. The drag force equation is given below:

$$F_D = \frac{1}{2} C_D A \rho_l v^2 \tag{3.5}$$

Where C_D is the drag coefficient, A is the projected area of the robot, v is the velocity of the robot in vertical motion and the combination of $\frac{1}{2}\rho_l v^2$ gives the dynamic pressure. Combining the expressions for buoyancy, the forces acting on the NDTBOT are due to its mass and drag force.

The resultant force acting on the body is:

$$M(t)g - \rho_l \vartheta g - \frac{1}{2} C_D A \rho_l v^2 \tag{3.6}$$

The equation of motion for the NDTBOT is expressed using Newton's Second Law as follows:

$$M(t)g - \rho_l \vartheta g - \frac{1}{2} C_D A \rho_l v^2 = M(t)a \tag{3.7}$$

Where a is the acceleration of the body due to the resultant force acting on the NDTBOT. For an object of changing mass $M(t)$, undergoing acceleration a, another mass m_a needs to be added equivalent to the displaced liquid mass which also has to be accelerated. Therefore, the

equation (3.5) is rewritten as follows:

$$m_0 g + m_v(t)g = \rho_l \vartheta g + \frac{1}{2} C_D A \rho_l v^2 + (m_0 + m_v(t) + m_a)a \quad (3.8)$$

Where m_a is the added mass with $m_a = \rho\pi R^2 L$.

R is the radius of the NDTBOT cylindrical tank and L is its length.

The time-varying mass $m_v(t)$ is calculated from the equation of the volumetric flow as follow:

$$\dot{m}(t) = m_v(t) = \rho_l \dot{v}(t) \quad (3.9)$$

Where $\dot{m}(t)$ is mass flow, ρ_l is the density of the liquid and $\dot{v}(t)$ is the time varying volumetric flow. The time varying volumetric flows as a function of an input voltage applied to the micropump are given in Table 3.3. The micropump works with multiple input voltages which is a great advantage for battery energy saving.

Table 3. 3: Input voltage with volumetric flow and mass flow (Micropump, 2015)

Input voltage (V)	**6.0**	**8.0**	**10.0**	**12.0**
Volumetric flow ($\boldsymbol{cm^3}$/s)	7.5× t	10× t	12.7 × t	15 × t

Table 3.4 shows the densities of water and petroleum medium with water having higher density than petroleum medium.

Table 3. 4 Density

Medium	**Water**	**Crude oil**	**Gasoline**	**Diesel fuel**
Density ($\boldsymbol{k_g/m^3}$)	1000	930	770	831

The mass flow into the NDTBOT buoyancy tank with different media was calculated using equation (3.9). Table 3.3 shows the mass flow with time.

Table 3. 5 Mass flow with input voltage

	mass flow $\boldsymbol{m_v(t)}$ ($\boldsymbol{k_{g/s}}$)			
Input voltage (V)	**Water**	**Crude oil**	**Gasoline**	**Diesel**
6	$7.5 \times 10^{-3}t$	$6.98 \times 10^{-3}t$	$5.78 \times 10^{-3}t$	$6.23 \times 10^{-3}t$
8	$1 \times 10^{-2}t$	$9.3 \times 10^{-3}t$	$7.7 \times 10^{-3}t$	$8.31 \times 10^{-3}t$
10	$1.27 \times 10^{-2}t$	$1.18 \times 10^{-2}t$	$9.78 \times 10^{-3}t$	$1.06 \times 10^{-2}t$
12	$1.5t \times 10^{-2}t$	$1.4 \times 10^{-2}t$	$1.16 \times 10^{-2}t$	$1.25 \times 10^{-2}t$

Figure 3. 15 shows the time variant mass flow in order to control the vertical motion of the robot in water, crude, diesel oil and gasoline using 6.0 volts as the input voltage. The mass flow of the NDTBOT buoyancy tank varies with the medium due to their different densities. The robot buoyancy tank gets to its maximum weight of 400 grams in 50.5 seconds. The weight of

the robot is adjusted according to the medium which will make it operate in any medium. This new feature will make the system usable in most storage Tanks.

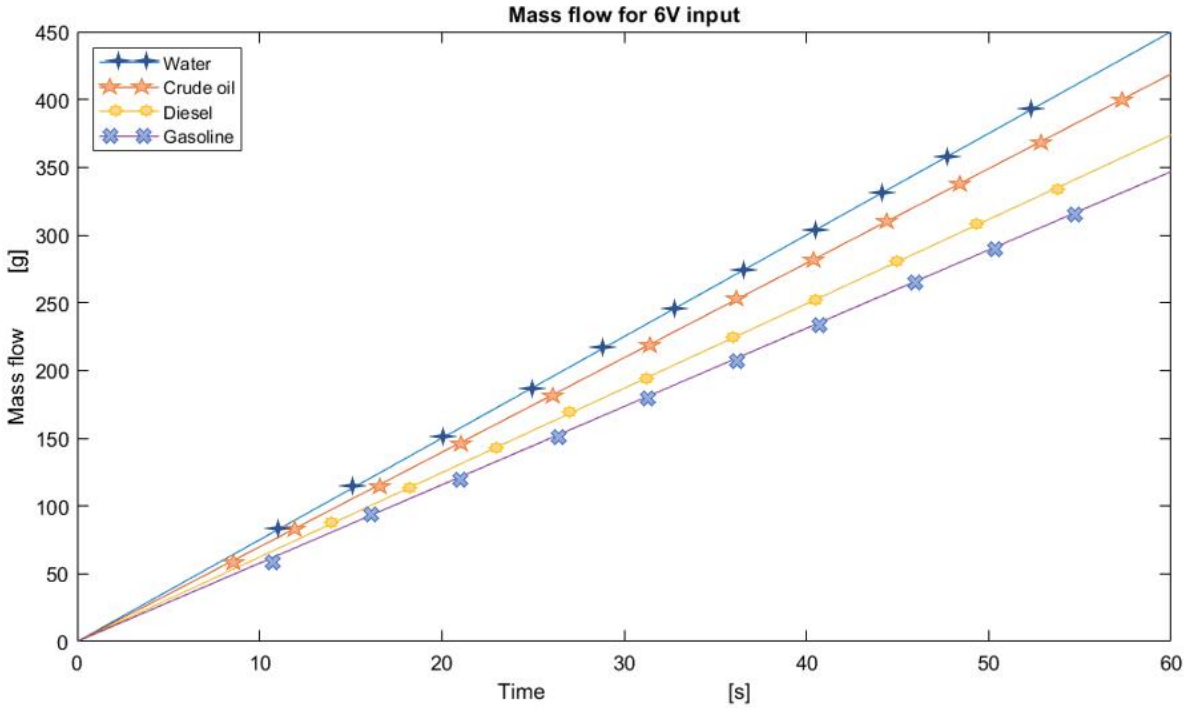

Figure 3. 15: Time-varying mass flow

Table 3.6 shows the calculated kinematic viscosity and Reynolds number Appendix A-3.

Table 3. 6 Medium Kinematic viscosity and Reynolds number.

Medium	**Density** (k_g/m^3)	**Kinematic viscosity** $\times 10^{-6}$ (m^2/s)	**Reynolds Number**
Water	1000	1.52	3.55×10^4
Crude oil	930	69.1	7.81×10^2
Gasoline	770	0.75	7.2×10^4
Diesel fuels	831	3.39	1.5×10^4

3.6.3 Drag coefficient

The drag coefficient is primarily a function of shape and altitude of the body which is under consideration. The magnitude of the drag coefficient for pressure drag depends on many factors, most notably the shape of the body, orientation of the body relative to the fluid stream, the Reynolds number of the flow, the surface roughness, and the influence of other bodies or surface in the vicinity. The drag coefficient of a long cylinder is about 0.81 so long as the ratio L/D (Length-to-Diameter ratio) is greater than 2, for a short cylinder the drag coefficient is about 0.91 provided the ratio L/D is less than 2; and Reynolds number is between 10^4 and 10^6, Sighard (1965). The NDTBOT drag coefficient was estimated using a short cylinder. When the robot is moving down in vertical motion, the result obtained from the calculation of the

Reynold number and the length-to-diameter ratio is shown (Appendix A-3) provides the information for drag coefficient estimation. Since the robot body shape moving down is different from that of moving up, the drag coefficient was estimated using the configuration of a semi-circular rod (Veritas, 2011) and the calculation of L/D is as shown in Table 3.7.

Table 3. 7: Medium characteristics.

Medium	**Density** (k_g/m^3)	**Kinematic viscosity** $\times 10^{-6}$ (m^2/s)	**Reynolds Number**	**L/D**	**Drag coefficient Moving Down**	**Drag coefficient Moving Up**
water	1000	1.52	3.55×10^4	0.83	0.91	To be estimated

The NDTBOT is a slow-moving robot with vertical motion when gaining the maximum weight in the buoyancy tank 400g; its velocity can be estimated 0.3m/s. In this case, the pump is off the robot moved with its weight. The dimension and payload of the robot in the air are shown in Table 3.8 below:

Table 3. 8: NDTBOT characteristics

Weight	**3. 1 kg**
Length	15cm
Diameter	18cm
Total volume	2219244.42mm^3
BT volume	783334.69mm^3
Gravitation	9.81m/s^2
v	0.3m/s
m_a	4.07 k_g
R	0.9cm

The equation of motion could be rewritten with each input voltage stated to choose the appropriate voltage to power and drive the NDTBOT. The equation will help to drive the robot at different speeds needed during its operation. The NDTBOT can have four different equations of motion expressed in Table 3.9. These equations are essential to calculate the robot on board batteries power saving and control.

Table 3. 9: NDTBOT equations of sinking motion

Voltages	**Equations of sinking motion**	
6.0	$0.074t + 7.19 = (7.5 \times 10^{-3}t + 7.17)a$	(3.10)
8.0	$0.098t + 7.19 = (10 \times 10^{-3}t + 7.17)a$	(3.11)
10.0	$0.125t + 7.19 = (12.7 \times 10^{-3}t + 7.17)a$	(3.12)
12.0	$0.147t + 7.19 = (15 \times 10^{-3}t + 7.17)a$	(3.13)

The acceleration of sinking motion of the NDTBOT from above equations with different input voltages is shown in Figure 3. 16. The robot acceleration in sinking motion varies with the input voltages as shown.

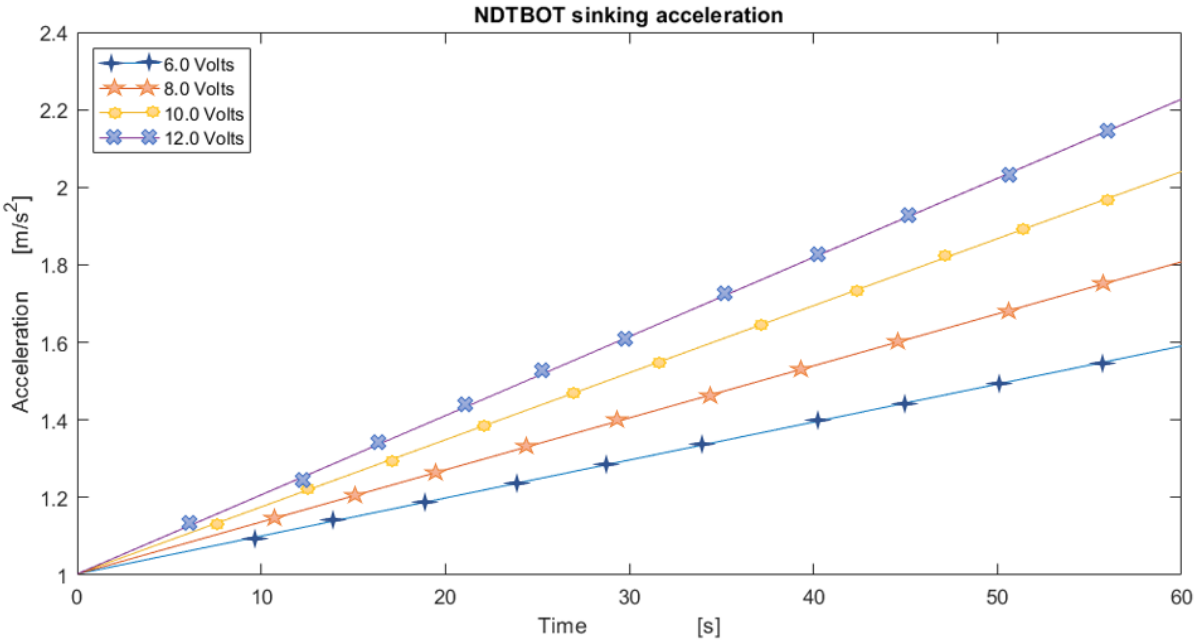

Figure 3. 16: NDTBOT sinking motion acceleration vs time

3.7 Computation of drag coefficient

The NDTBOT model optimisation was done by computer-based software SOLIDWORKS. Ansys CFX is a Computer Aided Engineering tool designed for analysing problems involved in fluid motion. It provides a good approximation simulation result of the real environment, and the numerical methods are very convenient in solving the associated geometric model.

3.7.1 Methodology

The Ansys CFX workflow process is shown in Figure 3. 17. It involves the generation or insertion of domain geometry, mesh, and setup solution. The geometry of the NDTBOT was imported from Solidworks. The estimation of the drag coefficient was done by using the 3D model of the NDTBOT subjected to boundary conditions as close as possible to the real-time conditions.

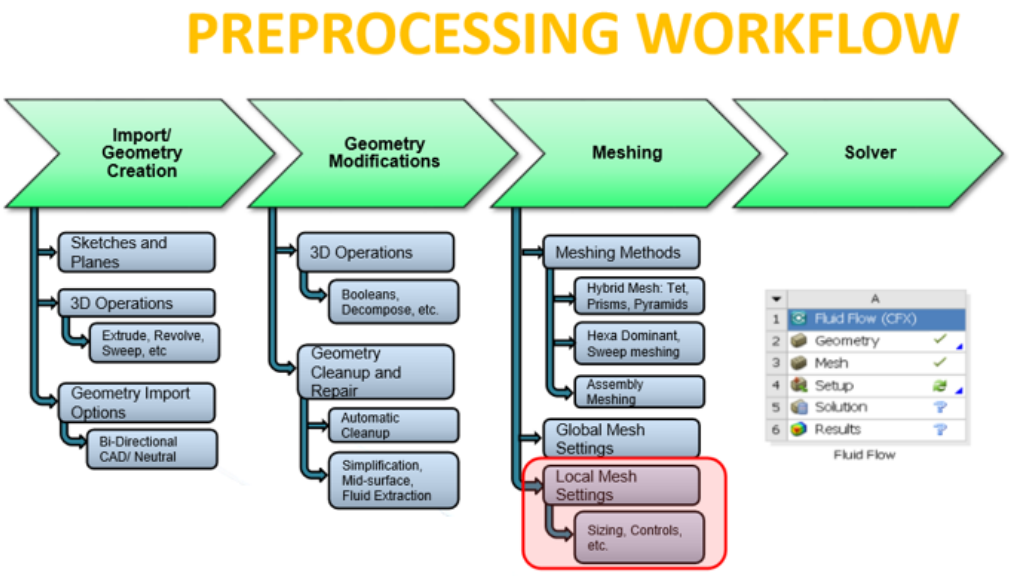

Figure 3. 17: Ansys CFX workflow.

3.7.2 Mesh

The meshing method used was Local Mesh Setting, and sizing was chosen because it allows proximity and curvature meshing to be used in case of multi bodies. Because the NDTBOT holds multiple bodies, LMS allows to set up the mesh according to the geometry. The fluid region was defined as water, the inlet, outlet, wall and robot wall were established, and the robot wall was subtracted from cylinder wall to make up the fluid domain and then meshed using Ansys-CFX. To avoid the wall of flow affecting the results of hydrodynamic analysis, the cylinder wall flow field was made big with 1.5 m diameter and 4m length. Due to the complexity of the NDTBOT structure the mesh element size selection needs to be very small to get an accurate result. The inlet boundary condition of flow velocity (0.3 m/s) was set as constant flow with velocity components $U_x = 0[m/s]$, $V_Y = -0.3\,[m/s]$, and $W_Z = 0[m/s]$ due to NDTBOT vertical motion. The minus sign indicated the orientation of the fluid motion with respect to Y orientation. Thus, for sinking motion, $V_Y = -0.3\,[m/s]$ and ascending motion $V_Y = 0.3\,[m/s]$. The outlet flow was set with constant outflow pressure of 0 $[P_a]$, so that it will have less influence in the upstream inflow. And the cylinder enclosure, the conduit of the flow and the NDTBOT was considered as a stationary wall. A no-slip and no-roughness condition was applied. Figure 3. 18 shows the NDTBOT meshing.

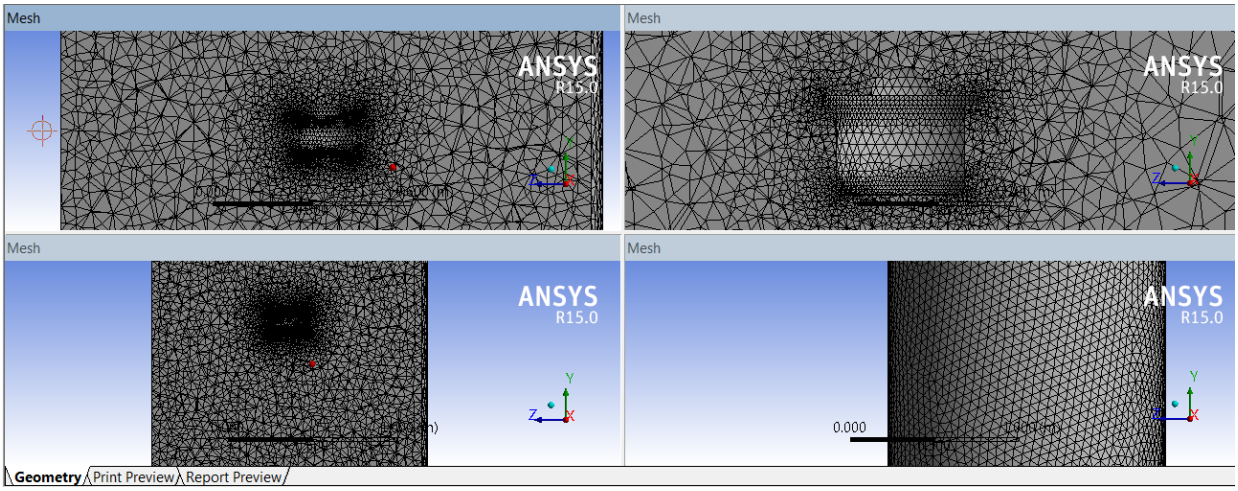

Figure 3. 18: NDTBOT mesh.

3.7.3 Validation of the drag coefficient obtained

In order to get an accurate simulation close to the calculated result, different mesh settings were considered to get reasonable results for the drag coefficient in Table 3.10. The simulation of the mesh convergent graphs is shown in Appendix A-4.

Table 3. 10: Number of elements with drag coefficient

Number of elements	**134851**	**274597**	**457588**	**865340**	**1282761**	**2021038**
sinking Drag coefficient [m²]	0.98979	0.98204	0.88301	0.79144	0.75989	0.75134
Ascending Drag coefficient [m²]	1.81628	1.78053	1.38233	1.02989	1.02012	1.02520

The number of mesh elements vs drag coefficient is shown Figure 3.19(a) for the ascending and Figure 3.19(b) sinking motion.

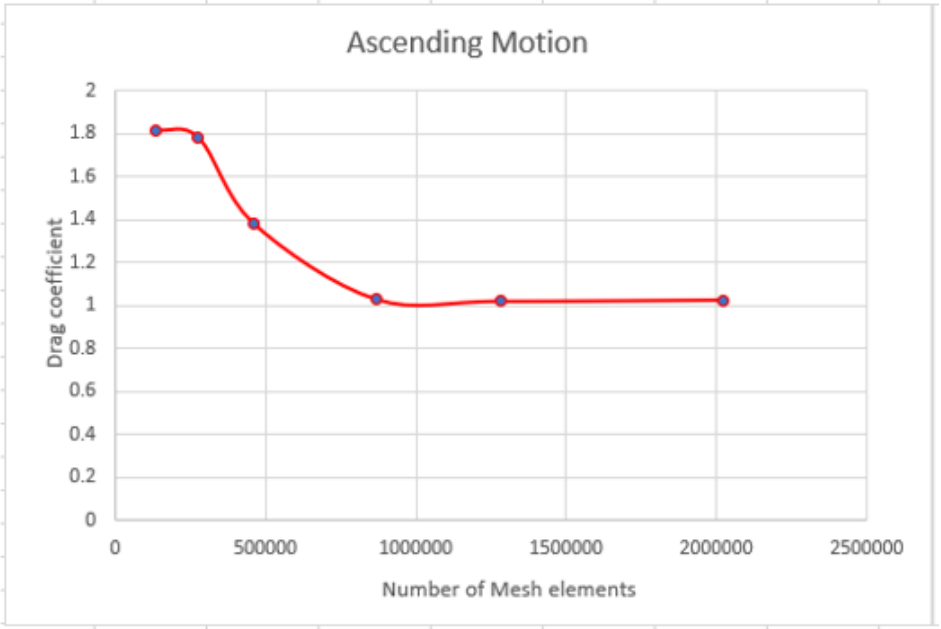

(a)

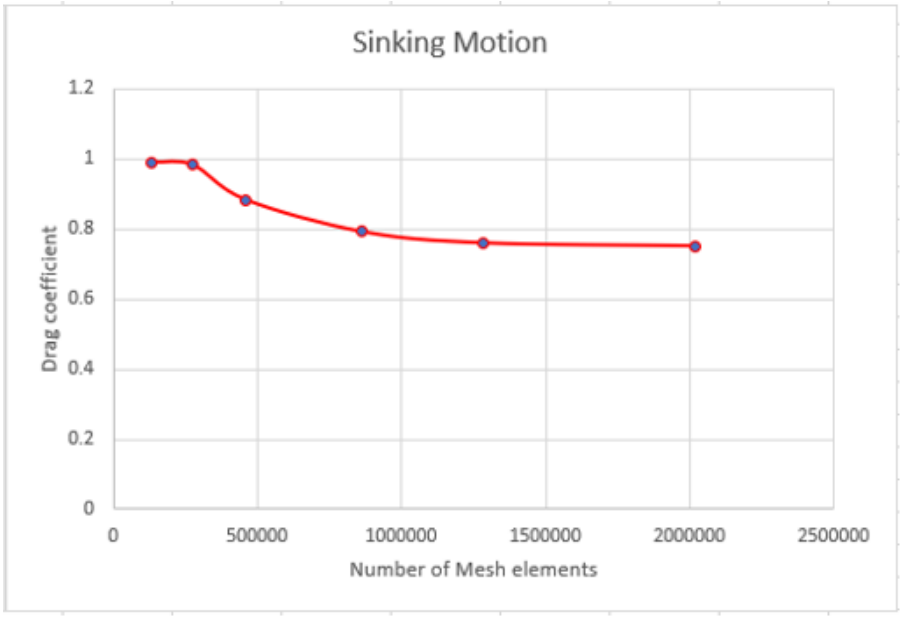

(b)

Figure 3. 19: NDTBOT drag coefficient vs mesh elements.

The NDTBOT ascending (a) and sinking (b) motions stated in Figure 3. 19 show the change of the drag coefficient with increasing mesh elements. After element size of 1000000, the drag coefficient does not change by much. Therefore, the drag coefficient obtained with simulation for both ascending and sinking motions are accurate.

3.7.4 Solver setup domain

The solver setting was used for input /output parameter initialisation. Four domains were set up with the annotation shown in Figure 3. 20 with boundary conditions respectively as inlet boundary type inlets, outlet boundary type outlets and wall and robot wall as boundary type walls. All necessary initialisation calculations were applied.

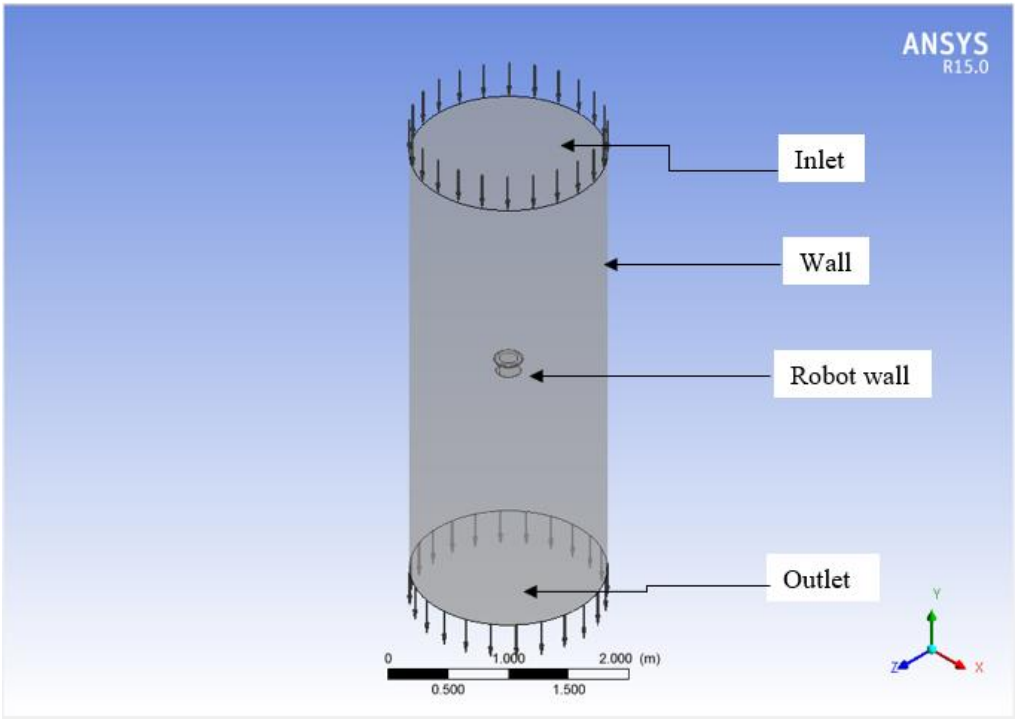

Figure 3. 20: NDTBOT setup in the flow field.

The boundary condition is velocity flow at the inlet with static pressure at the outlet. The turbulence flow at the inlet was set with common turbulence condition of low with the intensity of 1%. The wall domain velocity component $U_x = 0[m/s]$, $V_Y = -0.3\ [m/s]$, and $W_Z = 0[m/s]$ for sinking motion with $V_Y = -0.3\ [m/s]$ and ascending motion $V_Y = 0.3\ [m/s]$, in order to avoid the wall influence on the drag coefficient result in this study.

3.7.5 NDTBOT sinking motion

The robot sinking movement was set with the fluid flow, since the robot and the fluid move relative to each other, the robot was set as static, stationary wall and the fluid as a constant velocity flow. Figure 3. 21 shows the velocity vectors of the flow around the robot with maximum velocity around the robot edges

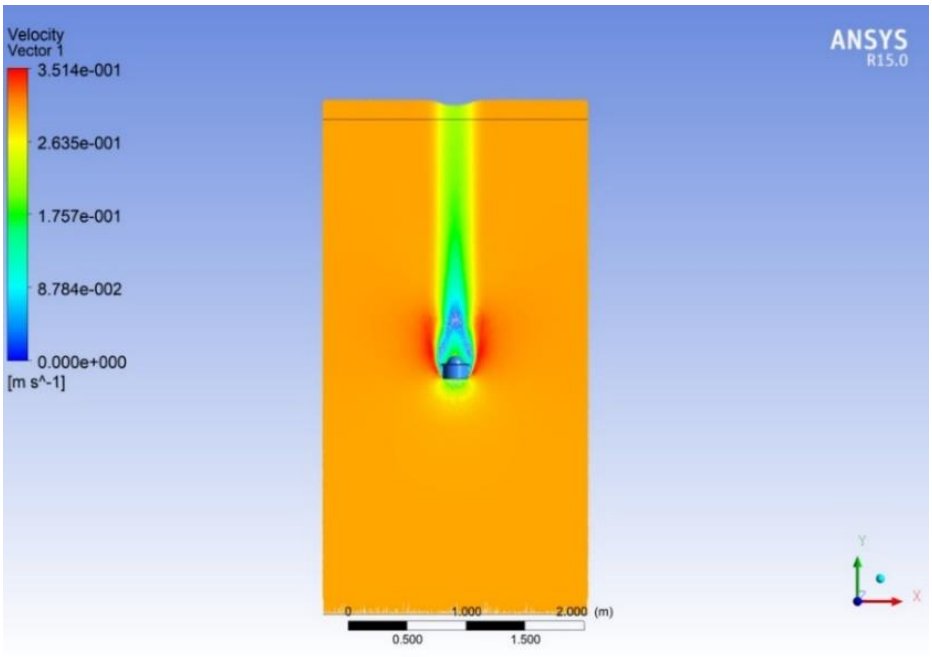

Figure 3. 21: Velocity vectors of sinking motion.

The pressure contour of the NDTBOT in sinking motion is shown in Figure 3. 22 with the maximum pressure appearing at the bottom while the dome geometry presents low pressure.

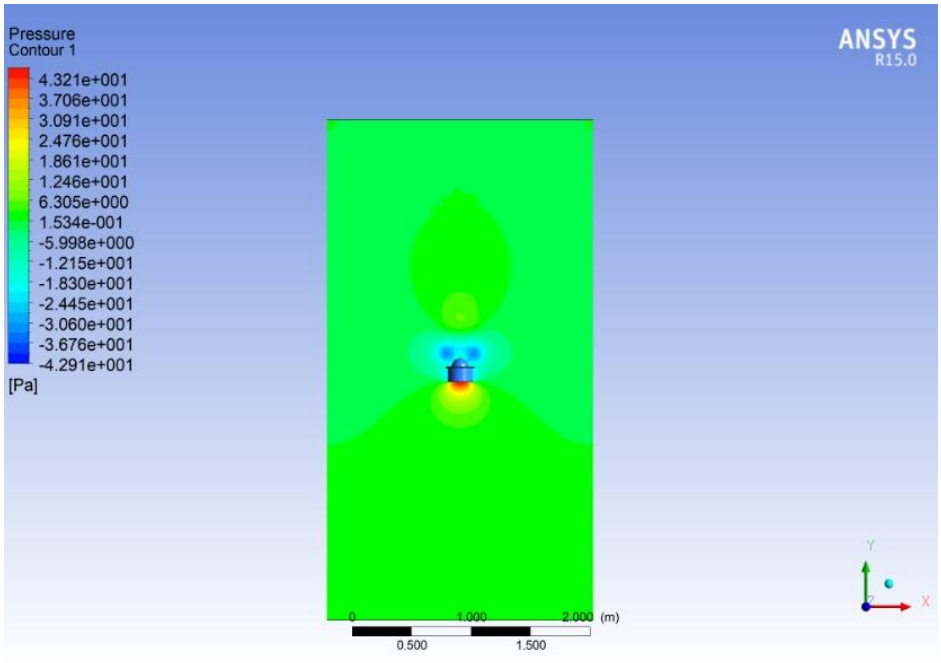

Figure 3. 22: Pressure contour of sinking motion.

The drag coefficient given by Ansys simulation was 0.75834 and compared to the estimated drag which is 0.91. The obtained result in the simulation is close to the estimated with a difference of 0.14. Therefore, the estimated drag coefficient could be used to evaluate the robot sinking motion. The drag coefficient equation applied in the simulation using water for environment simulation was stated with equation 3.14, and the drag coefficient of the sinking motion is shown in Figure 3. 23.

$$\text{DragCoeff} = (\text{DragRobotBody})/(0.5 * \text{DensityWater} * \text{VELOCITY}\hat{}2 * \text{ProjectedArea}) \quad (3.14)$$

Where DragCoeff is the drag coefficient.

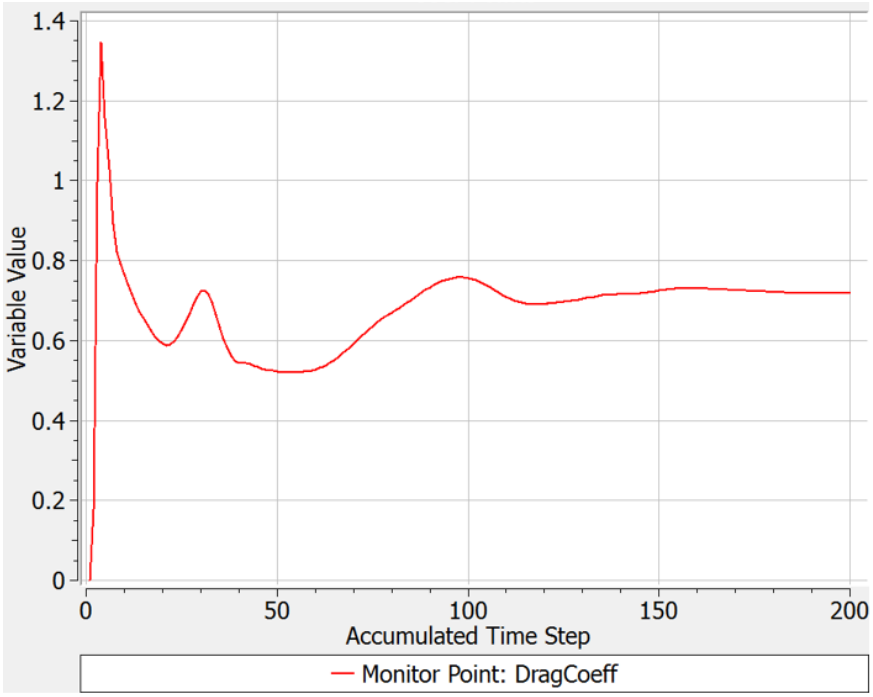

Figure 3. 23: Drag coefficient of sinking motion

3.7.6 NDTBOT ascending motion

Similar to the NDTBOT sinking motion mentioned above, the robot ascending motion and the fluid move relative to each other. The NDTBOT was set as a stationary wall while the fluid was set with constant velocity. The velocity vectors of the flow are shown in Figure 3. 24

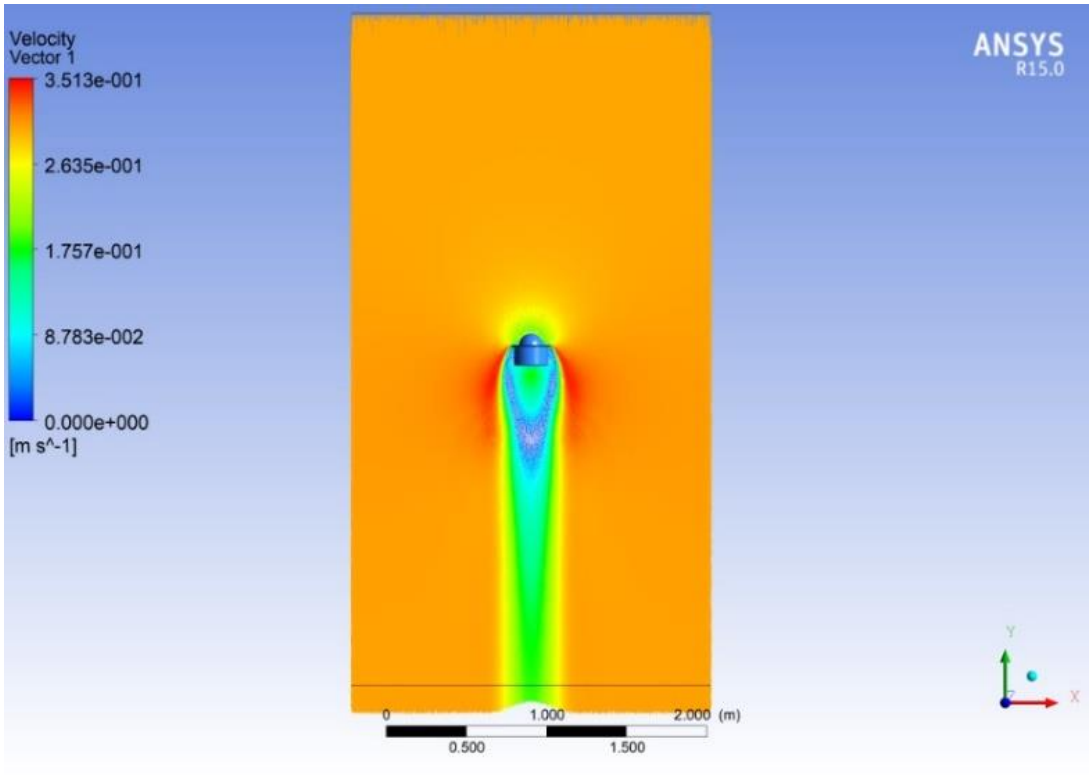

Figure 3. 24: Velocity vectors of ascending motion

The pressure contour of the NDTBOT in ascending motion is shown in Figure 3. 25 with the maximum pressure appearing around the dome geometry while the bottom presents low pressure. By superimpose pressure contour Figure 3. 25 on the velocity vectors Figure 3. 24, it is observed that the higher the velocity, the lower the pressure and the higher the pressure, the lower the velocity.

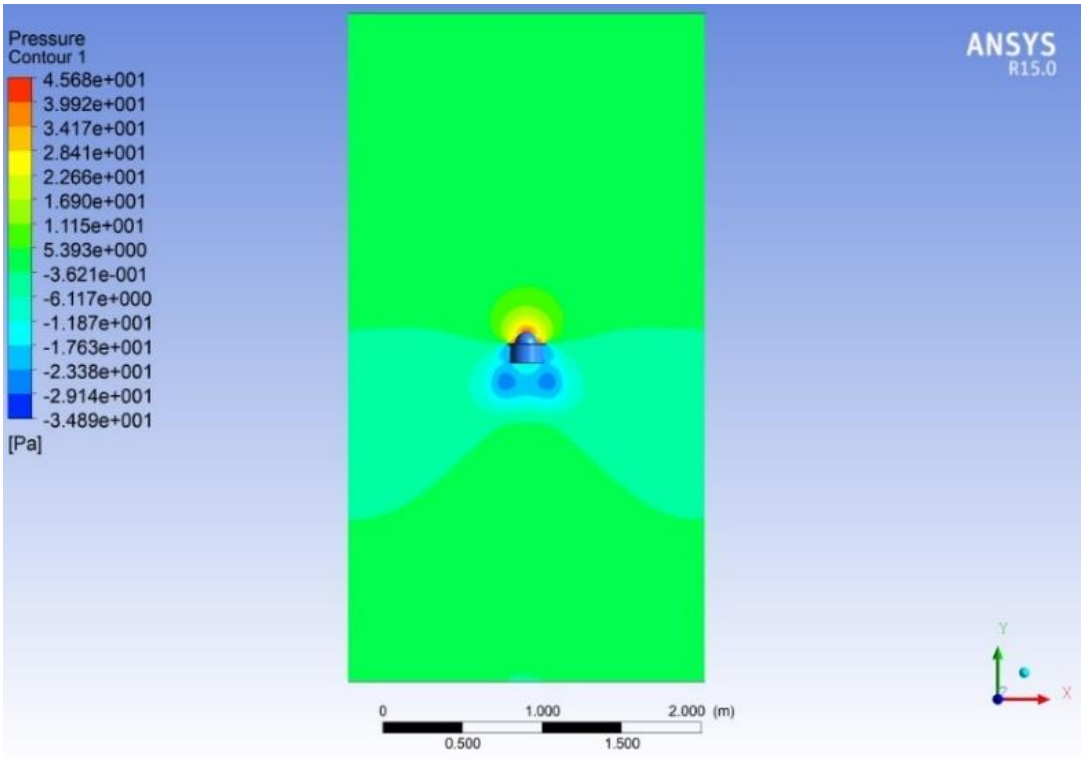

Figure 3. 25: pressure contour of ascending motion

The ascendant motion equations were calculated with the drag coefficient obtained by Ansys simulation due to the unusual top shape of the NDTBOT. From the convergence Figure 3. 19, the result of the drag coefficient obtained with the simulation was 1.0252, and Figure 3. 26 shows the steady state of the drag coefficient from time step of 65 to 100. The result obtained with mesh convergence is more accurate and reasonable and is used to evaluate the NDTBOT ascending motion. The drag coefficient applied in the simulation is stated by equation 3.15:

$$DragCoeff = \text{DragRobotBody}/(0.5 * \text{DensityWater} * \text{VELOCITY\^{}2} * \text{ProjectedArea}) \quad (3.15)$$

Where DragCoeff is the drag coefficient.

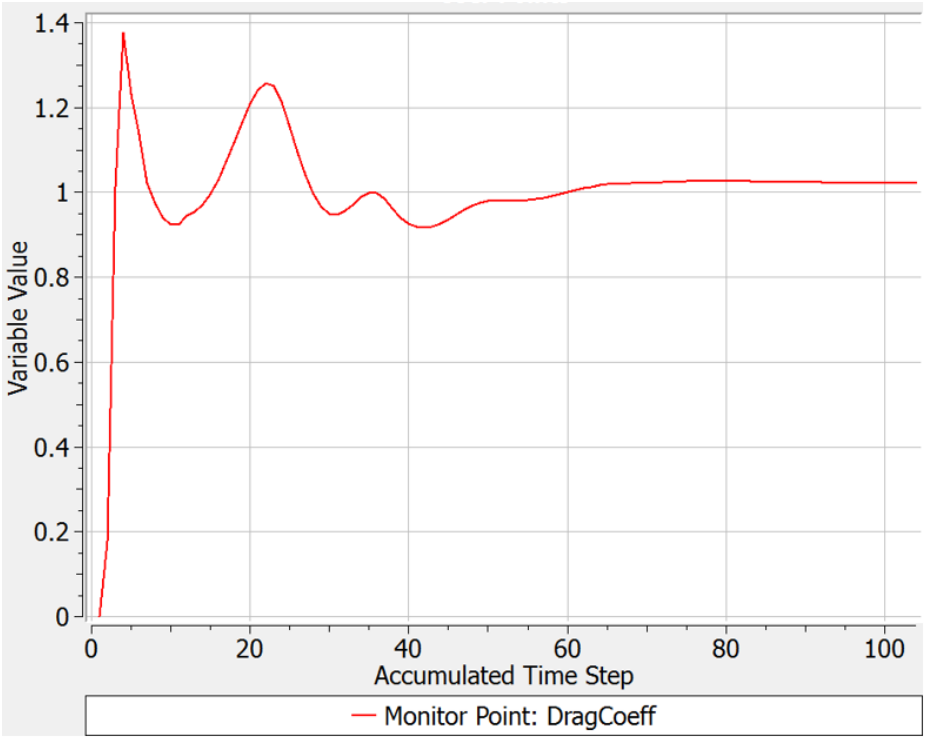

Figure 3. 26: Drag coefficient of ascending motion

The drag coefficient obtained from the simulation with ascending motion of the NDTBOT was used to calculate the equations of ascending motion with different operating voltage with the general equation of motion as shown Table 3. 11.

Table 3. 11 NDTBOT equations of ascending motion

Voltages	**Equations of ascending motion**	
6.0	$0.074t + 7.47 = (7.5 \times 10^{-3}t + 7.17)a$	(3.16)
8.0	$0.098t + 7.47 = (10 \times 10^{-3}t + 7.17)a$	(3.17)
10.0	$0.125t + 7.47 = (12.7 \times 10^{-3}t + 7.17)a$	(3.18)
12.0	$0.147t + 7.47 = (15 \times 10^{-3}t + 7.17)a$	(3.19)

The acceleration of the robot from the above equations with different input voltages is shown in Figure 3. 27; the robot acceleration varies with the input voltages as shown.

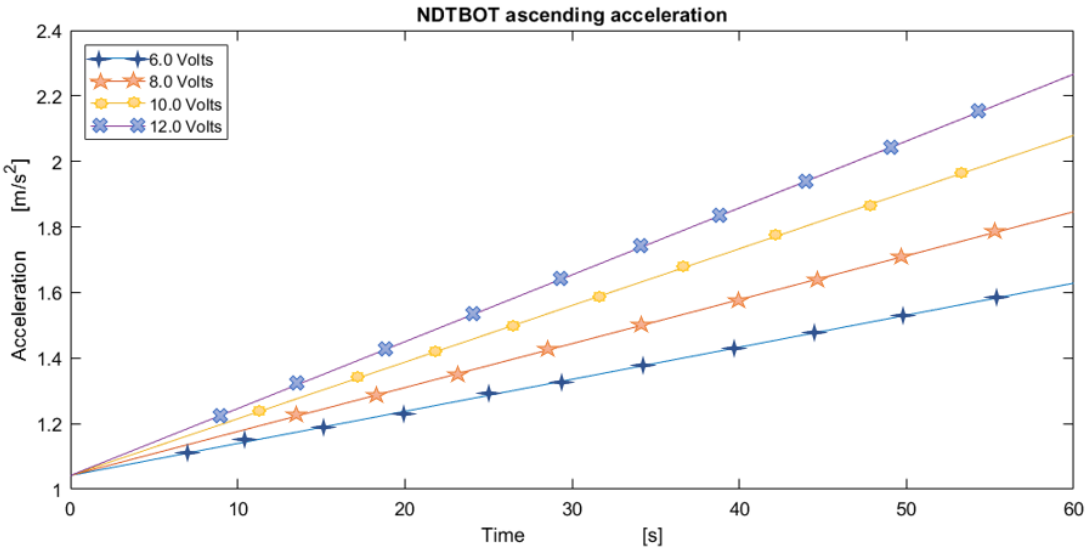

Figure 3. 27 NDTBOT sinking motion acceleration vs time.

3.8 Chapter summary

In this chapter, a new prototype robotic system has been designed to carry ultrasonic UT probe for in-service inspection of storage tank floors. To develop an appropriate system, the environment of inspection was studied. Two robotic systems were developed. The first prototype was designed to test the buoyancy system of the NDTBOT which is the primary method of locomotion for the robot. An ultrasonic UT probe was mounted on the side of NDTBOT to inspect the thickness of steel plates placed in the water tank. The NDTBOT buoyancy system was successfully tested in a water tank with accurate plate thickness measurement with the ultrasonic UT probe. The advanced prototype of NDTBOT was designed to incorporate the buoyancy system tested in the first prototype. The user interface and control system (up/down) were designed to control the NDTBOT. All electronics and ultrasonic flaw detector and on-board power batteries were chosen to meet intrinsic safety requirements for operation in hazardous environments. With this design, encapsulation of the NDTBOT will be more straightforward for deployment in a hazardous environment. The robot was designed to avoid any spark which can create an explosion in storage tanks by avoiding any moving parts in the robot. Very low DC voltage was used to drive the robot which is recommended for ATEX certification in zone 0. Ansys simulation was used to study the robot motion using the drag coefficient obtained from the simulation to obtain the required NDTBOT acceleration by applying different input voltages to the pump in order to control the robot.

Chapter 4

Robotic Non-Destructive Testing

Ultrasonic testing is one of the most popular non-destructive testing techniques for detection of internal flaw. Widely used in industry for inspection of incoming materials as well as for quality control. The flaws to detect may be voids, cracks, inclusions, segregations, delaminations, bursts, flakes, or similar type of flaws. An ultrasound wave oscillates at a frequency, in the range from 20kHz to 200MHz (Figure 4.1). Most ultrasonic flaw detection applications utilise frequencies between 500KHz to 10MHz (Drury, 2005).

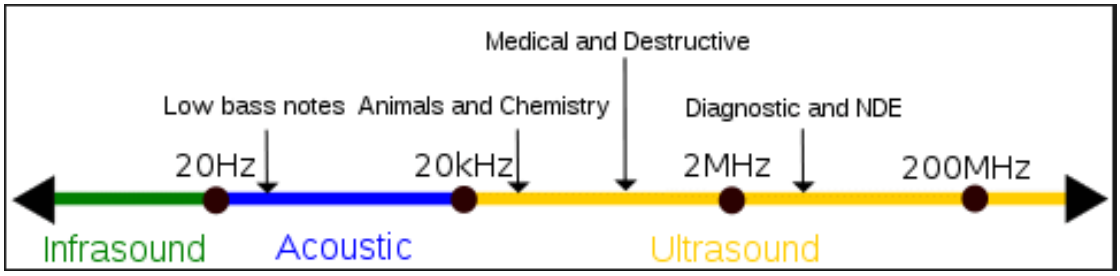

Figure 4. 1: Ultrasonic range diagram (Ultrasound, 2017).

Any mechanical vibration associated with a sound wave of frequency (f) is related to the speed of the propagation in the medium (c), and the wavelength of the oscillation (λ), expressed by the equation below:

$$f = \frac{c}{\lambda} \tag{4.1}$$

Ultrasonic is the application of ultrasound, and UT is a testing technique that utilises ultrasound. UT is an essential tool for inspection in various fields such as construction, aerospace, nuclear, medical, oil and gas, petrochemical, and the food industry (Choi and Popovics, 2015).

This chapter review NDT ultrasonic wave propagation in materials, types of wave, the acoustic impedance of tested objects, and the refraction-diffraction effects that might occur during the test. It describes use of the NDTBOT to gather plate thickness data for different steel plates placed inside a water tank.

4.1 Ultrasonic wave propagation

The problem NDT arises when the test material is composed of unfriendly ultrasonic materials such as composites and concrete which are difficult to inspect because of high attenuation of the ultrasonic signal. To perform post-processing of recorded signals, it is necessary to know the principles of ultrasonic wave propagation in materials. To perform a correct measurement, one must understand the type of wave, the acoustic impedance of the tested object, and refraction-diffraction effects that might occur during the test.

4.1.1 Types of ultrasonic waves

There are three types of ultrasonic waves, longitudinal waves, transverse waves or shear waves and surface waves. This classification of the kinds of ultrasonic waves is based on the direction of the propagation of particle vibration when an ultrasonic wave travels through a medium (Prakash, 2015). Longitudinal waves are the most commonly occurring. They can propagate in solids, liquids, and gases. In this type of waves, particles have the same direction of vibration as the travel direction (Figure 4.2a). Shear waves or transverse waves are as important as longitudinal waves. They can propagate only in solid objects and are polarised because particles vibrate only in one direction in a plane perpendicular to the travel direction (Figure 4.2b). While changing the position of a shear wave source, the plane of particle vibration is also changing. The velocity of a shear wave is always lower than the velocity of a longitudinal wave; therefore, with the same frequency, they have different wavelengths.

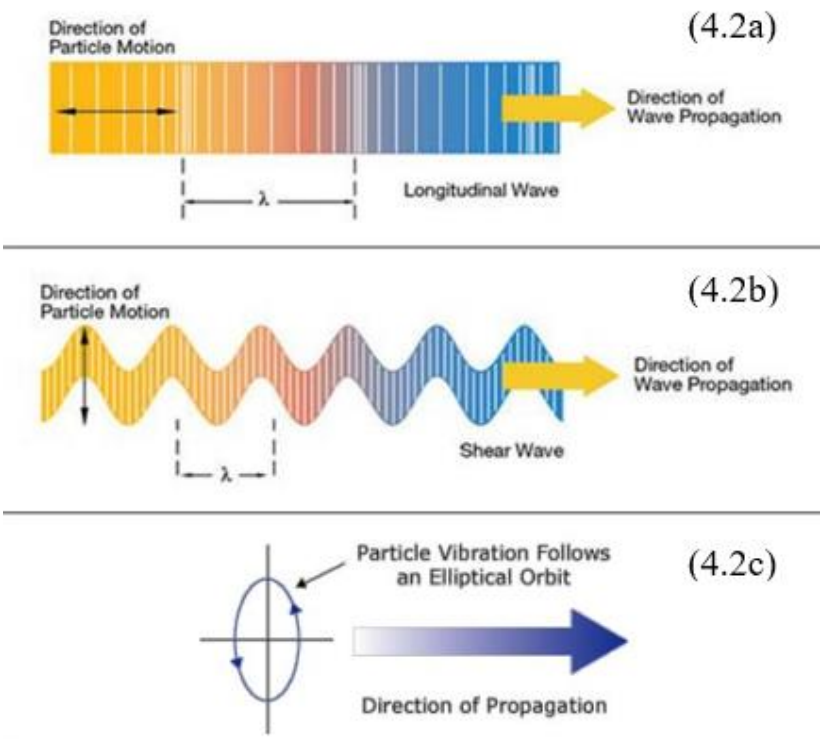

Figure 4. 2: Typical ultrasonic wave propagation (Olympus, 2016).

Surface waves are also known as Rayleigh waves because they propagate at the surface of the material (Figure 4.2c). They penetrate the object only to a depth approximately equal to the wavelength. The particle vibration direction consists of two vectors. A vector that is perpendicular to the wave travel direction has a higher value than a vector that is parallel to that direction. Hence, the particle moves in ellipses in planes perpendicular to the surface and parallel to the direction of propagation. Longitudinal waves are the fastest ultrasound mode among all the modes that are commonly used in ultrasonic NDT. The velocities with different materials of Longitudinal and transverse waves are illustrated in Table 4.1 knowing that the velocity of the transverse wave in a liquid is zero. The transverse wave reflection coefficient at the boundary of liquid or gas to a solid material is equal to the incident wave, thus a total reflection of the transverse wave with a coefficient of reflection is equal to 1.

Table 4. 1: Densities, the velocity of sound and acoustic impedances of some materials.

Material	**Density** $10^3 kg/m^3$	**Velocity of sound** Long. c_l $10^3 m/s$	Transv. c_t $10^3 m/s$	**Acoustic impedance** $Z = \rho c_l$ $10^6 kg/m^2 s$
Metals				
Aluminium	2.7	6.32	3.13	17
Brass	8.4	4.40	2.20	37
Cast iron	6.8 to 5.8	3.3 to 5.8	2.2 to 3.2	25 to 45
copper	8.9	4.70	2.26	42
Iron (steel)	7.7	5.90	3.23	45
Non -metals				
Paraffin wax	0.83	2.2	-	1.8
Ice	0.9	3.98	1.99	3.6
Epoxy resin	1.1 to 1.25	2.4 to 2.9	1.1	2.7 to 3.6
Liquid				
Glycerine	1.26	1.92	-	2.5
Methylene	3.23	0.98	-	3.2
Diesel oil	0.831	1.20	-	1
Water(20^o)	1	1.483	-	1.5
Crude oil	0.930	1.40	-	1.3
Kerosene	0.780	1.37	-	1.07
Gasoline	0.770	1.30	-	1

4.2 Ultrasonic attenuation

Ultrasonic attenuation is due to a decrease in the amplitude of the transmitted beam, and different materials have different ultrasonic attenuation. A material having a higher value of ultrasound attenuation reduces the ultrasonic beam as compared to a material having a lower value of ultrasonic attenuation. Also, the presence of defects or a discontinuity area in a material increases the value of ultrasonic attenuation in the region containing defects. The attenuation of the ultrasound transmitted signal is calculated by the relation:

$$I_t = I_i e^{-\alpha t} \tag{4.2}$$

Where I_t is the intensity of the transmitted beam, I_i is the intensity of incident beam, α is a constant and t is the thickness of the material through which the ultrasound beam has travelled.

Ultrasonic scattering is encountered when the elastic waves propagate within heterogeneous media where either density or phase velocity (known as acoustic impedance) varies. When ultrasonic waves pass through an interface with irregular shape, and its dimensions are smaller than the diameter of the ultrasound beam, the incident beam will be reflected in different directions, known as scattering (Hardt et al., 2012). The concept used in ultrasonic testing is based on the scattering phenomena that occurs from defects such as cracks, flaws, etc. Scattering materials reduce the ability to distinguish signals from noise, often quantified by

Signal-to-Noise Ratio (SNR), illustrated in Figure 4.3. It shows a typical pulse-echo ultrasonic immersion inspection of cylindrical defect measurements in transparent (a) and scattering (b) materials. The effect of the scattering material is seen clearly with increased attenuation, and the introduction of coherent noise.

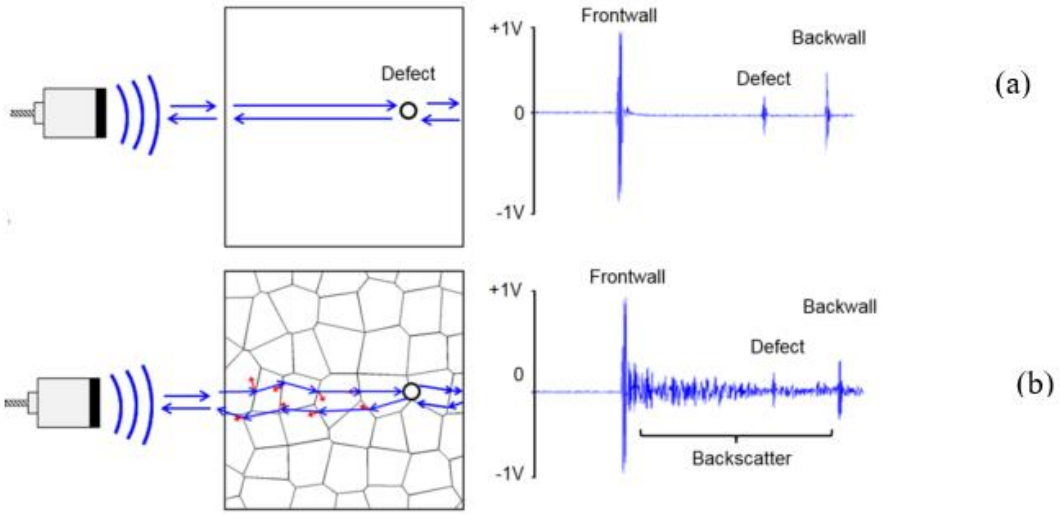

Figure 4. 3: Schematic of pulse-echo ultrasonic immersion inspection (Feuilly et al. 2009).

Noise is a ubiquitous limitation on sensing applications which can arise from a variety of sources. Two important sources of noise can be considered in the ultrasonic signal case. The first source is the scattering of ultrasonic waves from coarse material grains, the effect is known as backscattering noise. Thus, larger grain size or large number of grains in a metal leads to higher noise levels. Another source of noise is related to the electronic circuitry of a sensor. Compared to backscattering noise, the electronic noise level is much smaller.

4.3 Characteristic acoustic impedance, reflection, and transmission

Acoustic impedance is a measure of resistance that is offered by the material in which the wave propagates. The impedance of a material is the product of the material's density and velocity described by the relation:

$$Z = \rho c_l \tag{4.3}$$

Where ρ is material density and c_l is a longitudinal wave velocity in the material. At the interface between two materials, the acoustic impedance either side of the interface will determine what proportion of the incident sound wave will reflect and what proportion will transmit into the second material. Reflexion illustrated in Figure 4.4 shows the interface between two materials whose acoustic impedances are Z_1 and Z_2 respectively.

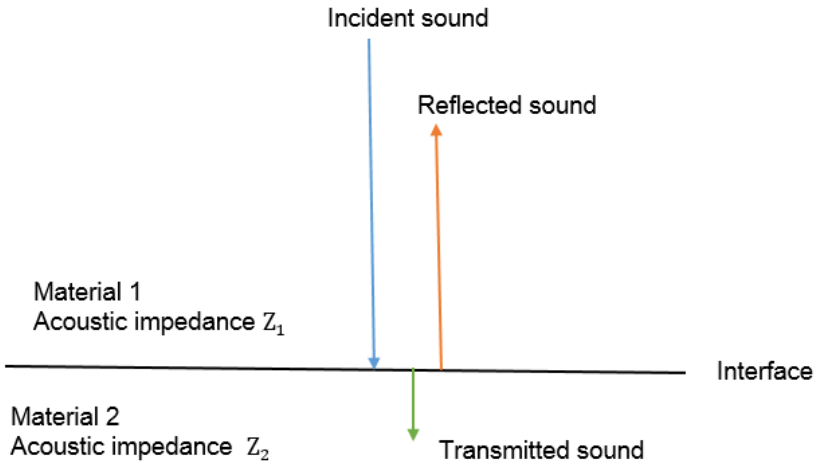

Figure 4. 4: Interface of two materials.

In the example, part of the energy is transmitted into material 2, and part is reflected in material 1. The incident energy that is reflected is given by the equation:

$$R = \left(\frac{Z_2 - Z_1}{Z_2 + Z_1}\right)^2 \tag{4.4}$$

Where R is the reflected energy and Z_1, Z_2 are the acoustic impedances. Since the amount of reflected energy plus the transmitted energy must be equal to the total amount of incident energy, the transmission coefficient is calculated with following equation.

$$T = 1 - R \tag{4.5}$$

4.4 Refraction and diffraction

The phenomena of refraction occur when an ultrasonic wave crosses from one medium to another with different speeds, at any angle other than normal incidence (0^o or 90^o) it will be reflected (Inoue et al., 2006). Both the speed and wavelength will cause the incident wave to bend according to the speed in the medium. Refraction is a change of the wave travel direction at the boundary between two materials due to the change of the wave propagation velocity. The relationship between the angles of the wave before and after it passes the boundary of the two materials is described by Snell's law which states that the ratio of the sines of the angles of incidence θ_1 and refraction θ_2 is equivalent to the ratio of phase velocities in the two media, or equivalent to the opposite ratio of the indices of refraction shown in Figure 4.5.

$$\frac{sin\theta_1}{sin\theta_2} = \frac{V_1}{V_2} \tag{4.6}$$

Where V_1 and V_2 are the wave velocity in a respective medium.

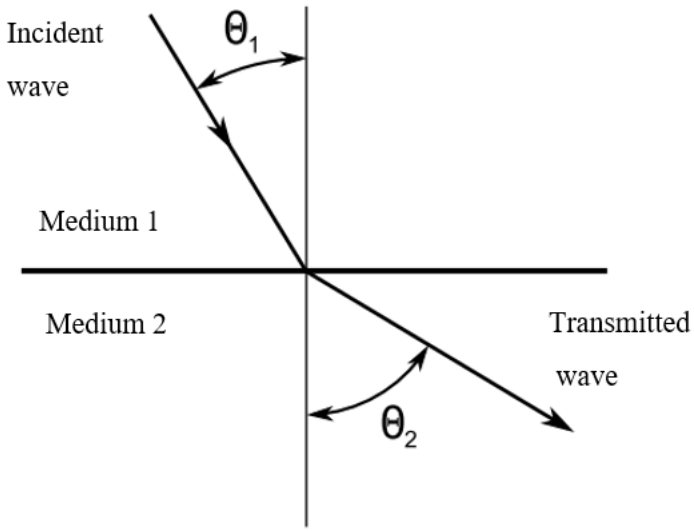

Figure 4. 5: Refraction angle of an incident plane wave at an interface between two media.

However, the incident angle is known as the critical angle when $V_2 > V_1$. It is possible to have an incident angle with the refraction angle $\theta_2 = 90^o$, where the transmitted wave travels along the interface between the two media. When the incident angle is greater than the critical angle, the wave is completely reflected, and no energy is transmitted into the second medium (Bouhadjera, 2006).

Another important aspect is the mode conversion that occurs when one of the mediums is solid (Hoegh, and Khazanovich, 2015). In this case, the incident angle and the critical angle of the material are used to determine the occurrence of mode conversion. Several ultrasonic applications have been designed to utilise the mode conversion phenomena (Castro et al., 2005). Example of mode conversion is when the longitudinal wave reaches the interface between two solid material at an angle, some of the energy can cause particle movement in a transverse direction to start a shear wave. Figure 4.6 shows example of mode conversion of a longitudinal wave.

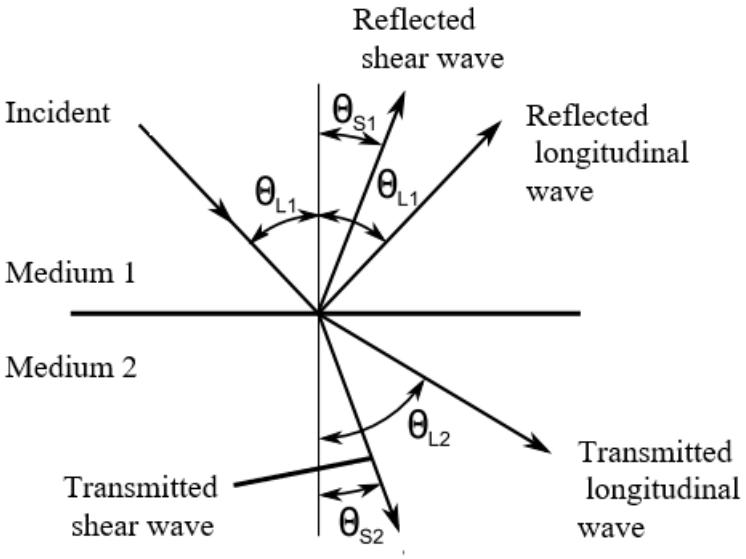

Figure 4. 6: Mode conversion of longitudinal wave incident upon a boundary between two materials.

Snell's law holds true for both longitudinal waves and shear waves and is expressed as follows:

$$\frac{sin\Theta_{L1}}{V_{L1}} = \frac{sin\Theta_{L2}}{V_{L2}} = \frac{sin\Theta_{S1}}{V_{S1}} = \frac{sin\Theta_{S2}}{V_{S2}} \tag{4.7}$$

Where V_{L1} and V_{S1} are the velocity of the longitudinal and shear waves in medium 1 and V_{L2} and V_{S2} are the velocity of the longitudinal and shear waves in medium 2. Two critical angles at which surface waves are produced appear with the mode conversion. The first critical angle, if the longitudinal wave is incident upon a surface, the generated surface wave will have a longitudinal component in the direction of propagation, and the transverse component is perpendicular to the surface is also known as a Rayleigh wave. If the wave is incident upon a plate of finite thickness, then the transmitted wave will be bounded between the two surfaces of the plate with mode conversion occurring as the wave is reflected. As a result, the longitudinal and shear waves inside the plate are coupled together, and the resultant wave is a Lamb wave.

The diffraction effect can be illustrated by Huygens principle which states that at every point to which a luminous disturbance arrives, becomes a source of a spherical wave, and the sum of these secondary waves determines the form of the wave. When the propagating plane wave passes through an opening, the spherical element waves again form the plane wave in the centre zone of the opening. In the case of a straight edge, the elementary waves of the edge from a cylindrical wave whose axis is the edge. Superimposing the plane wave and edge wave produces a field of maxima and minima of the sound pressure (Krautkramer and Krautkramer, 1990). The effect is presented in Figure 4.7, where the dots represent pressure maxima. The

diffraction is most pronounced when the object size is comparable with the wavelength. The ratio of the radiator diameter d and the wavelength λ determines the field spread and the number of minima and maxima. The diffraction occurs with all types of waves, such as acoustic waves, water waves and electromagnetic waves.

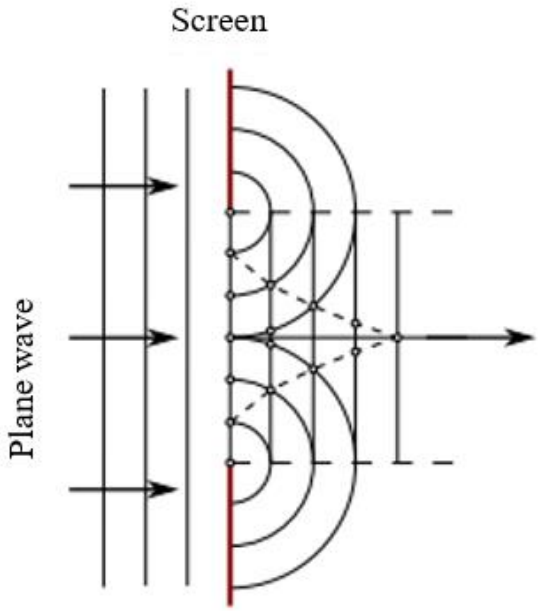

Figure 4. 7: Diffraction of the plane wave.

4.5 The pulse-echo method

Ultrasonic testing is used in engineering applications such as flaw detection and its evaluation, and measurement including the medical field. Usually, UT uses high-frequency sound waves in the range of 0.5 to15MHz to conduct the inspection. In general, ultrasonic is based on the capture and quantification of either the reflected waves (pulse-echo) or the transmitted waves (through-transmission). Different applications use either transmitted waves or pulse-echoes. Generally, pulse-echo is used more due to the requirement that only one side of the test surface is sufficient to inspect the material. The probe generates the pulse wave that propagates into the specimen with corresponding material velocity. When the ultrasonic wave hits the specimen, part of the wave is reflected, the remaining will travel further to a boundary of the material and will be reflected back to the receiver. Figure 4.8 shows the ultrasonic pulse-echo method with transceiver (a), and the display screen shows the A-scan with transmitter pulse, defect echo and back well echo (b), with t_R the transit time to the reflector and t_B is the transit time to the back wall.

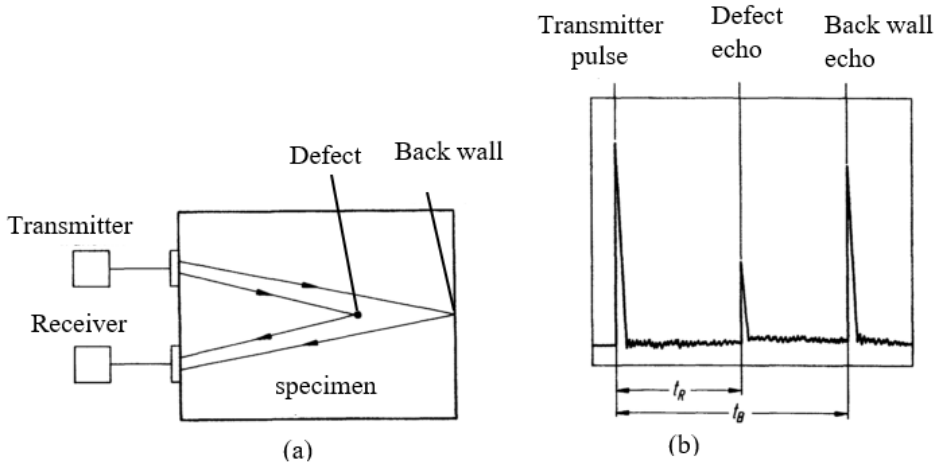

Figure 4. 8: The principle of the pulse-echo method (Moore and Washer, 2004)

The distance (d) to the reflector or back wall can be calculated with the velocity (c) of sound as:

$$d = \frac{ct_R}{2} \; or \; d = \frac{ct_B}{2} \tag{4.8}$$

4.5.1 Important factors influencing the received echo amplitude

The amplitude of the received echo illustrated in Figure 4.9 depends on several influences such as:

- transmitted pulse power entering the specimen,
- the direction of transmission,
- attenuation of the sound wave due to absorption and scattering,
- shadow effects,
- the signal loss at receiver due to reflection and coupling,
- size of the reflector,
- the directivity of the transmitter probe.

The signal amplitude from two equivalent defects is reduced for the defect at greater amplitude as shown in (a), the effect of shadow is illustrated in (b) in this case the larger defect masked the small defect from the ultrasonic signal. In the case of (c), strong attenuation of the sound beam due to scattering, no display of the defect due to its orientation, but in reality, a much more reduced signal would be detected, describing the effect of defect orientation. The impact of the influence of defect size is shown in (d), the more substantial defect will reflect more ultrasonic energy thus greater display amplitude.

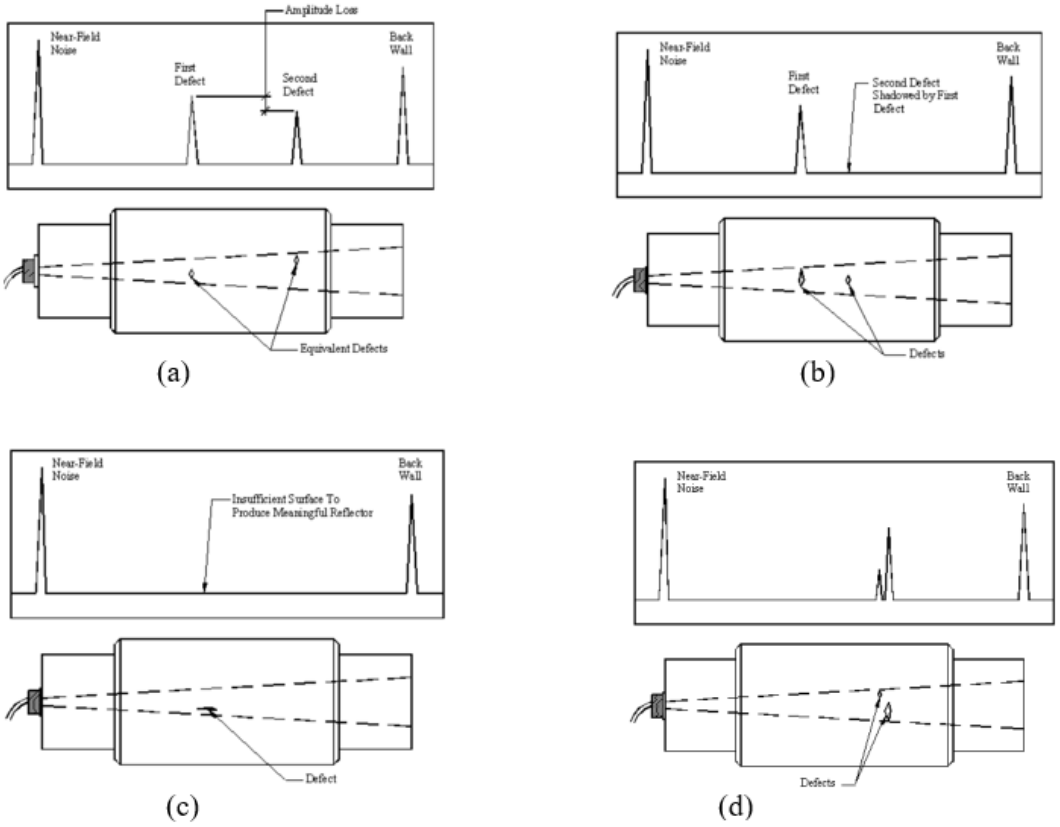

Figure 4. 9 Schematic screen picture obtained by the pulse-echo method, (Moore and Washer, 2004).

4.6 Ultrasonic transducer

The essential component of an ultrasonic system is the transducer or probe. The essential part of the probe is the piezoelectric element that converts the electric signals into mechanical vibrations (ultrasonic waves) and converts mechanical vibration (ultrasonic wave) into electric signals. Several factors influence the behaviour of a transducer such as the type of material, mechanical and electrical construction and external mechanical loads. The mechanical assembly parameters that affect performance are the radiation surface area, mechanical damping, the housing, the connector type and other variables. There are several types of transducers for a specific application according to the need.

To choose the appropriate transducer for an application, it is important to understand the concept of frequency range or bandwidth of ultrasound. In general, lower frequency provides greater energy and penetration in the material. While higher frequency offers greater sensibility to small discontinuity even though their penetrating power is not optimal. Meanwhile, a highly damped transducer or probe will respond to a broader frequency range, and it can give the sensor better resolution power.

The majority of ultrasonic NDT transducers contain piezoelectric materials, (IOlympus, 2006). The construction of the typical conventional piezoelectric transducer is shown in Figure 4.10. Usually materials are tested using a contact method, where the sensors are held against the sample, with some form of coupling gel to remove any air layer that would prevent transmission. The most important element of an ultrasonic probe is the active element known as a piezoelectric or ferroelectric material which determines the central frequency and other proprieties. Also, other components include the backing material, wear plate, matching plate, and electrical circuits.

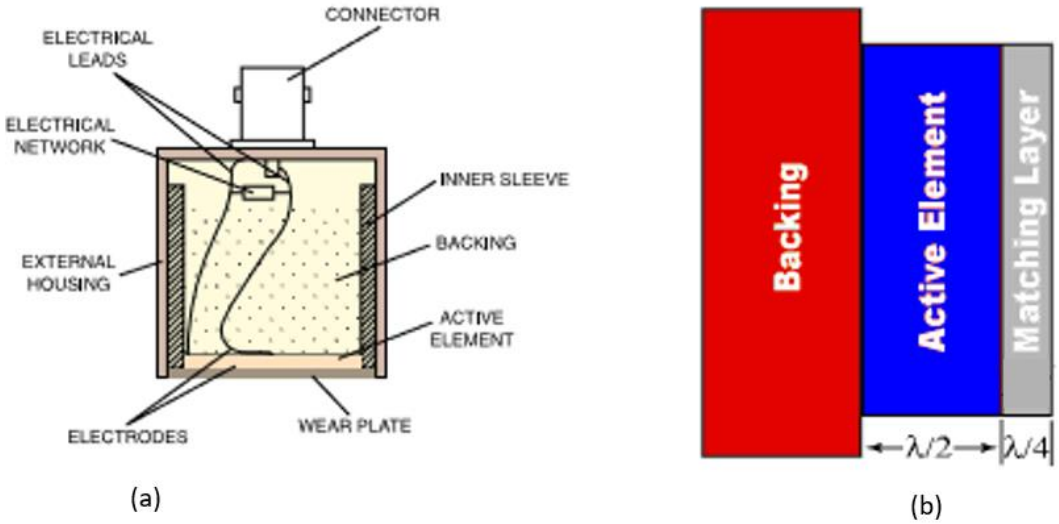

Figure 4. 10: Schematic of the typical construction of a piezoelectric transducer. (a) A typical contact probe and (b) use of a matching layer in water immersion, (IOlympus, 2006).

In immersion ultrasonic probes, a suitable liquid such as oil or water is used as the coupling medium. To get as much energy out of the transducer, an impedance matching layer is placed between the active element and the face of the transducer as shown in Figure 4.10. Optimal impedance matching can be achieved by having the matching layer with a thickness of ¼ of the desired wavelength for maximum transmission amplitude into the medium.

Besides the active element, the backing material is also one of the essential components for an ultrasonic probe. The backing material has a significant influence on the damping characteristics of the transducer. The most effective backing material is one with impedance similar to the active element as well as the one that has a wider bandwidth. This kind of backing material can produce better sensitivity when used in the ultrasonic probe. As the mismatch in impedance between the active element and the backing material increases, medium penetration increases but transducer sensitivity is reduced.

4.7 NTDBOT medium of inspection

The NDTBOT environment for inspection is a petrochemical storage tank. However, for initial experiments without going to the expense of making the NDTBOT intrinsically safe, thickness measurement with ultrasonic is done in water. The robot utilised a zero-degree probe to measure the thickness of steel plates placed inside a water tank. Corrosion is detected by measuring the plate thinning from a nominal value. For the NDTBOT to be able to do a similar in-service inspection in the petrochemical storage tank and correctly read the thickness of the bottom plate, the transmitted sound pressure into the specimen becomes an important factor. Therefore, the sound pressures of certain petroleum products are calculated and compared to the experiment done in a water environment. In this calculation, two materials are used with material 1 to be water and material 2 to be a steel plate. The incident wave is transmitted from material 1 to material 2 with acoustic impedance $Z_1 = \rho_1 c_1$, and material 2 impedance is $Z_2 = \rho_2 c_2$. The equations (4.4 and 4.5) are used together with Table 4.1 to calculate the reflection and transmitted coefficients of the incident wave for water /steel and different petroleum media in terms of percentages shown in Table 4.2.

Table 4. 2: Reflection and transmitted coefficients.

Materials (Z_1/Z_2)	**Reflection coefficient (R) %**	**Transmitted coefficient (T) %**	**Margin % with respect to Water/ steel**	
Water/ steel	87.5	12.5	Reflection coef.	Transmitted coef.
Crude oil / steel	89.1	10.9	+1.6	-1.6
Kerosene / steel	90.9	9.1	+3.4	-3.4
Diesel / steel	91.5	8.5	+4	-4
Gasoline / steel	91.5	8.5	+4	-4

The attenuation of the signal as it travels through the material is not considered in this calculation. From Table 4.2 the positive and negative signs in the margin percentage respectively show the increase in reflected energy coefficient and the decrease in transmitted energy in petroleum products. The amount of energy transmitted into material 2 decreases by 4% for (gasoline/steel) and in case of crude/steel the energy transmitted decrease by 1.6% compared to water/steel.

4.8 Ultrasonic testing performance of NDTBOT

To evaluate the NDTBOT's performance and ability to inspect a tank floor to get the state of the floor thickness, three measurement techniques were used. First the initial thickness was measured with a Vernier calliper, second, the thickness measurement was made with a hand-held ultrasonic sensor probe and flaw detector and last the NDTBOT was submerged into

a water tank to remotely measure the thickness of various steel plates. The goal of this experiment was to measure the thickness of different steel plates using the NDTBOT submerged in a water tank and compare these measurements with prior measurements of original thickness with a Vernier calliper and results obtained with hand-held contact UT.

4.9 Experimental setup

4.9.1 Calliper thickness measurement

In this part of the experiment, a digital Vernier calliper was used to measure the average thickness of different sizes of steel plates. To get an average reading of the original thickness of each steel plate, several readings were taken at different parts of the plate. Figure 4.11 shows the setup measurement in the lab.

Figure 4. 11: Calliper thickness measurement

In this work, ten steel plates with different sizes were used, and the average thickness of each steel plate was calculated. The average thickness of each plate represents the initial thickness of the plate. Equation 4.9 is used in this calculation and Table 4.3, shows the calculated result known as the initial or real thickness of the steel plate.

$$AV = thickness_{intial} = \frac{1}{n}\sum x_i \quad (4.9)$$

Where AV is the average thickness, x_i represents a measurement and n is the number of measurements.

Table 4. 3: Real plate thickness.

Steel plate	**1**	**2**	**3**	**4**	**5**	**6**	**7**	**8**	**9**	**10**
Initial average thickness (mm)	21.45	19.80	21.82	21.41	13	14	19.74	21.20	18.99	13.4

4.9.2 Handheld UT thickness measurement

Choosing the right frequency and diameter of the Ultrasonic probe for thickness measurement with consideration of material type are the first things to take into account. Table 4.4 compares the lower and higher frequency ultrasonic transducer used in the material testing.

Table 4. 4: Low /Higher frequency advantages.

Low-frequency ultrasonic transducer (0.5MHz -10MHz)	-Provide greater energy and penetration in the material. -Increase the chance to get a strong return echo. -Good quality measurement of absorption materials -Best for material that absorbs sound (plastic and composites).
Higher frequency ultrasonic transducer (15MHz -25MHz)	-Provide reduced penetration in the material. -Greater sensitivity to the small discontinuity. - can improve flaw resolution when used with proper instrumentation. -Ideal for precision because the pulse they emit is highly focused -Have shorter wavelengths and are absorbed and attenuated more easily. -Suitable to measure thin materials. -Reduce troublesome “surface noise” that can be present on some metals (aluminium or titanium) that can cause measurement error.

A low-frequency ultrasonic transducer was used for the hand-held UT thickness measurement due to the advantages mentioned in Table 4.4. Because the interest is in the thickness measurement, therefore, a probe that can provide ultrasound to penetrate a material and get strong echo, a low-frequency transducer was preferred. A conventional immersion ultrasound transducer, 2.25 MHz with diameter 12.75 mm, zero-degree was used in this

experiment. The goal was to determine the thickness by manual scanning (contact NDT), the same ten steel plates measured previously with a Vernier calliper were used. To obtain precision and accuracy measurement of the experiment, a steel test calibration block with artificially induced flaw was used to calibrate the probe as shown in Figure4.12.

Figure 4. 12: Steel calibration block with a thickness of 25 mm

The micro-ultrasonic hardware used was from EROSONIC with very low input voltages of 5 V connecter to the computer via USB cable. The device is suitable for embedded applications for real-time data acquisition. It can be used in several applications such as Time of Flight Detection and for flaw detection in metal and composite materials, process monitoring, weld inspection and pipe and tube inspection. Figure 4.13 shows the top and bottom views, with Pulse / Receiver (P/R) or pulse-echo mode connection with the same probe, and Through Transmission (T/T) mode connection when used for work in transmission mode. This means that one probe is used as a transmitter and another one as a receiver.

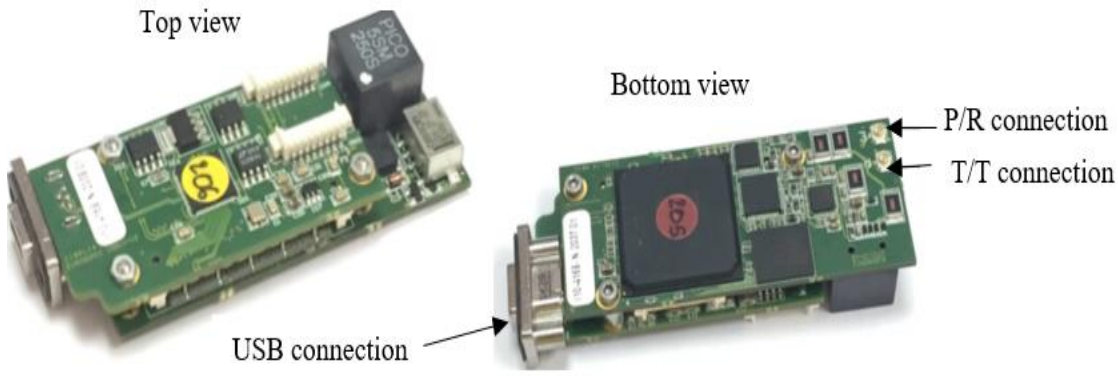

Figure 4. 13: UTC 110 Ultrasonic

The Hand-Held Ultrasonic Thickness Measurements (HHUTM) was done with the same number of steel plates as mentioned earlier, couplant was used between the transducer and the test piece to facilitate the transmission of sound energy. Several tests were done, and the average of the thickness is calculated for each steel plate. The hand-held inspection thickness was calculated with the time of flight given by the EROSONIC graphical user interface and the speed of sound with following equation.

$$thickness = \frac{TOF \times C}{2} \tag{4.10}$$

Figure 4.14 (a) shows the thickness measurement and Figure 4.14 (b) the GUI with an A-scan display (Amplitude of signal). It is a basic visualisation of the ultrasound wave which uses defectoscopy for flaw detection. In the experiment, the A-scan was used for thickness measurements. Other types of scan are the B-scan which is performed to obtain information about flaw width, and C-scan is used to evaluate the flaw position in two dimensions. These types of scan are the most basic and conventional methods of ultrasound imaging, where no signal processing is needed.

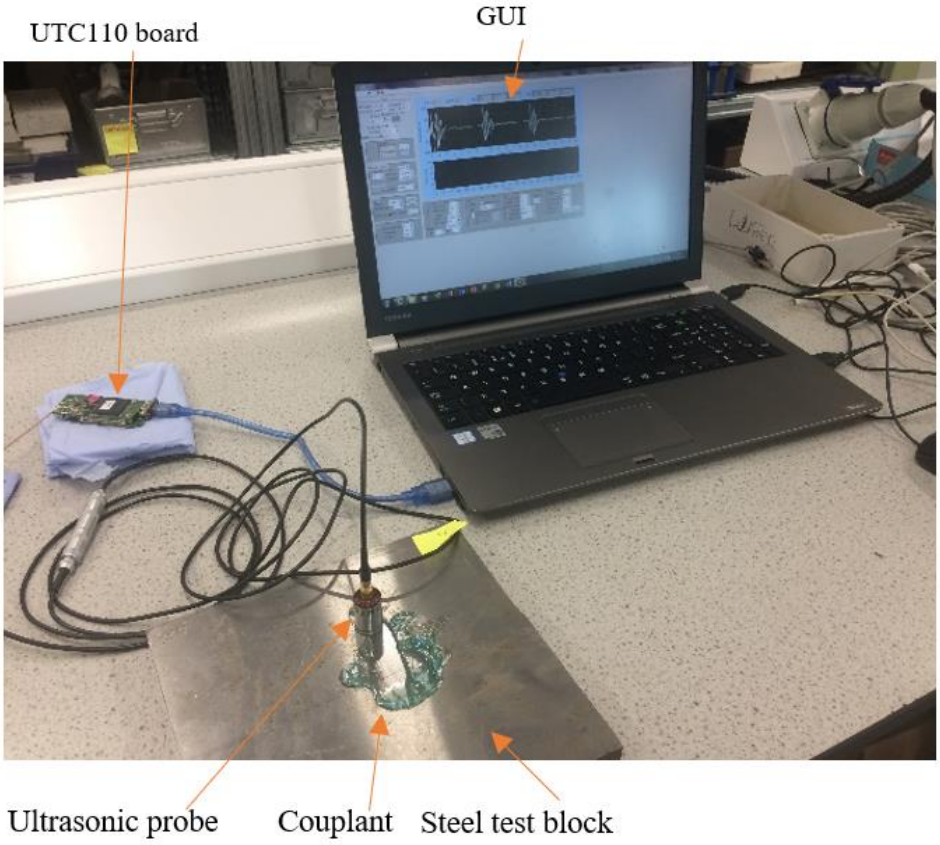

(a)

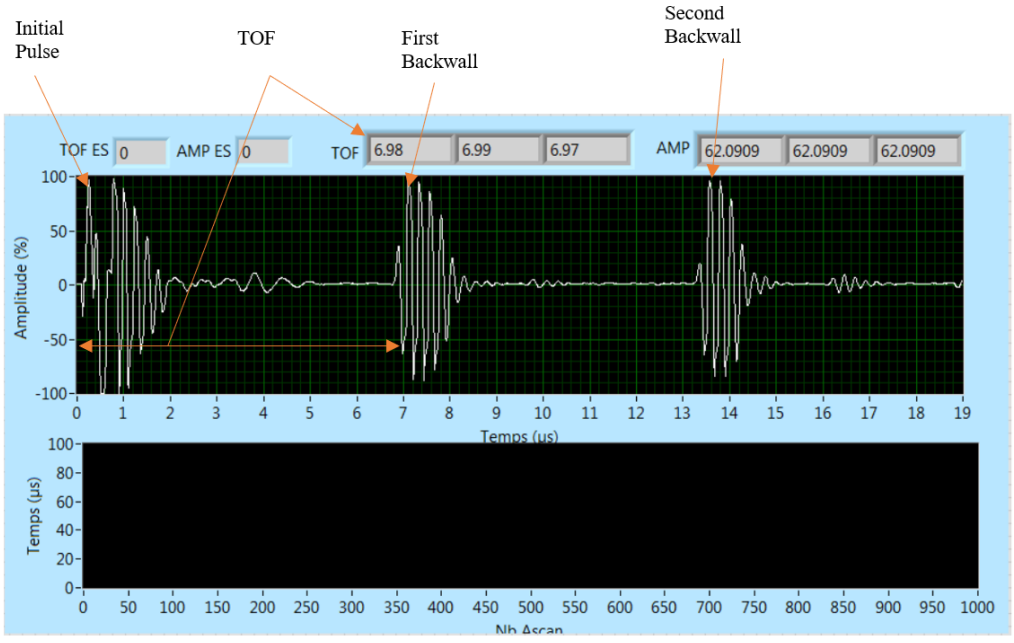

(b)

Figure 4. 14: UTC 110 Ultrasonic

$$AV_{thickHand-held} = thickness_{\text{Hand-held}} = \frac{1}{n}\sum y_i \quad (4.11)$$

Where $AV_{thickHand-held}$ is the Hand-held thickness, y_i is a value of thickness and n is the number of thickness readings.

The results obtained with the Hand-Held Ultrasonic Thickness Measurement (HHUTM) using the A-scan are shown in Table 4.5.

Table 4. 5: Hand-held ultrasonic thickness measurement

Steel plate	**1**	**2**	**3**	**4**	**5**	**6**	**7**	**8**	**9**	**10**
HHUTM (mm)	21.90	20.75	21.64	21.90	14.38	15.1	20.25	21.83	19.10	13.80

4.9.3 Thickness measurement with NDTBOT

The ultrasonic testing method used in the experiment is the non-contact pulse-echo technique with immersion probes. In section 4.9.2, the probe contacts the surface via an ultrasound couplant. In the NDTBOT thickness measurement case, the ultrasound probe is kept at a constant stand-off distance from the surface with sound transmission through the liquid (in this case water). A single transducer which acts as a transmitter, as well as the receiver, was used to measure the thickness of the same ten steel plates.

The EROSONIC UT probe and hardware were integrated with an on-board microcomputer together with all electronics and battery were placed inside into the NDTBOT watertight enclosure. The probe was held at a constant stand-off distance from the plate surface (non-contact NDT) to ascertain the thickness of the same ten steel plates. At this stage, the on-board microcomputer processes the robot control commands, and sends NDT data via a very lightweight Ethernet RJ45 cable. Figure 4.15 shows the experiment with submerged steel plates. The probe used in this experiment was a conventional UT, single element, diameter 12.75 mm, of frequency 2.25 MHz used in earlier hand-held thickness measurements

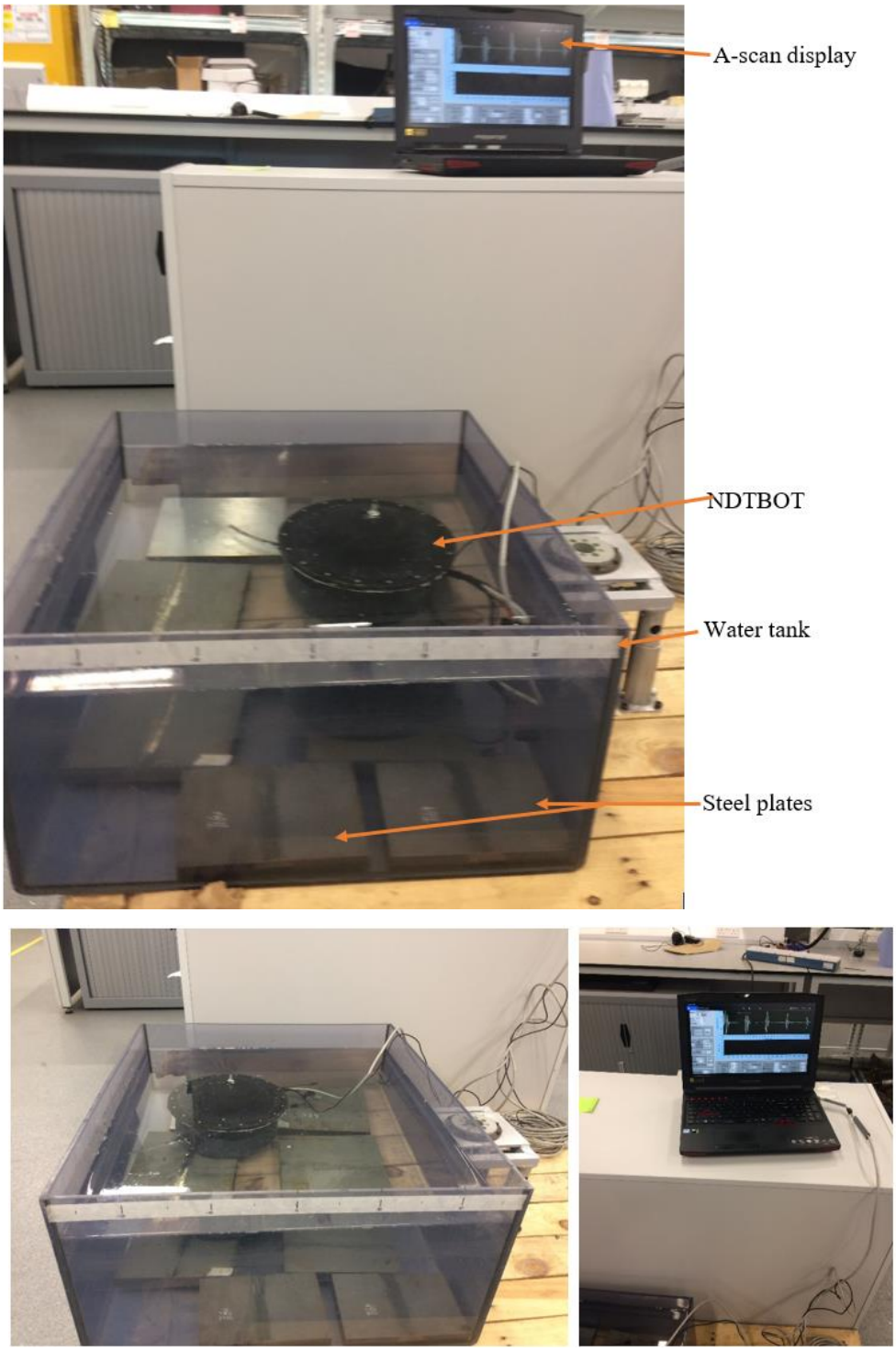

Figure 4. 15: NDTBOT in water tank inspection

The NDTBOT was driven to hop around inside the water tank to read the thickness of different steel plates. The results of the NDTBOT thickness measurement are shown in Table 4.6. A similar calculation was done using the time of flight method explained earlier with hand-held thickness measurement and the equation following is used to calculate the thickness.

$$AV_{thickNDTBOT} = thickness_{\mathbf{NDTBOT}} = \frac{1}{n}\sum v_i \quad (4.12)$$

Where $AV_{thickNDTBOT}$ is the average NDTBOT thickness reading, v_i is a value of thickness reading with the NDTBOT and n is the number of reading.

Table 4. 6: NDTBOT ultrasonic thickness measurement.

Steel plate	**1**	**2**	**3**	**4**	**5**	**6**	**7**	**8**	**9**	**10**
NDTBOT UT thickness (mm)	21.31	19.48	20.72	21.31	12.94	13.76	19.90	21.50	19.05	13.60

The purpose of the experiment was to use NDTBOT submerged in a water tank, randomly measure the thickness of the steel plate and compare with hand-held contact thickness measurement to determine the NDTBOT performance with respect to the real or initial thickness measured with the calliper. The measured thickness of the ten steel plates is summarised in Figure 4.16. It shows that the readings with the NDTBOT were much closer to the real thickness than the hand-held thickness measurements.

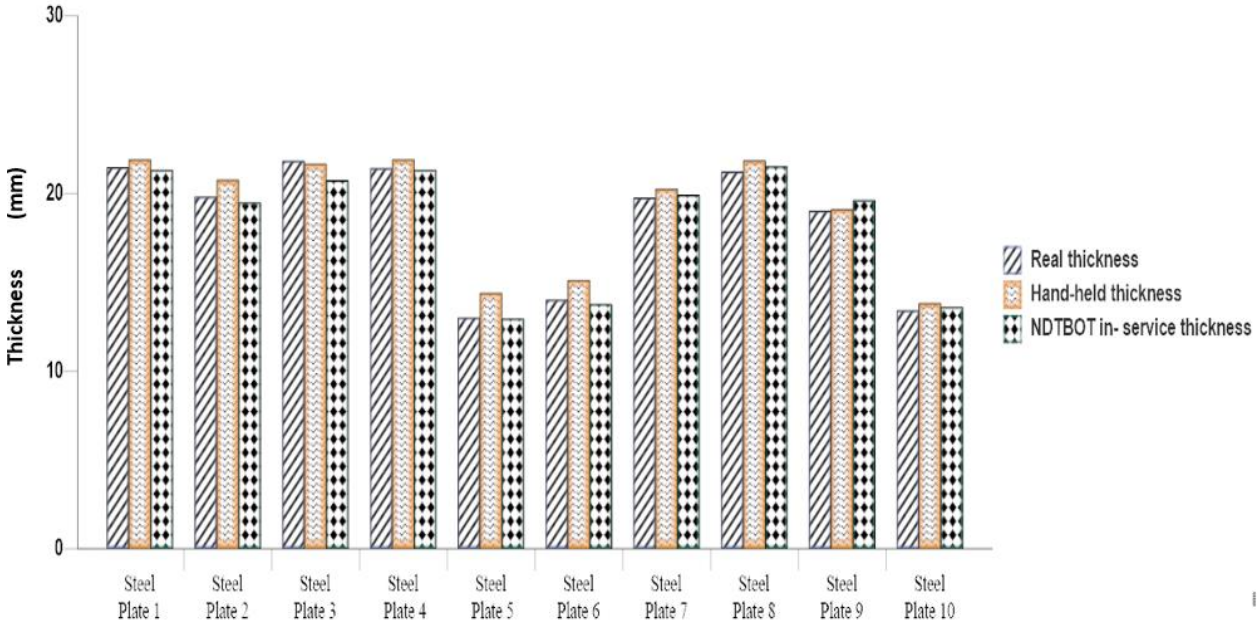

Figure 4. 16: Steel plate thickness measurement.

The percentage margin error between hand-held contact and the NDTBOT inspection was calculated with the following equation where measured thickness refers to a hand-held or NDTBOT in-service inspection and real thickness refers to calliper measurement.

$$\%\text{Margin error} = \frac{\frac{1}{n}\sum w_i - \frac{1}{n}\sum x_i}{\frac{1}{n}\sum x_i} \times 100 \tag{4.13}$$

The expression could be rewritten as:

$$\%\text{Margin error} = \frac{\frac{1}{n}\sum (w_i - x_i)}{\frac{1}{n}\sum x_i} \times 100$$

$$\%\text{Margin error} = \frac{\sum (w_i - x_i)}{\sum x_i} \times 100$$

Where w_i is the Hand-held thickness or NDTBOT UT thickness measurement.

Table 4.7 shows the percentage error of different steel plates used in the experiment.

Table 4. 7: Initial, measured thickness and margin errors.

Steel plate	**1**	**2**	**3**	**4**	**5**	**6**	**7**	**8**	**9**	**10**
UT contact margin error (%)	+2.1	+4.8	-0.82	+2.29	+10.62	+4.85	+2.58	+2.97	+0.58	+2.98
NDTBOT UT margin error (%)	-0.65	-1.61	+5.04	-0.47	-0.46	-1.71	+0.81	+1.41	+0.32	+1.5

The UT contact or hand-held margin of error is higher than the NDTBOT margin error when compared to the real material thickness. This is due to greater variation of pressure applied to the hand-held ultrasonic transducer during UT contact scanning and the couplant applied to the test plate. Therefore, NDTBOT measurement of plate thickness with non-contact NDT could give more accurate results for in-service inspection tank.

4.10 Chapter summary

The prototype of the NDTBOT has been developed to test its motion capability with a simple active buoyancy control method and to determine the quality of plate thickness measurements with non-contact ultrasound NDT. The robot can stand up to 10 m deep which is the rating of the micropump. The NDTBOT thickness measurements with an immersion ultrasound probe obtained more accurate results than manual or hand-held contact NDT. Therefore, the results increase confidence that using NDTBOTS to look for corrosion thinning on the floors of storage tanks can give at least equivalent results to standard NDT performed by a human operator.

Chapter 5

Investigation of Radio Frequency Communication with the NDTBOT

Radio Frequency (RF) is a promising technology for many wireless applications due to its broad bandwidth, good ratio of transmission data and low cost. So far, all RF devices are designed to work in atmospheric environments. Research is growing on the application of RF for underwater wireless sensor communications (Lloret et al., 2012). A static multi-hop underwater wireless sensor network using RF electromagnetic communication has been proposed by (Che et al., 2009) and re-evaluation performed of RF electromagnetic communication in underwater sensor networks (Che et al. 2010). However, in this chapter, RF is proposed for data transmission in a dielectric media such as petroleum products and vegetable oil. In such applications, the frequency becomes an important consideration for the propagation aspects of electromagnetic waves in such medium. Therefore, the primary goal of this chapter is to determine an RF frequency suitable for this purpose. To achieve this goal, simulation with commercial electromagnetic software FEKO (Altair, 2017) was performed to analyse the behaviour of EM propagation parameters such as the radiation pattern in petroleum and vegetable oil.

5.1 Background

Radio frequency transmission, known as non-ionizing radiation, is a series of energy waves composed of oscillating electric and magnetic fields travelling at the speed of light. Higher-powered RF radio transmitters can induce current in a metal structure and create hazards to personnel. This includes long and medium wave radio, ship communication and radar systems, radio beacons, amateur radio, FM and VHF/UHF radio, TETRA communication system, radio telephones, civilian and military radar, satellite communications, television broadcasts, mobile phone networks and local site radio communication systems (Bradby, 2008). High power radio frequency transmissions can produce spark ignition at a distance of up to 30 km (NAVSEA OP 3565/NAVAIR 16-1-529, 2003). TV, radio, radar systems, communication system, etc, all fall within the RF range as shown in the electromagnetic spectrum, Figure 5.1.

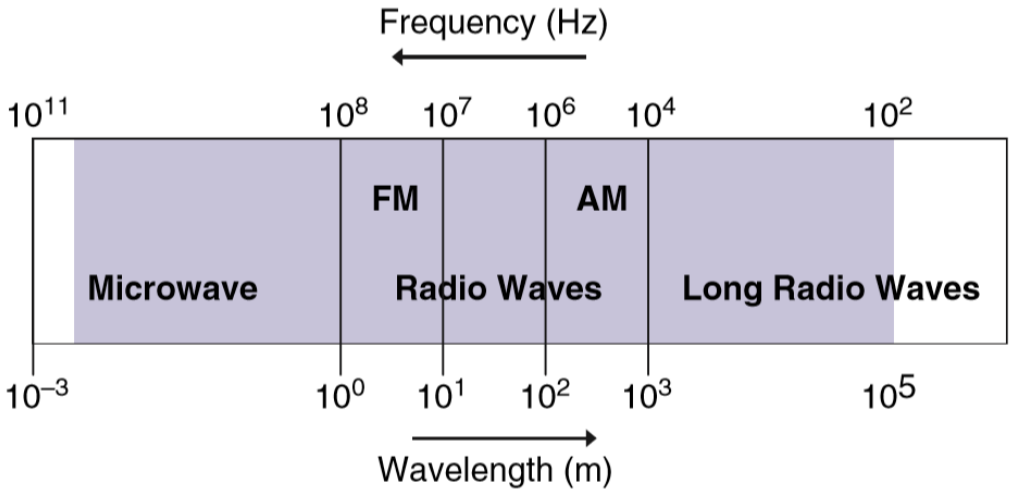

Figure 5. 1: Electromagnetic spectrum, RF-induced ignition risk (Bradby, 2008).

Spark initiated by electromagnetic waves occur if the source of current power is sufficiency large from 50 Watts above as reported in (NAVSEA OP 3565/NAVAIR 16-1-529, 2003) and (British Standards, 2002). Typical transmission sources that could initiate a spark in a flammable atmosphere are shown pictorially in Figure 5.2.

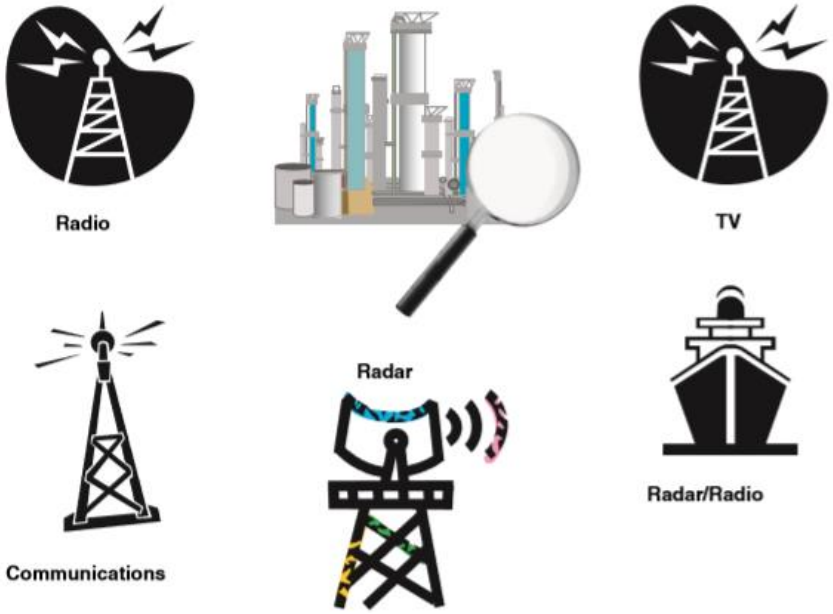

Figure 5. 2: RF transmission sources (Bradby, 2008).

5.2 Traveling Waves

A disturbance that propagates waves is a natural consequence of many physical processes: waves manifest themselves as ripples on the surface of lakes and oceans; mechanical waves modulate stretched strings; sound waves constitute pressure disturbances that travel through media; and electromagnetic waves carry electric and magnetic fields through free space and material media as microwaves, light, and X-rays. Electromagnetic waves in a vacuum travel at a speed of 3×10^8m/s, and sound waves in air travel at a speed of 330 m/s, approximately a million times slower. An essential feature of a propagating wave is that it is a self-sustaining disturbance of the medium through which it travels.

5.3 Maxwell's equation and sources

Maxwell's equations in the phasor domain for a linear isotropic, and homogeneous medium with the charge density ρ_v, current density J, magnetic permeability μ, electric permittivity ε, and conductivity σ, (David and Cheng, 2006), assume the following form:

$$\nabla . \widetilde{\boldsymbol{E}} = \widetilde{\boldsymbol{\rho}}_{\boldsymbol{v}}/\boldsymbol{\varepsilon}. \quad \text{Gauss's law} \tag{5.1a}$$

$$\nabla \times \widetilde{\boldsymbol{E}} = -\boldsymbol{j\omega\mu}\widetilde{\boldsymbol{H}}. \quad \text{Faraday's law} \tag{5.1b}$$

$$\nabla . \ \widetilde{\boldsymbol{H}} = \boldsymbol{0}. \quad \text{Divergence law} \tag{5.1c}$$

$$\nabla \times \widetilde{\boldsymbol{H}} = \tilde{\boldsymbol{J}} + \boldsymbol{j\omega\varepsilon}\widetilde{\boldsymbol{E}}. \quad \text{Ampere's law} \tag{5.1d}$$

5.4 Plane-wave propagation in a medium

Electromagnetic propagation in any medium is described by the homogeneous wave equation where the attenuation constant (α) and the phase velocity (β) are obtain by solving Maxwell's equations Appendix B-1.

Given the properties of the medium (μ, ε, σ), we may determine equations for the attenuation and phase constants as follow:

$$\alpha = \omega \sqrt{\frac{\mu\varepsilon}{2}\left[\sqrt{1 + (\frac{\sigma}{\omega\varepsilon})^2} - 1\right]} \tag{5.2}$$

$$\beta = \omega \sqrt{\frac{\mu\varepsilon}{2}\left[\sqrt{1 + (\frac{\sigma}{\omega\varepsilon})^2} + 1\right]} \tag{5.3}$$

Where ω is the angular frequency (rad/s), μ is the magnetic permeability, which is equal to the free space permeability, ε is the dielectric permittivity in media.

5.5 Non-conductive or lossless medium

The properties of an electromagnetic wave, such as its phase velocity (u_p) and wavelength (λ), depend on the angular frequency and medium's three constitutive parameters; permittivity (ε), permeability (μ) and conductivity (σ). In a non-conducting medium, the wave does not suffer any attenuation as it travels and hence the medium is said to be lossless therefore conductivity is equal to zero ($\sigma = 0$). Therefore equations (5.2) and (5.3) give $\alpha = 0$ and the phase constant is given by:

$$\beta = k = \omega\sqrt{\mu\varepsilon} \tag{5.4}$$

Where k is the wavenumber

5.5.1 lossless medium phase velocity, wavelength and impedance

- phase velocity (u_p)

The phase velocity of a wave is the rate at which the phase of the wave propagates in the medium. It is clear that with equation (5.5) an electromagnetic wave with a phase velocity is slower than the speed of light in the conventional dielectric, the relation between u_p and the phase constant, β is

$$u_p = \frac{\omega}{k} = \frac{\omega}{\omega\sqrt{\mu\varepsilon}} = \frac{1}{\sqrt{\mu\varepsilon}} = \frac{c}{n} \tag{5.5}$$

Where $n = \sqrt{k}$ is the refractive index of the medium.

- wavelength (λ)

$$\lambda = \frac{2\pi}{k} = \frac{2\pi}{\beta} = \frac{u_p}{f} \tag{5.6}$$

- impedance

$$\eta = \frac{\omega\mu}{k} = \frac{\omega\mu}{\omega\sqrt{\mu\varepsilon}} = \sqrt{\frac{\mu}{\varepsilon}} \tag{5.7}$$

5.6 Conductive medium

A conducting medium can be divided into two categories, low-loss dielectric and a good conductor. Low-loss medium is defined as a good but imperfect insulator with nonzero conductivity such that $\sigma/\omega\varepsilon \ll 1$. A good conductor a medium for which $\sigma/\omega\varepsilon \gg 1$. Table 5.1 summarises the propagation parameters in various types of media with attenuation constant α, phase constant β, impedance η, phase velocity u_p, and wavelength λ.

Table 5. 1: Initial, measured thickness and margin error.

Any medium	**Lossless Medium**	**Low-loss Medium**	**Good Conductor**	**units**
$\boldsymbol{\alpha = \omega\sqrt{\frac{\mu\varepsilon}{2}\left[\sqrt{1+(\frac{\sigma}{\omega\varepsilon})^2}-1\right]}}$	0	$\frac{\sigma}{2}\sqrt{\frac{\mu}{\varepsilon}}$	$\sqrt{\pi f\mu\sigma}$	(Np/m)
$\boldsymbol{\beta = \omega\sqrt{\frac{\mu\varepsilon}{2}\left[\sqrt{1+(\frac{\sigma}{\omega\varepsilon})^2}+1\right]}}$	$\omega\sqrt{\mu\varepsilon}$	$\omega\sqrt{\mu\varepsilon}$	$\sqrt{\pi f\mu\sigma}$	(rad/m)
$\boldsymbol{\eta = \sqrt{\frac{\mu}{\varepsilon}}\left(1 - j\frac{\sigma}{\omega\varepsilon}\right)^2}$	$\sqrt{\frac{\mu}{\varepsilon}}$	$\sqrt{\frac{\mu}{\varepsilon}}$	$(1+j)\frac{\alpha}{\sigma}$	(Ω)
$\boldsymbol{u_p = \frac{\omega}{\beta}}$	$1/\sqrt{\mu\varepsilon}$	$1/\sqrt{\mu\varepsilon}$	$\sqrt{4\pi f/\mu\sigma}$	(m/s)
$\boldsymbol{\lambda = 2\pi/\beta = u_p/f}$	u_p/f	u_p/f	u_p/f	(m)

5.7 Overview of three central wireless proven communication in a medium

None of the current research in EM-RF wireless communication is related to data transmission in petrochemical storage tanks and through liquid petroleum products. All research is focussed on underwater wireless communication with three main communication

techniques: Acoustic, Optical and Radio Frequency. Reviewing these communication techniques in an underwater environment gives a better idea of their advantages and limitations. Acoustics is a proven technology for marine sensor applications which offers long transmission ranges of up to 20 km (Dario et al., 2010). It presents specific challenges and limitations (Clementet al., 2012) because acoustic communications are affected by the low speed of sound underwater and time-varying multipath propagation. Together, these factors result in a communication channel of poor quality and high latency. While optical wave technology has recently stimulated several attempts at research in underwater optical communications, it presents some challenges in realisation (Kumar, 2016). Optical waves only deliver excellent performance in clear water and require tight alignment of the node. Electromagnetic waves suffer from strong attenuation when propagating in water and as a result have the limitation of transmission range. However, they have some valuable features that enable flexible deployment of an underwater vehicle. Table 5.2 outlines the three major underwater communication technologies with benefits and limitations in water which will be more or less similar to petroleum or vegetable oil medium considered in this chapter.

Table 5. 2: Evaluation of different types of communication.

	Benefits	**Limitations**
RF	• Crosses air/water/seabed boundaries easily Prefers shallow water • Unaffected by turbidity, salinity, and pressure gradients • Works in non-line-of-sight; unaffected by sediments and aeration • Immune to acoustic noise • High bandwidths (up to 100 Mb/s) at the very close range • The possibility of converting communications, with a low probability of interception, due To the low power spectral density. • Simplicity in implementation, low cost of devices. Propagation through solid materials, due to the presence of energy at different frequencies.	• Susceptible to EMI • Limited range through water
Acoustic	• Proven technology • Range: up to 20 km	• Strong reflections and attenuation when transmitting through the water/air boundary • Poor performance in shallow water • Adversely affected by turbidity, ambient noise, salinity, and pressure gradients • Limited bandwidth (0 b/s to 20 kb/s) • Impact on marine life
Optical	• Ultra-high bandwidth: gigabits per second • Low cost	• Does not cross the water/air boundary easily • Susceptible to turbidity, particles, and marine fouling • Needs line-of-sight • Requires tight alignment of nodes • Very short range

Electromagnetic waves propagate better in lossless medium (petroleum product, vegetable oil, etc.) than low loss medium (water or seawater, etc.). From Table 5.2 it is clear that acoustic and optical technologies, radio frequency-EM have some distinct advantages that make them suitable for communication environments.

The w environment inside a petrochemical storage tank can make better use of radio frequency over acoustic and optical technologies because it can propagate in petroleum medium without significant attenuation and has the advantages stated in Table 5.2 over water as well as lossless mediums. Acoustic and optical waves cannot perform a smooth transition through the air to the medium interface or from the medium to the air interface and are poor in shallow water communication. Electromagnetic wave transmissions are tolerant to turbulence and EMW can cross from one medium to another easily following the path of least resistance. EMW can work in dirty conditions, while optical waves are susceptible to particles. However, EMW propagation in a petroleum environment is limited due to safety regulations.

5.8 Hazard of EM propagating in flammable atmospheres

Hazardous area classification becomes an important factor when using EM-radio frequency in the area around a process or activity where a flammable atmosphere exists section 1.3 gives details of existing different regions in a petroleum storage tank where gases or vapours are likely to be present.

5.8.1 Thermal radiation and EM radiation as a form of heat

The basic structure of matter involves charged particles bound together in many ways. When electromagnetic radiation is incident on a medium, it causes the charged particles to oscillate and gain energy. Any electromagnetic radiation can heat a material when it is absorbed. EMW produced by radio-frequency transmitters (e.g. radio, television and radar) will induce electric currents and voltages in any conducting structure. The magnitude of the induced voltages and current depends upon the shape and size of the structure relative to the wavelength of the transmitted signal and on the strength of the electromagnetic field.

5.8.2 Electromagnetic power radiation to petroleum tank

The probability of ignition of fuel vapours induced by radio frequency is small. The following conditions must occur simultaneously for the fire to take place: a flammable fuel-air mixture must be present within the range of the induced arcing, the arc must contain a sufficient amount of energy to cause ignition, and the gap across which the arc occurs must be an absolute

minimum distance. The minimum arc energy necessary to produce fire has been determined. The tests were conducted under laboratory conditions (NAVSEA OP 3565/NAVAIR 16-1-529, 2003) and it was found that the apparent power required to ignite gasoline and fuel in a explosive vapour test device was 50 Watts or more and the spark gap needed in term of metal to metal contact was 0.5 millimetre (0.02 inch). Similarly, British Standards (BSI PD CLC/TR 50427, 2004) state that the output power of the transmitter might need to be about 50 to 100 Watts to provide sufficient signal to the plant. Figure 5.3 illustrates the process of ignition of EM wave in flammable vapour atmospheres:

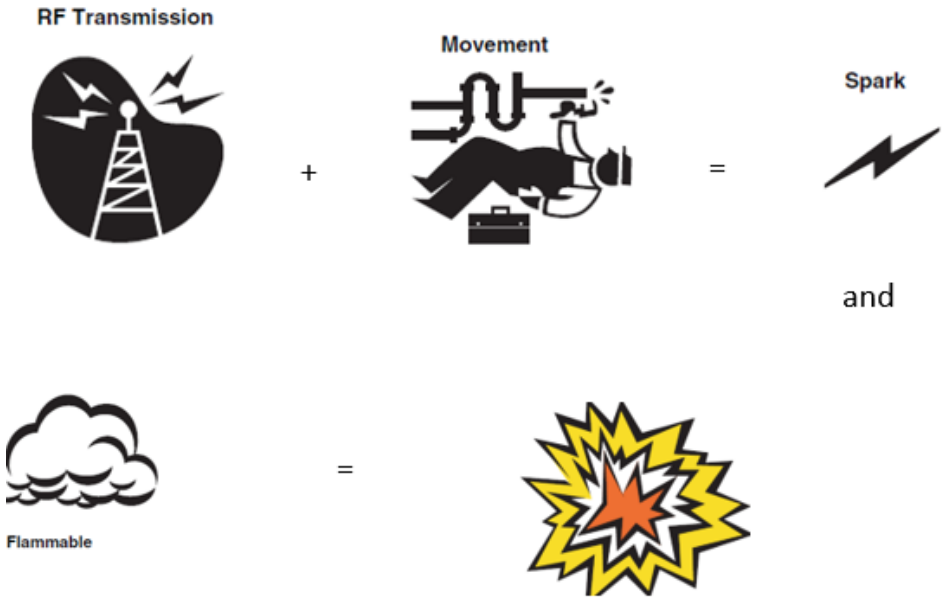

Figure 5. 3: RF transmission sources (Bradby, 2008).

The spark in the flammable atmosphere occurs when the power or energy in a spark exceeds the specific threshold value, which depends on both the nature and concentration of the combustible gas or vapour. (BSI PD CL/TR 50427, 2004) reports the threshold values of RF power which if exceeded will cause ignition, for continuous transmissions and for pulsed transmissions whose pulse duration exceed the thermal initiation time (e.g. pulsed radar). Table 5.3 shows flammable gases and vapours grouping according to their ignition time.

Table 5. 3: Radio-frequency power thresholds.

Gas group	Representation gas	Threshold power (W)	Thermal initiation time (averaging period) (μs)
I	Methane	6 for long narrow structure structures, e.g. cranes, 8 for all other structures	200
IIA	Propane	6	100
IIB	Ethylene	3.5	80
IIC	Hydrogen	2	20

5.8.3 Dielectric properties of the medium

Dielectrics or insulators are material whose dominant charges in atoms and molecules are bound by negative and positive charges that are held in place by atomic and molecular forces; they are not free to travel. Therefore, ideal dielectrics do not contain any free charges (such as in conductors), and their atoms and molecules are microscopically neutral. When external fields are applied, these bound negative and positive charges do not move to the surface of the material as would be the cause for conductors, but the centroids can shift slightly in positions relative to each other, thus creating numerous electric dipoles. Figure 5.5 illustrates the range of dielectric (insulators) and electrical conductors and semiconductors material properties.

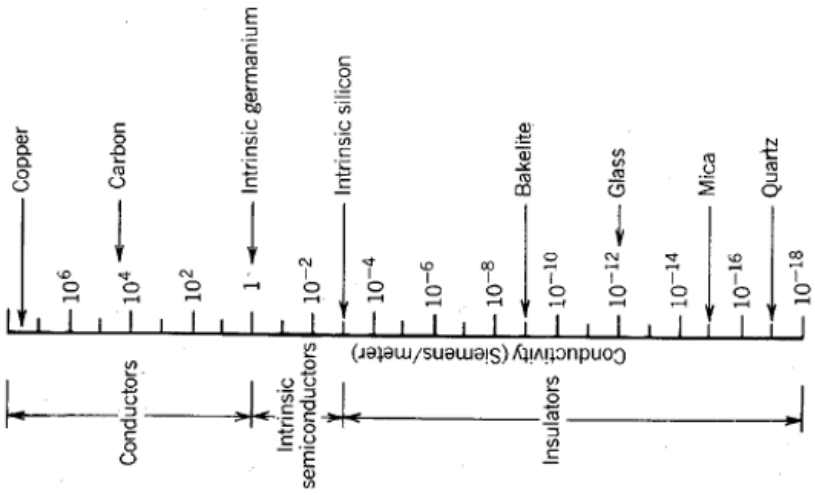

Figure 5. 4: Range of insulators, semiconductors, and conductors (David, 2006).

From the above conductivity of material or medium classification, petroleum products and

vegetable oil are in the range of insulator and water is in the semiconductor range, Table 5.4 shows their conductivity.

Table 5. 4: Medium conductivity.

Medium	**Crude oil**	**Gasoline, gas**	**Diesel oil, Fuel**	**Jet fuel**	**Kerosene**	**Vegetable oil**	**water**
Conductivity $\boldsymbol{\sigma}$	1×10^{-10}	2.5 $\times 10^{-11}$	5 $\times 10^{-11}$	5 $\times 10^{-11}$	5 $\times 10^{-11}$	0	0.01

5.9 Electromagnetic waves in dielectric medium and water

The best media for electromagnetic waves propagation is an insulator, where the conductivity is zero ($\sigma = 0$ S/m). Those media are said to be lossless, because electromagnetic waves are not attenuated. Conductivity of a medium has direct relationships to the propagation of the electromagnetic wave, this means that with the increase in conductivity of the material, attenuation will be increased, and the EMW will travel less distance. The propagation of an electromagnetic wave through matter is governed by three properties of the material: conductivity, permeability and permittivity or dielectric constant. These parameters change with the type of the medium and the electrical conductivity value associated with the medium often varies, thus the wave propagation speed and absorption coefficient, which are directly related to the working frequency, also vary. Table 5.5 lists the three main EM properties for certain medium.

Table 5. 5: Medium conductivity, dielectric and permeability.

Medium	**Crude oil**	**Gasoline, gas**	**Diesel oil, Fuel**	**Jet fuel**	**Kerosene**	**Vegetable oil**	**water**
Conductivity $\boldsymbol{\sigma}$	1 $\times 10^{-10}$	2.5 $\times 10^{-11}$	5 $\times 10^{-11}$	5 $\times 10^{-11}$	5 $\times 10^{-11}$	0	0.01
Dielectric or Relative permittivity $\boldsymbol{\varepsilon}$	$2-3$	2.0	2.1	1.8	1.7	3.1	81
Permeability $\boldsymbol{\mu}$	1.25 $\times 10^{-6}$	1.25 $\times 10^{-6}$	1.256 $\times 10^{-6}$	1.25 $\times 10^{-6}$	1.25 $\times 10^{-6}$	1.25 $\times 10^{-6}$	1.25$\times$ 10^{-6}

The magnetic permeability is the ability of a medium to store magnetic fields. The mediums listed in Table 5.5 are non-magnetic and their relative permeability is the same. Therefore, the permeability of the medium does not affect EM propagation. The magnetic permeability can be calculated with equation (5.8). Table 5.5 shows clearly that petroleum crude oil and vegetable oil dielectric almost same and their conductivity is zero, therefore they could be

considered as insulators or dielectrics (Oleksandr, 2012).

$$\mu = \mu_0(1 + \chi_v) \tag{5.8}$$

Where χ_v is volume magnetic susceptibility.

Independent of the working frequency of the transmitted signal, the propagation speed of the signal and absorption coefficient can be calculated respectively with Equation (5.9), (5.11)

$$\mathcal{C} \approx \frac{1}{\sqrt{(1+\chi_e)\varepsilon_o \times \mu_r \times \mu_o}} \tag{5.9}$$

Where: χ_e is the electric susceptibility of the medium could be calculated with equation (5.10), ε_o the electric permittivity, μ_r is relative magnetic permeability of medium and μ_o is magnetic permeability of free space.

$$\chi_e = \varepsilon_r - 1 \tag{5.10}$$

$$\alpha \approx \frac{\sigma}{2}\sqrt{\frac{\mu_r \times \mu_o}{(1+\chi_e)\varepsilon_o}} \tag{5.11}$$

Table 5. 6 shows that Electromagnetic waves propagation through petroleum and vegetable oil medium does not absorb, and propagation speed is reduced by the reflection coefficient compared with propagation in air.

Table 5. 6: Propagation speed and absorption coefficient of matter.

Medium	**Crude Oil**	**Gasoline, gas**	**Diesel oil, Fuel**	**Jet fuel**	**Kerosene**	**Vegetable oil**
Propagation speed (m/s)	1.73×10^8	2.12×10^8	2.07×10^8	2.24×10^8	2.30×10^8	1.70×10^8
Absorption coefficient	5.34×10^{-9}	3.32×10^{-9}	$6.50 \times 10^{-}$	7.01×10^{-9}	7.22×10^{-9}	0

5.9.1 Electromagnetic attenuation through dielectric or insulator medium

Plane waves propagate through dielectrics with phase velocity (equation 5.5) that is independent of the frequency of the waves (with the assumption that the permeability and permittivity are constants). However, in reality, the Phase velocity of an EMW through dielectric does depend on the frequency of the wave, this effect is known as dispersion and is readily observed in a simple experiment. For example, the "splitting" of white light by a prism shows that the refractive index increases with increasing frequency. So, the purple and blue light travels more slowly than red light through glass and is reflected more strongly by a prism.

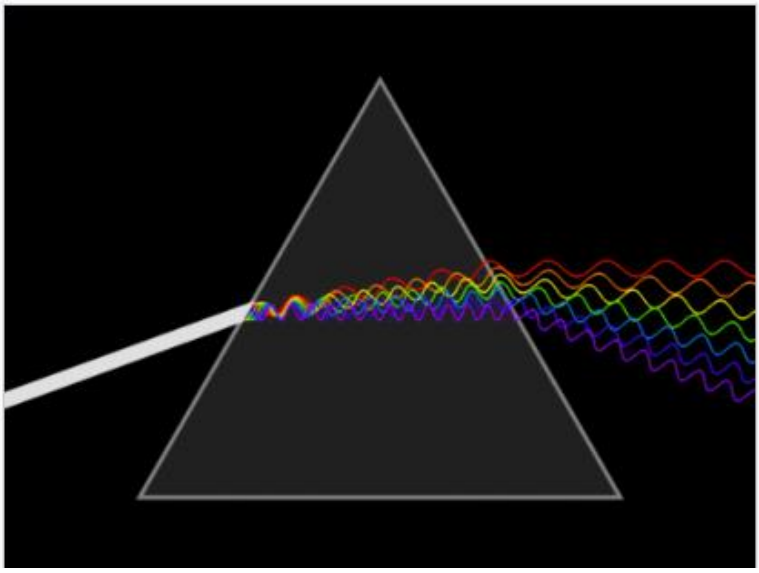

Figure 5. 5: Triangular prism, dispersing light (Lucas, 2007).

The speed of light changes as it moves from air into the glass of the prism; this speed change causes the light to be refracted and to enter the new medium at a different angle. The effect of dispersion of EMW in the dielectric medium is associated with absorption of the energy of the wave.

5.9.2 Electromagnetic wave absorption and dispersion through petroleum products and other medium

The electromagnetic wave absorption and dispersion for wave propagation through medium could be calculated using equations (5.2) and (5.12). Table 5.7 shows the absorption and dispersion of EM waves with given petroleum medium, air, seawater and vegetable oil.

$$k_d = \omega\sqrt{\mu\varepsilon_0 k} \tag{5.12}$$

Where k is dielectric constant.

Table 5. 7: EMW absorption and dispersion in a given medium.

Frequency	Medium	Air	Seawater	Vegetable oil	Crude oil	Gasoline	kerosene
433 MHz	Absorption (N/p)	0	0.06	0	0	0	0
	Dispersion (rad/s)	9.07	81.66	15.97	13.15	12.83	11.83
300 MHz	Absorption (N/p)	0	0.059	0	0	0	0
	Dispersion (rad/s)	6.27	56.22	11.08	9.10	8.89	8.20
250 MHz	Absorption (N/p)	0	0.0598	0	0	0	0
	Dispersion (rad/s)	5.24	47.85	9.22	7.59	7.40	6.83
200 MHz	Absorption (N/p)	0	0.045	0	0	0	0
	Dispersion (rad/s)	4.19	37.71	7.38	6.63	6.63	5.46

The table shows that the dispersion of the EMW varies with the frequency, a higher frequency means strong scattering of the wave and less travel distance. However, the absorption of EMW in Air, Vegetable oil, Crude oil, Gasoline and Kerosene is zero, therefore, there is no resistance to EMW propagation due to their very low electrical properties. Seawater on the other hand absorbs EMW which decreases as the frequency decreases. The dielectric constant is the most critical factor that affects the propagation of petroleum. Their properties are a function of temperature, so the increase in temperature leads to an increase of attenuation during communication in petroleum. Another factor that could affect the signal depends on water concentration in the petroleum product. Increasing water content will increase power loss. The selection of the optimal RF frequency is an essential factor for realising robot ultrasonic sensor data transfer or robot localisation in a storage tank Selecting higher frequency than the optimal will increase the attenuation due to wave absorption and limit the distance of propagation.

5.9.3 Electromagnetic waves propagation path loss in oil

The signal propagation in petroleum medium depends on the path loss. The received power as a function of the transmitted signal, path loss and antenna gain at transmitter and receiver are given by Friis as shown in (Stube, 1996):

$$P_{rec}(dBm) = P_i(dBm) + G_t\,(dB) + G_r(dB) - L_{path\,loss}\,(dB) \tag{5.13}$$

Where P_i is the transmit power, G_t and G_r are the gains of the transmitter and receiver antenna and $L_{path\,loss}$ is the path loss in the medium. The path loss is written as follow:

$$L_{path\ loss}\ (dB) = L_0(dB) + L_w(dB) + L_{att}(dB) \quad (5.14)$$

Where the path loss in air denoted L_0 is given by:

$$L_0(dB) = 20\log(\frac{4\pi df}{C}) \quad (5.15)$$

Where d is the distance between the transmitter and the receiver in meter, f is the operating frequency in Hertz and C is the velocity of light in air expressed in meter/second. The path loss due to medium change denoted L_w is given by (Elleithy et al 2012):

$$L_w(dB) = 20\log(\frac{\lambda_0}{\lambda}) \quad (5.16)$$

Where λ_0 is the signal wavelength in the air obtained with ($\lambda_0 = C/f$), λ is the wave factor and given by ($\lambda = 2\pi/\beta$), β is the phase constant calculated from equation (5.3). The path loss (L_{att}) due to attenuation in the medium is given by:

$$L_{att}(dB) = 10loge^{-2\alpha d} \quad (5.17)$$

Where α is the attenuation constant.

5.9.4 Calculation of propagation path loss in petroleum and vegetable oil

The path loss is a significant component in analysis and design a telecommunication system. It is the reduction in the power density of the electromagnetic wave as it propagates through the medium. The path loss is calculated using equation (5.14), the medium is known as a dielectric. From equation (5.2), the attenuation constant $\alpha = 0$, therefore equation (5.14) becomes:

$$L_{path\ loss}\ (dB) = L_0(dB) + L_w(dB) \quad (5.18)$$

The effect of frequency on the path loss at a distance of 1 m between the transmitter and receiver antenna is illustrated in Figure 5.6, which shows that as the frequency increases the path loss also increases. Path loss increased in vegetable oil compared to gasoline and kerosene fuel due to its high dielectric constant.

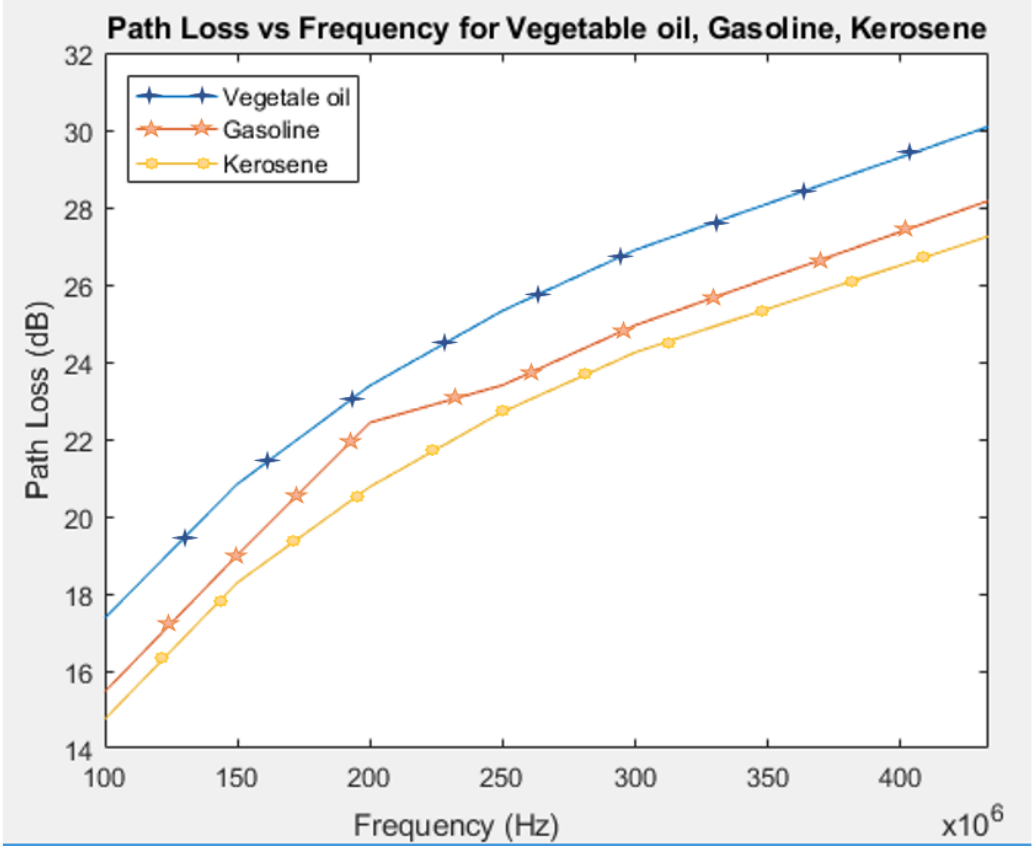

Figure 5. 6: Path Loss (dB) as a function of frequency (MHz) for Vegetable oil, Gasoline and Kerosene.

5.10 Simulation of electromagnetic wave propagation in different mediums

5.10.1 Medium characteristics

Communication in oil needs a very efficient antenna for wireless data communication. This type of antenna must meet some requirements to overcome the high value of path loss when propagating in such a medium. Therefore, the selected antenna must have very low transmission power (below the threshold stated in Table 5.3). The frequencies used in this work were 200 MHz, 300 MHz, and 433 MHz to avoid high absorption. Path loss due to high frequency results in high attenuation when propagating in petroleum medium and the antenna has to be small in dimension so that it can be fitted into the NDTBOT for Ultrasonic data transmission and possibly for its localisation in the tank. Electromagnetic wave propagation through the medium is governed by three properties of the material known as conductivity, permeability and permittivity. These will be used for medium set up in the simulation. The mediums used in this simulation are petroleum, water and vegetable oil.

5.10.2 Dipole antenna

The antenna used in this simulation was a Dipole Antenna with a set of three different frequencies 200 MHz, 300 MHz and 433MHz. The selection of those frequencies in the simulation were related to Table 5.7 in order to observe the dispersion and attenuation of the wave when propagating in that medium. The dipole antenna is simple to design, very effective for a wide range of communication needs, and has been used in numerous applications including underwater applications (Inacio et al., 2016). It is made up of two identical conductive elements or rods, which are fed at the centre by a balanced transmission line, which is equal to opposite flowing currents (Milligan, 2005). Dipole antenna comes in several types and shapes, which includes half-wave dipole, folded dipole, bow-tie, V-shaped and other configurations (Balanis, 2005).

The software used in this design simulation was the popular commercial electromagnetic software FEKO (Altair, 2017) . A dipole antenna was designed with the frequency specification using CADFEKO, Figure 5.7. To simulate electromagnetic propagation in the medium, a box cube with a size of 5 x 5 x 5 meters was used to represent the medium in which the electromagnetic wave will propagate, see Figure 5.7. The simulation involved three different types of the medium based on Table 5.5 such as diesel fuel, kerosene and vegetable oil. The antenna was placed in air at 3 meters away from the medium represented by the box cube. The three meter placement away from the medium represents zone 2 in a petroleum tank environment.

In Figure 5.7, the transmission was done through the air to the medium. The simulation environment was set for all electric fields to be tangential to the Y = 0 plane, and normal to the Z = 0 plane and creation of horizontal far field requested to be ($0 \leq \phi \leq 360^{o}$ with $\theta \leq 90^{o}$ and $\phi = 2^{o}$ increments). In this particular simulation the aim was to observe the antenna directivity in the far field radiation in order to observe the maximum concentration of radio frequency energy in a particular direction and also the wave attenuation.

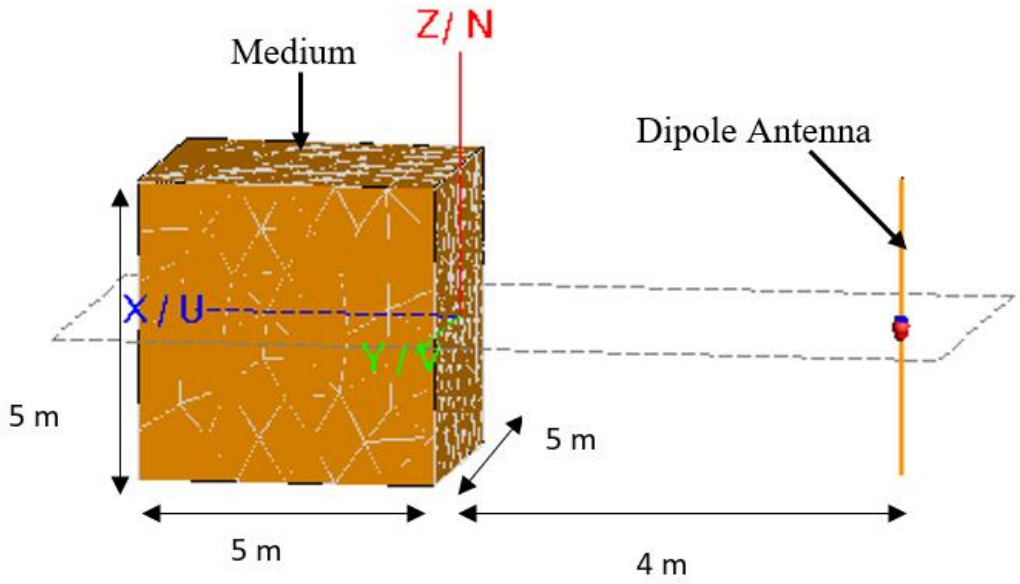

Figure 5. 7: A 3D view of the dipole with a cube (medium) model.

5.10.3 Far field radiation

The directivity of an antenna is a measure of how much it concentrates power in a given direction. The directivity of the antenna represents the additional power collected or transmitted in a certain direction relative to an isotropic radiator. Mathematically, the directivity of an antenna is defined as:

$$\mathbb{D}(\theta, \phi) = \frac{U_m}{U_0} \tag{5.19}$$

Where U_0 is the average radiation intensity that produced by the antenna, $U_m = U(\theta, \phi)$ is the maximum radiation intensity produced by the antenna at some angle (θ, ϕ). The average radiation is expressed in term of radiated power density as follow:

$$U_0 = \frac{W_{rad}}{4\pi} \tag{5.20}$$

Directivity can also be re-written in terms of power densities and radiated power as follow;

$$\mathbb{D}(\theta, \phi) = \frac{4\pi U(\theta,\phi)}{P_{rad}} \tag{5.21}$$

The horizontal plane far field radiation pattern of the dipole antenna propagation through free space with no obstacle or medium in front of the antenna was simulated with different frequencies as shown in Figure 5.8. The plot shows a number of equal lobes and maximum gain is distributed in all direction as the requested horizontal plane far field request ($0 \leq \phi \leq 360^o$ with $\theta \leq 90^o$ and $\phi = 2^o$ increments.

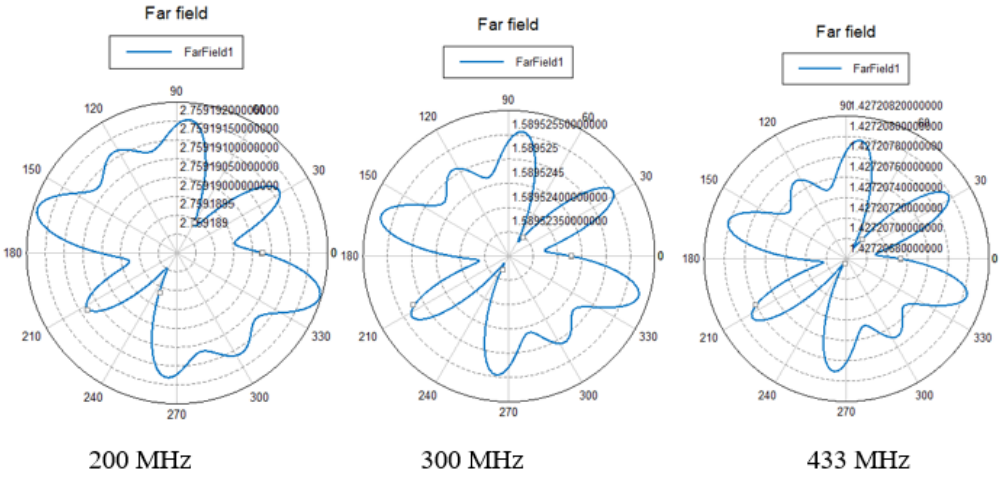

200 MHz 300 MHz 433 MHz

Figure 5. 8: free space far field radiation directivity.

The polar plot for far field radiation of the electromagnetic wave in the three medium vegetable oil, diesel fuel and kerosene fuel is shown in Figure 5. 9. The radiation pattern varies with the medium and the frequency. In general observation, attenuation of the electromagnetic wave in each of the select petroleum medium and vegetable oil is compared to the free space far field. The attenuation increased with increase of the radio frequency and with reduction of the transmitted energy. The attenuation of the electromagnetic wave due to the dispersion of the wave when propagated through the medium was calculated earlier. Another factor affecting the electromagnetic wave is reflection which is the sudden change in the direction of the propagation of the wave that strikes the boundary air and petroleum medium or vegetable oil. The speed of the electromagnetic wave in free space is $3x10^8$ m/s and reduces with the medium properties such as permeability, permittivity and conductivity of the medium it penetrated. The main properties of the media are related to the electromagnetic propagation and Table 5.6 states the propagation speed of the EMW in vegetable oil and petroleum which vary with the index of refraction of the medium.

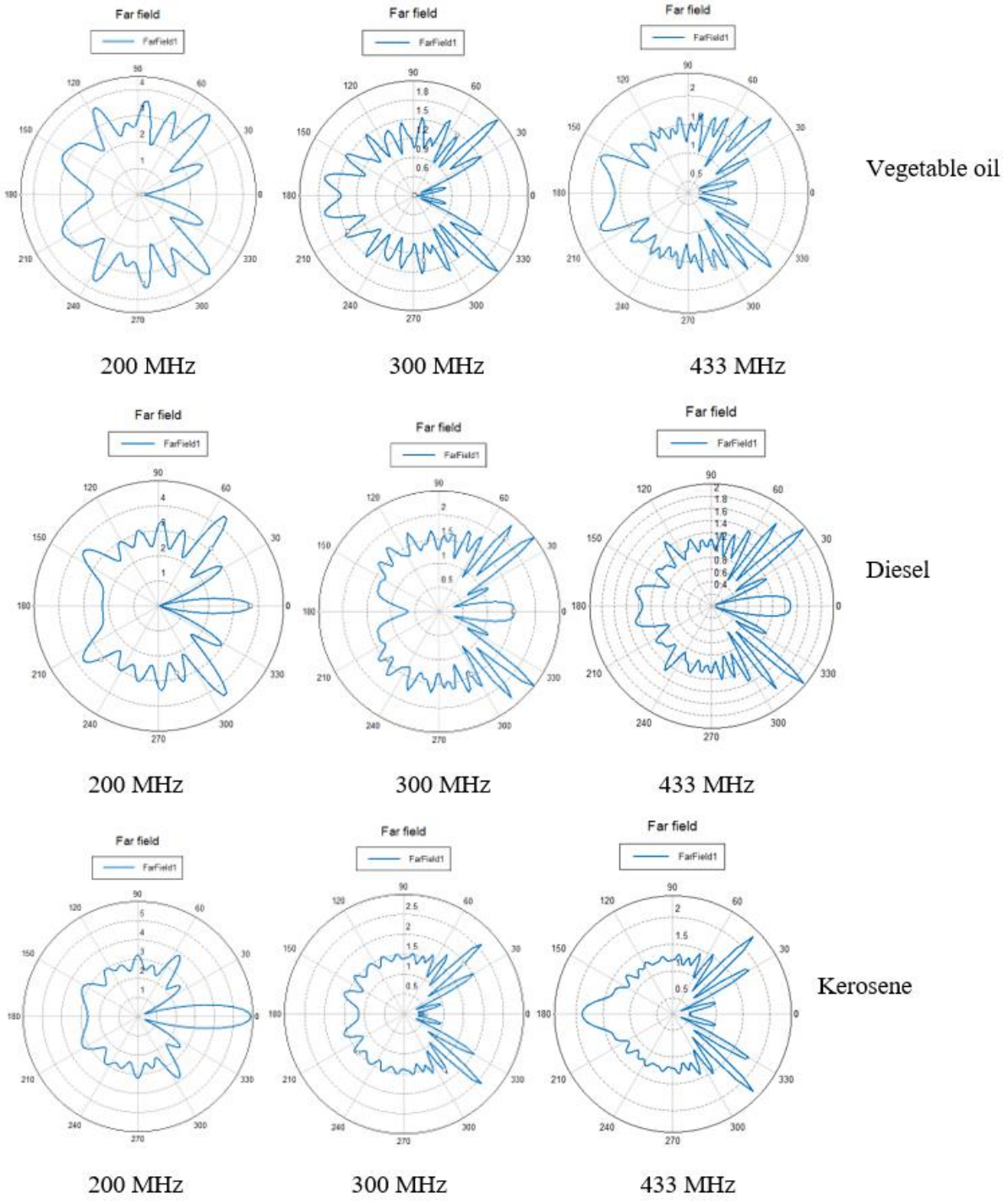

Figure 5. 9: Medium far field radiation directivity Phi (0.00 to 360.00).

The electromagnetic surface current distributions induced by a dipole antenna on selected petroleum medium with different frequencies are displayed (contact EMW at LHS and RHS internal propagation) in Figures 5.10, 5.11 and 5.12 respectively with vegetable oil, diesel fuel and kerosene fuel. The surface current distribution induced by a dipole antenna reduced in intensity with increase of the frequency. The simulation shows that the surface current distribution extends over all the medium surface. The distribution of the current is affected by the interface between air-medium however the distribution of the current shows that a receiver antenna placed inside the medium will receive the transmitted signal.

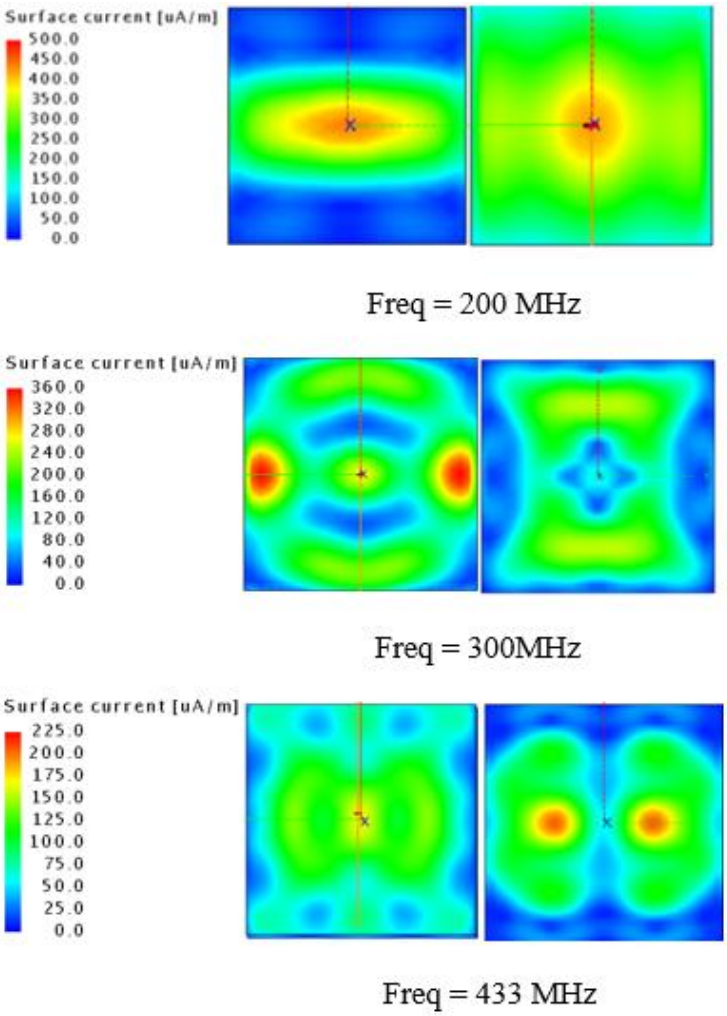

Figure 5. 10: Surface current distribution in vegetable oil medium.

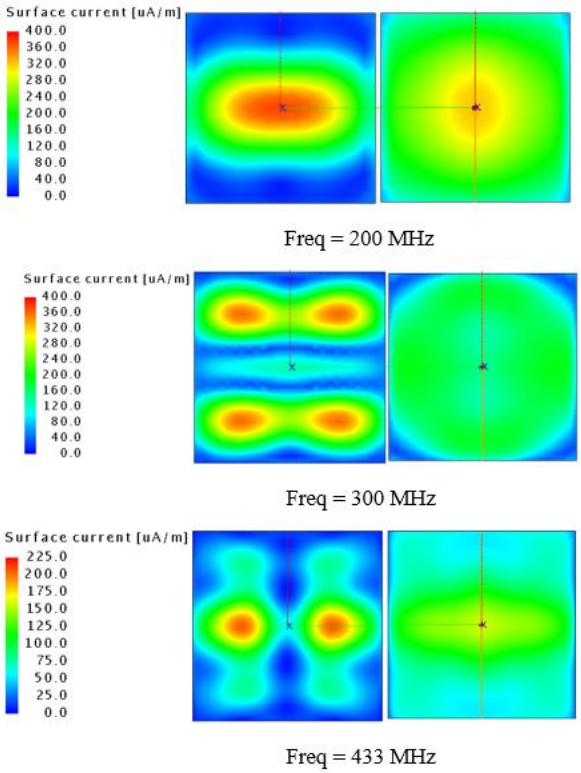

Figure 5. 11: Surface current distribution in diesel fuel medium.

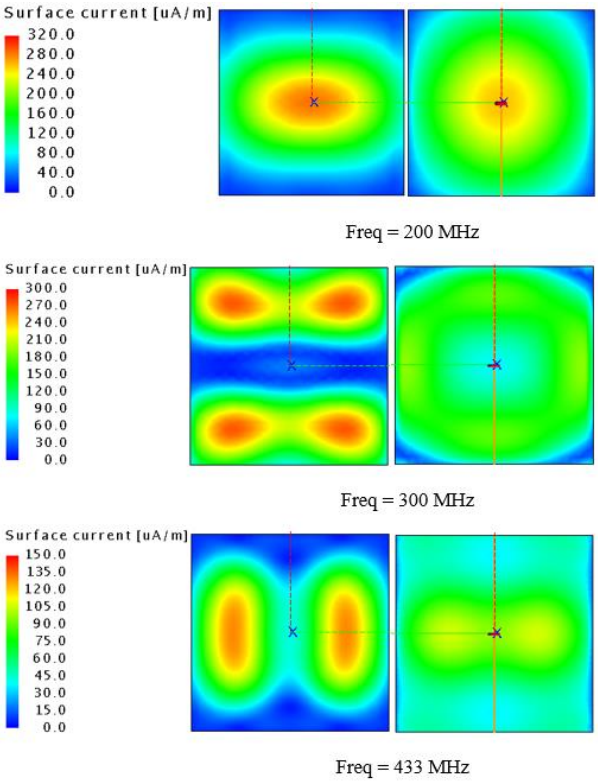

Figure 5. 12: Surface current distribution in kerosene fuel medium.

5.10.4 Time domain electric field

The time domain simulation was setup with the LoRa611Pro wireless transceiver data transmission module properties. LoRa611Pro is a commercial radio frequency module for data transmission. In order to observe whether attenuation of the electromagnetic wave crossing the steel wall of the storage tank will be detected at the receiver the electric field, signals were studied with different types of medium such as vegetable oil and petroleum (diesel fuel and kerosene). The simulation medium was selected with Table 5.5 e.g. vegetable oil permittivity or dielectric constant is in range of crude oil same for kerosene and jet fuel with a tinny difference. Real dimension of petrochemical storage tank was setup with an appropriate tank wall thickness in this simulation. Figure 5.13 shows a 2D drawing of the storage tank, two wireless transceivers were used, one of the transceivers located at 25 meters submerged in steel tank with petroleum medium or vegetable oil and the other transceiver located at 3 meters from the tank wall in the air. The thickness of the steel tank wall was setup to be 6.35 mm and the size of the tank was 50 meters in diameter. The tank properties were selected using the American Petroleum Institute standard (API 650 section 5.6.1.1) which specifies the range of petrochemical storage tank sizes and defines the minimum wall thickness required to avoid tank stress.

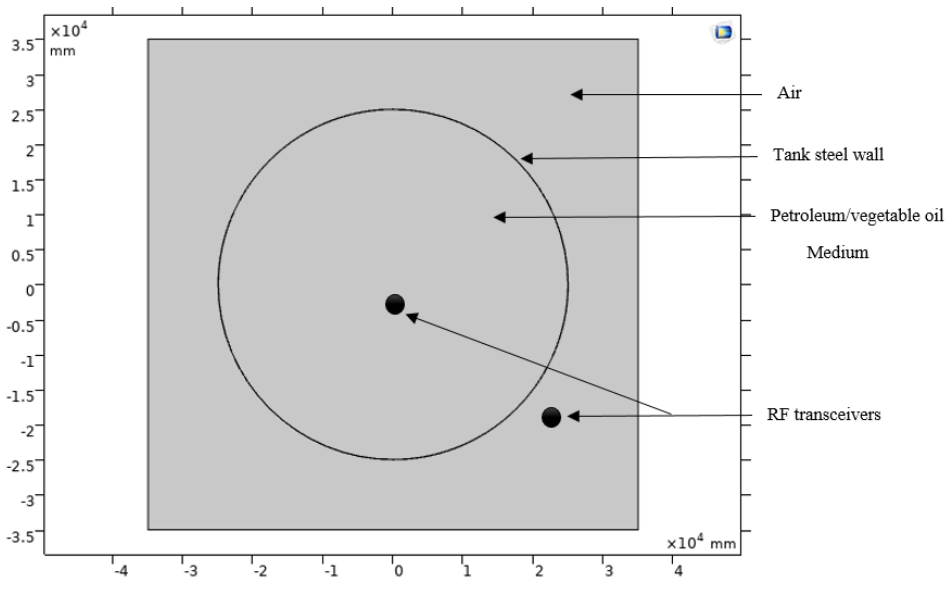

Figure 5. 13: 2D storage tank setup with two transceivers antenna.

Figure 5. 14 shows two sets of simulation in the air, with propagation of electromagnetic wave in the air with no steel wall between both transceivers and another set with a steel. Propagation in the air with no steel wall shows that the maximum electric field strength is 0.0024 V/m at about 35 seconds compared to propagation in the air with steel wall where the maximum electric field strength was 0.85 $x10^{-3}$ at about 46 seconds. The presence of the steel wall attenuates the electromagnetic wave which is evidenced by the reduction in the electric field strength.

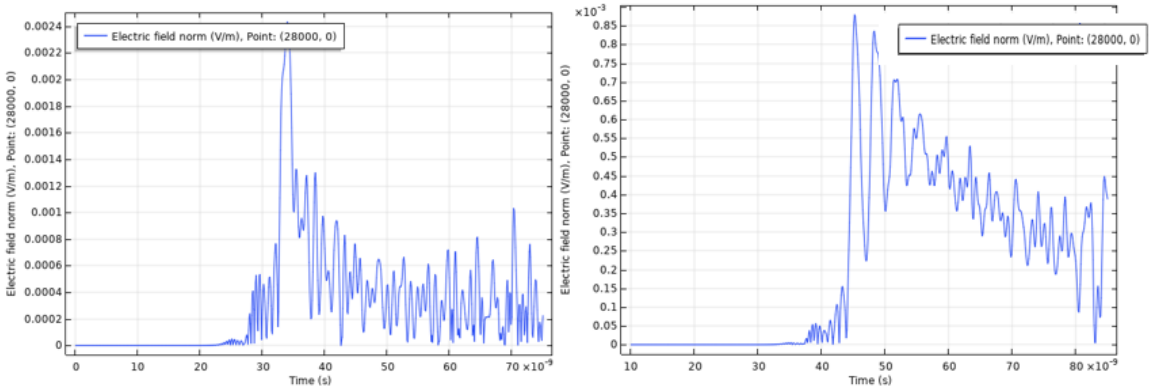

Just propagation in air no steel wall

Propagation in air with steel wall

Figure 5. 14: Electric field propagation between two 433 MHz transceivers antenna beacon in air.

The simulation results for the electric field strength for vegetable oil, diesel fuel and kerosene medium. The electric field strength was tested with electromagnetic wave transmission in both directions from air to the medium and medium to air through the steel tank wall. Electromagnetic wave propagation through vegetable oil as medium (Figure 5. 15) has average electric field strength in both direction of 5.1 $x10^{-4}$ V/m compared to electric field strength in the air with steel wall stated in Figure 5. 14 which was 0.85 $x10^{-3}$ V/m. Similarly, the average of the electric field strength (Figure 5. 16) of the electromagnetic wave propagation in diesel fuel in both directions is 6.3 $x10^{-4}$ V/m compared to Figure 5. 14 where the electromagnetic wave propagation in the air with steel tank wall the electric field strength was 0.85 $x10^{-3}$ V/m. Finally, the average electric field strength (Figure 5. 17) in kerosene fuel medium is 6.95 $x10^{-4}$ V/m compared to 0.85 $x10^{-3}$ V/m for electric field strength in the air with steel tank wall in Figure 5. 14. The simulation shows the time that it takes the electromagnetic wave to get to the maximum electric field strength. The electromagnetic wave travels faster in the air than diesel fuel, kerosene fuel and vegetable oil medium. The simulation conforms to the calculation of propagation speed and absorption coefficient of matter in Table 5.6.

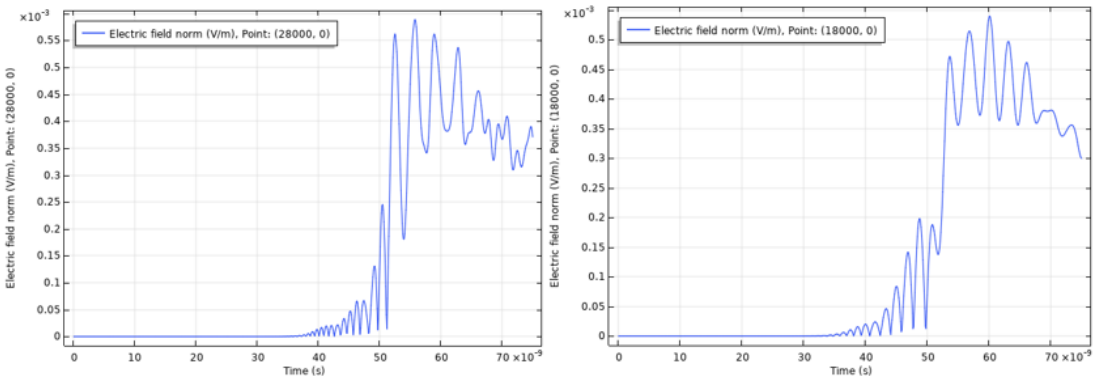

Receiver beacon located inside the tank Receiver beacon located outside the tank

Figure 5. 15: Electric field propagation between two 433 MHz transceivers antenna beacon in vegetable oil used as a medium.

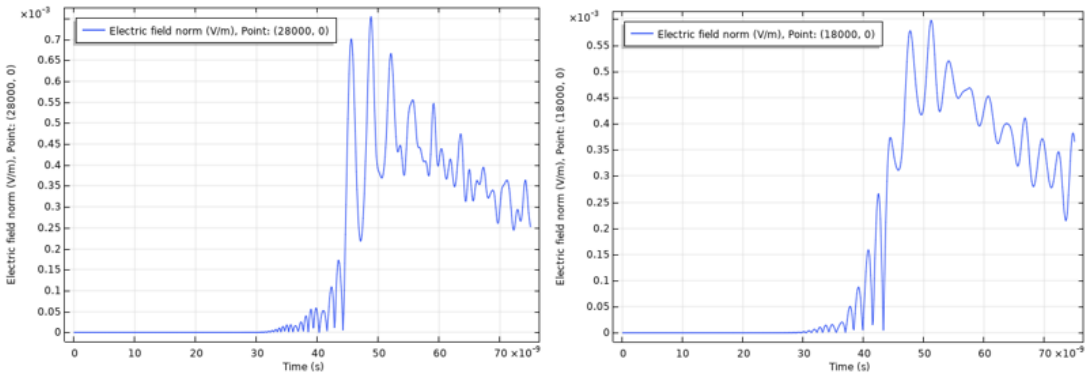

Receiver beacon located inside the tank Receiver beacon located outside the tank

Figure 5. 16: Electric field propagation between two 433 MHz transceivers antenna beacon in diesel fuel used as a medium.

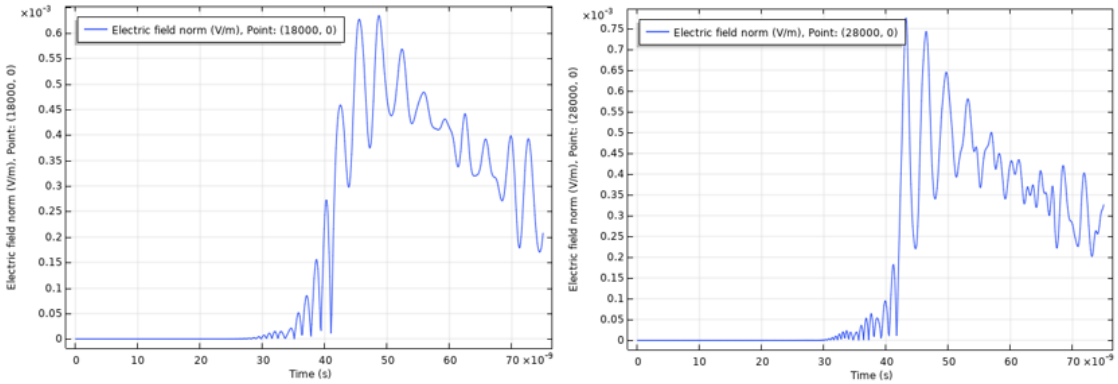

Receiver beacon located inside the tank Receiver beacon located outside the tank

Figure 5. 17: Electric field propagation between two 433 MHz transceivers antenna beacon in kerosene fuel used as a medium.

5.11 Chapter summary

This chapter presented a simulation and of radio frequency wireless communication through oil medium and through oil/steel/air interfaces. The simulation of electromagnetic wave radiation through petroleum products and vegetable oil has shown some attenuation of the wave through study of directivity patterns and surface currents. The time domain simulation shows faster propagation in petroleum medium than vegetable oil medium. The simulations and calculations have shown that the electromagnetic wave travels at lower speed in vegetable oil compared to other petroleum medium. Therefore, radio frequency could propagate better in petroleum products than vegetable oil with less dispersion and path loss.

Chapter 6

Results and analysis

The objective is to be able to propagate very low power wireless radio frequency signals which complies with regulations and standards in the petroleum storage tank. The internal structure of a petrochemical storage tank makes a robot with umbilical cable difficult to move inside the tank for corrosion inspection and NDT data collection. Another aspect is related to the robot localisation for online inspection which has not been investigated in this work but offers the opportunity for further work. The reason for using wireless RF communication was due to the advantages presented by radio frequency such as faster data transmission, low cost implementation over other communication media such as optical and acoustic shown. In this experiment, non-conducting vegetable oil is used to evaluate the data transmission from air to medium and medium to air. Vegetable oil medium was used due its dielectric property (Du and Li, 2017) and (Paranjpe and Deshpande, 1935) and to its similar properties with petroleum medium as stated in Table 5.5.

6.1 Electromagnetic wave propagation in vegetable oil

6.1.1 Radio frequency remote-control transmission

The investigation was done using two experiments. The first was set up with a four channel RF remote-control transmitter and receiver system operating with low voltage (5volts). The aim was to drive a DC motor via the RF wireless link. Figure 6.1 shows the RF transmitter, receiver and DC motor connected to a plastic propeller blade set up.

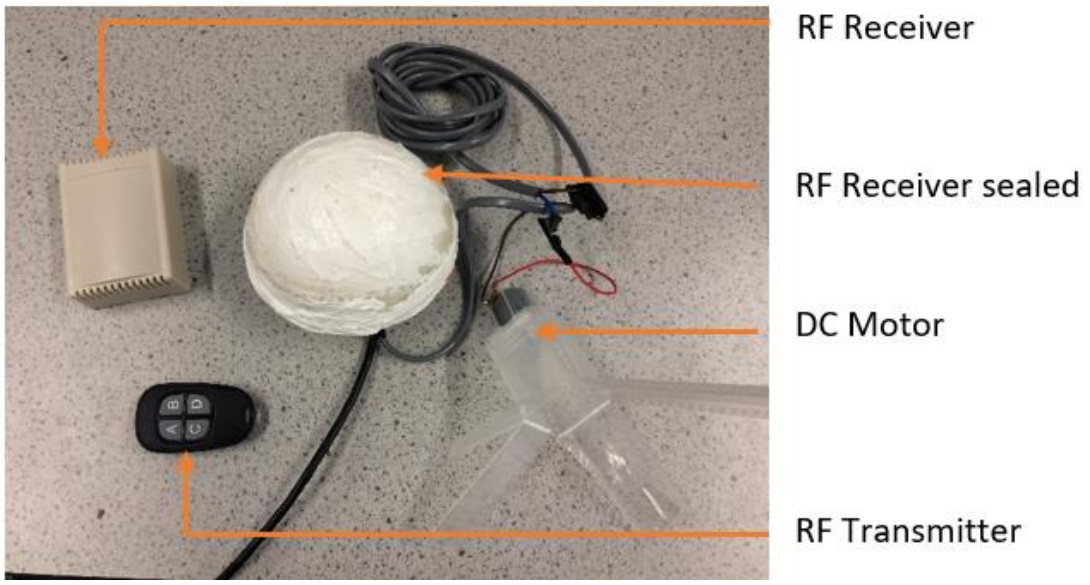

Figure 6. 1: RF remote-control transmitter and receiver system.

The receiver was sealed in a waterproof enclosure and submerged into a 1.5 meters long plastic pipe filled-up with vegetable oil. In order to see the effect of RF wireless communication, a connection was made via a cable from the submerged receiver to the DC motor driving a plastic propeller blade. The frequency used in this experiment was 433 MHz, Figure 6.2 shows the test set up with vegetable oil, RF receiver showing at the bottom of the pipe (a) and filled up with vegetable oil (b).

(a) (b)

Figure 6. 2: RF receiver submerge in vegetable oil.

The experiment results in Figure 6.3 (c) and (d) show respectively when the transmitter and receiver were both submerged in vegetable oil and when only the receiver was submerged, and transmission was done through air and the vegetable oil at a distance of 15 meters. In this experiment, a radio frequency wireless signal was sent to open and close the receiver switch through vegetable oil to turn on an off the DC motor. The electric motor connected to the RF receiver via cable was successfully driven on and off with a transmitter control button.

(c)

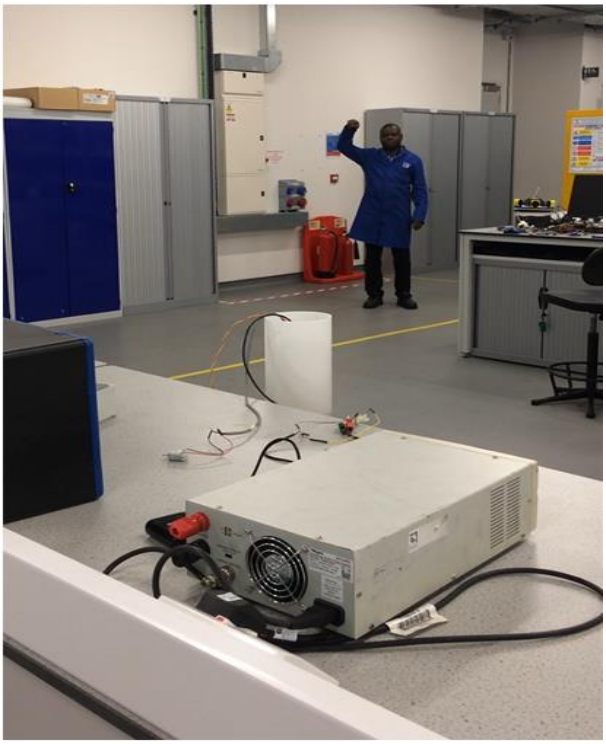

(d)

Figure 6. 3: RF transmission air/vegetable oil (a) and submerged transceiver.

6.1.2 Experiment case transmitter and receiver submerge

The Radio Frequency used in this experiment was low power LoRa611Pro wireless transceiver 433 MHz data transmission module based on SX1276/1278 chips from Semtech. The module implements Lora technology to achieve sufficient sensitivity and excellent anti-interference with 100mW output power. Table 6.1 shows the characteristics of the LoRa611Pro wireless transceiver data transmission module.

Table 6. 1: RF module electrical characteristics.

Parameters	Min.	Typ.	Max.	Unit	Condition
Working condition					
Voltage range	3.3	5.0	6.5	V	
Operation Temperature	-40	25	+85	^{0}C	
Current consumption					
Rx current		<15		mA	TTL.level
Tx current		<130		mA	@20dBm
Sleep current		<200		uA	
RF parameters					
Frequency range	414.92	433.92	453.92	MHz	@433MHz
Data rate	91	656	17353	bps	LoraTM
Output power	0		+20	dBm	Configurable
Sensitivity		-139		dBm	91bps

Two transceiver modules were used, and each transceiver was sealed into a waterproof enclosure with end connection adapter RS485 interface for computer connection. Figure 6.4 (a) and Figure 6.4 (b) show both antennas in an enclosure, the radio frequency wireless module can transmit a distance of up to 5000 meters at 91 bps with the antenna in an open area.

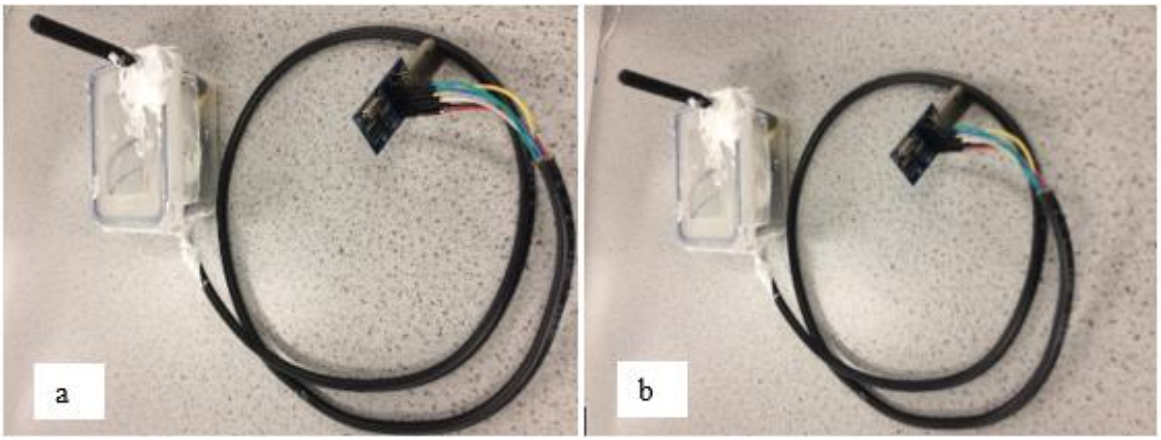

Figure 6. 4: RF transceivers.

Similar to experiment 1, both data transceivers were submerged into vegetable oil for data transmission. In order to observe the data link, commercial serial software was used to read the receiver antenna data from the transmitter. In this experiment text data were set up and transmitted from the computer (a) to the computer (b) (Figure 6.5) via a RF wireless link. The data text received were compared with the data sent from the transmitter. Figure 6.5 (a) and (b) shows that data was successfully transmitted within the medium (vegetable oil) with no information loss.

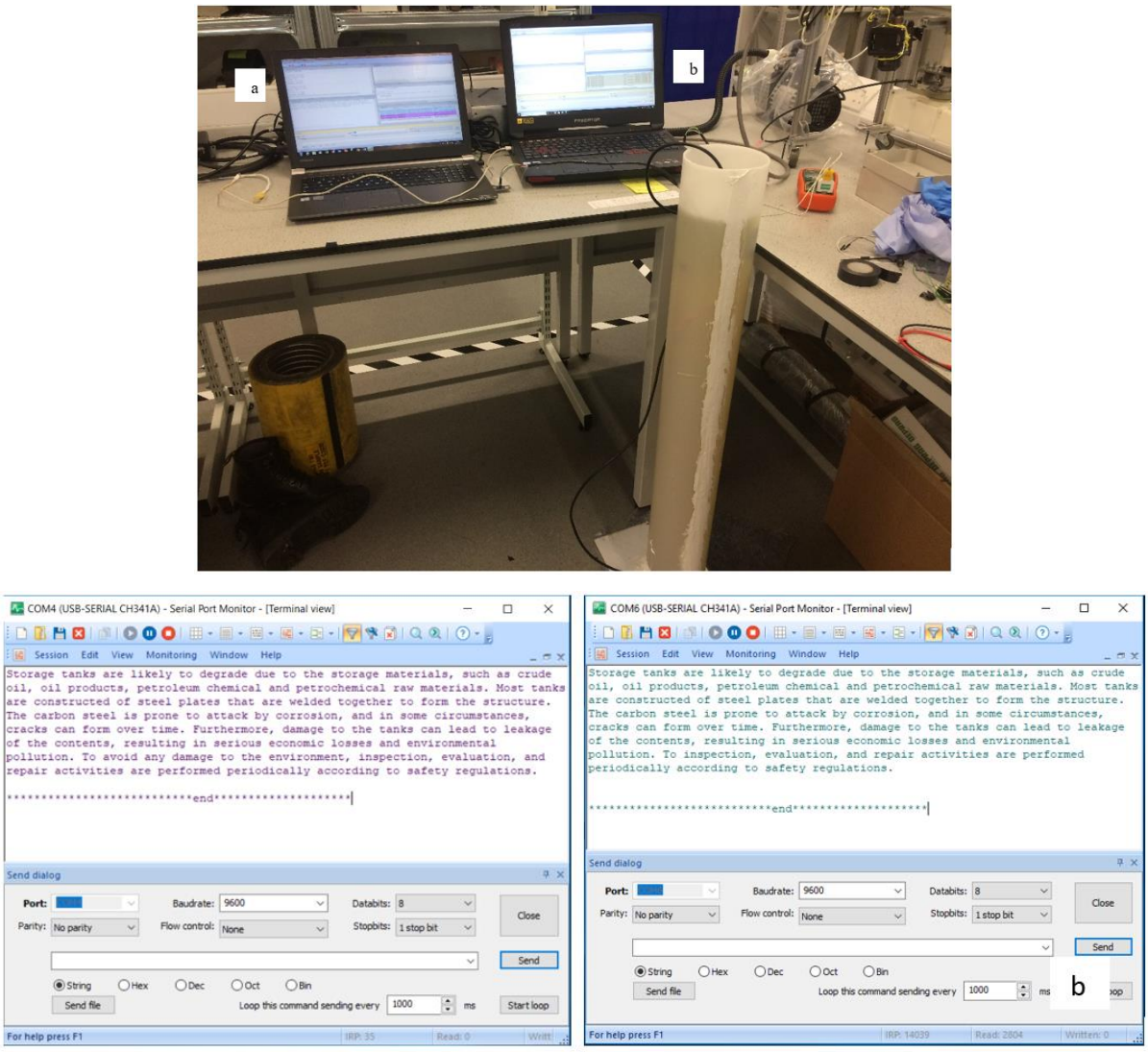

(a) (b)

Figure 6. 5: RF transmission in vegetable oil medium transmitter and receiver submerged.

Visual Studio C# (Appendix C-1) was used to design a user interface for the RF transceiver to read and send data. The GUI was connected to the RF antenna via computer communication port. In this investigation, different type of data was used such as string data sent through a computer connected to the antenna via communication port 4 (COM4). Figure 5.6 (e) and Figure 5.6 (h) shows the transmitter control user interface and the other computer conneced to the receiver antenna via communication port 6 (COM6). The data transmitted was identical to the data received, no loss of information while transmitting through vegetable oil.

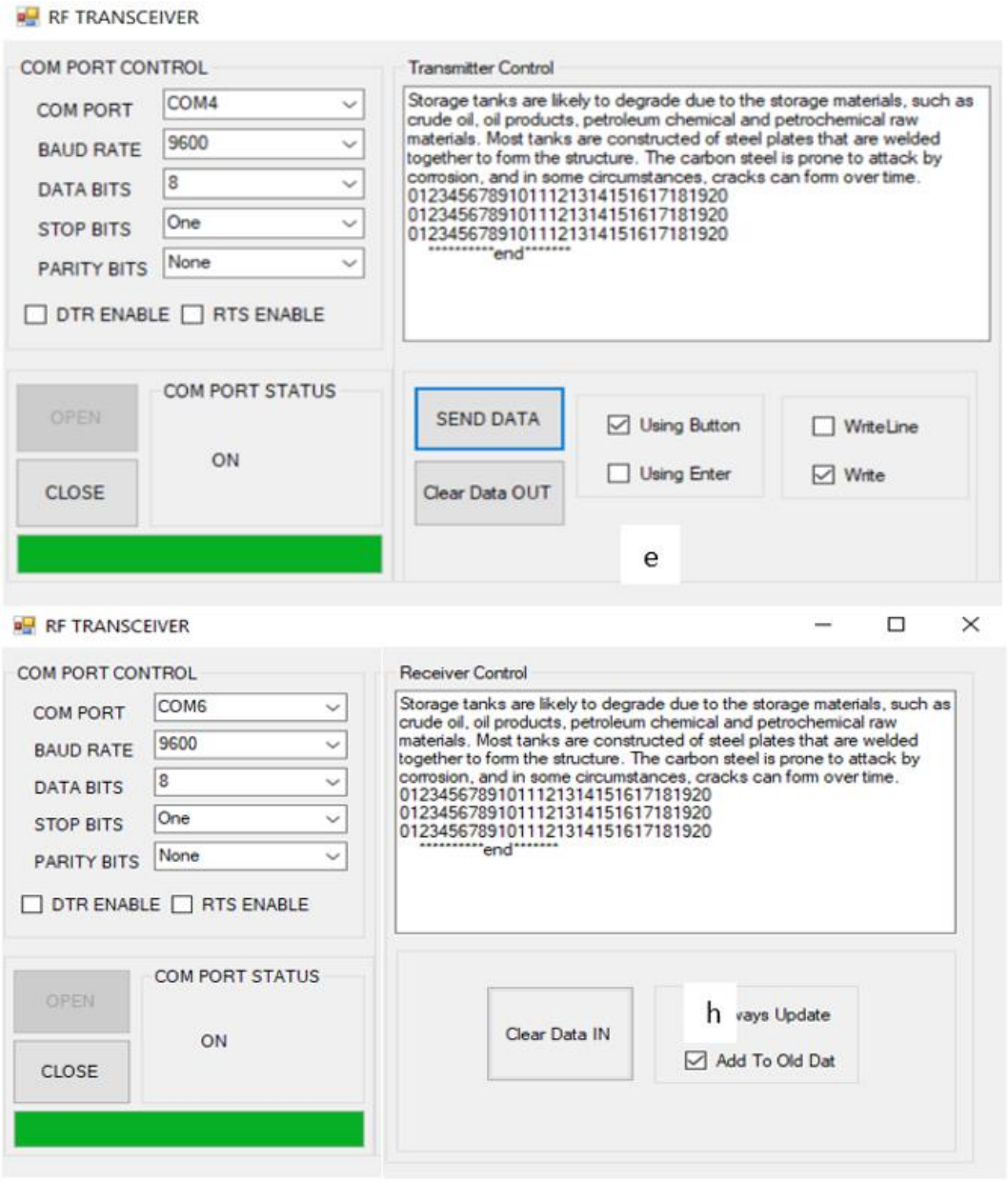

Figure 6. 6: RF GUI transceiver.

6.1.3 Experiment case transmitter in air and receiver submerge

Contrary to the first setup in experiment 1, where the pipe was plastic material, with an open end, and both transmitter and receiver were submerged. Experiment 2 was setup in a steel pipe with a wall thickness of 7.67 mm, diameter of 20 cm with both ends of the steel pipe closed. One antenna was submerging into the steel pipe as shown in Figure 6.7 (a) and Figure 6.7 (b) and connected to a computer in the air. To compensate the diameter of the steel pipe, the antenna connected to a computer in the air (b) was taken to different locations with distances as follow: 5 m, 10 m, 15 m, 20 m, 25 m, 30 m up to 40 m.

(a)

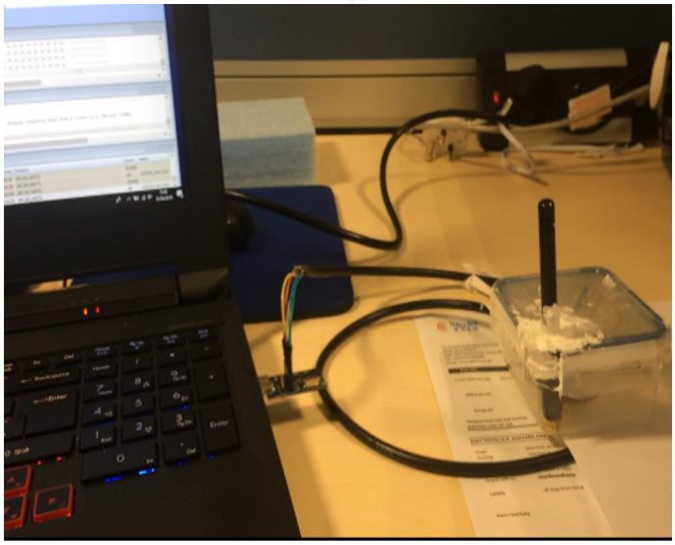

(b)

Figure 6. 7: RF transmission in vegetable oil/ air and air/vegetable oil.

The result shows that digital data was transmitted correctly in both directions from air to vegetable oil and vegetable oil to air. The data was transmitted and received in both direction at different distances as mentioned earlier. The data was collected with no information loss in both directions. The GUI in Figure 5.8 (g) displays the data transmitted via an antenna connected to communication port 6 (COM6) with the received data displayed in Figure 5.8 (f). Figure 5.8 shows the similarity of the data transmitted and received; no loss was observed.

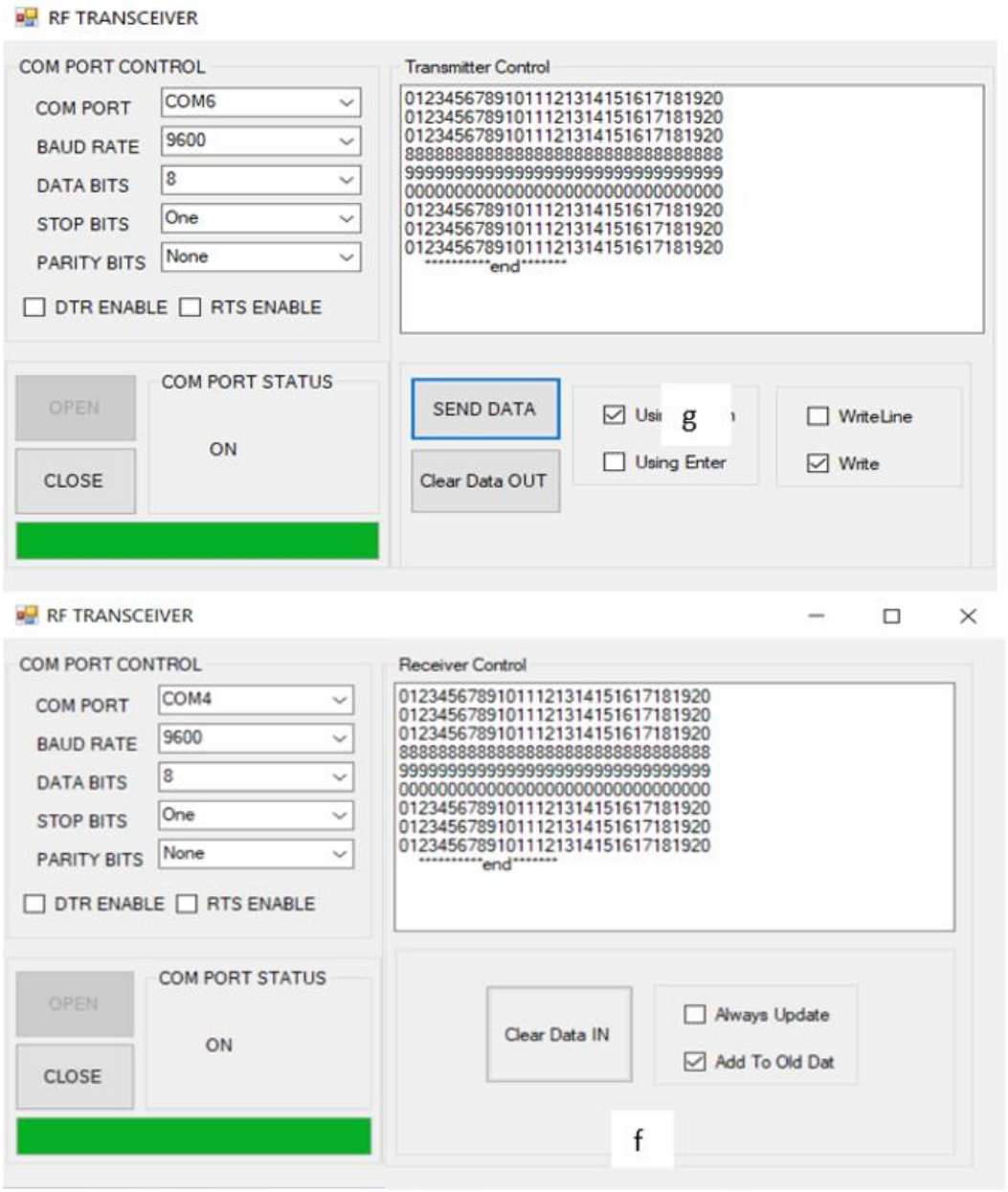

Figure 6. 8: RF transmission air/vegetable oil; vegetable oil/air.

6.1.4 Ultrasonic testing data transmission with radio frequency

Ultrasonic testing data is transmitted with radio frequency wireless link. The result obtained with the RF data Figure 6.9 (a) was compared to the initial reading Figure 6.9 (b). All data was transmitted with no loss as shows the signal time of flight for both 6.49 µs.

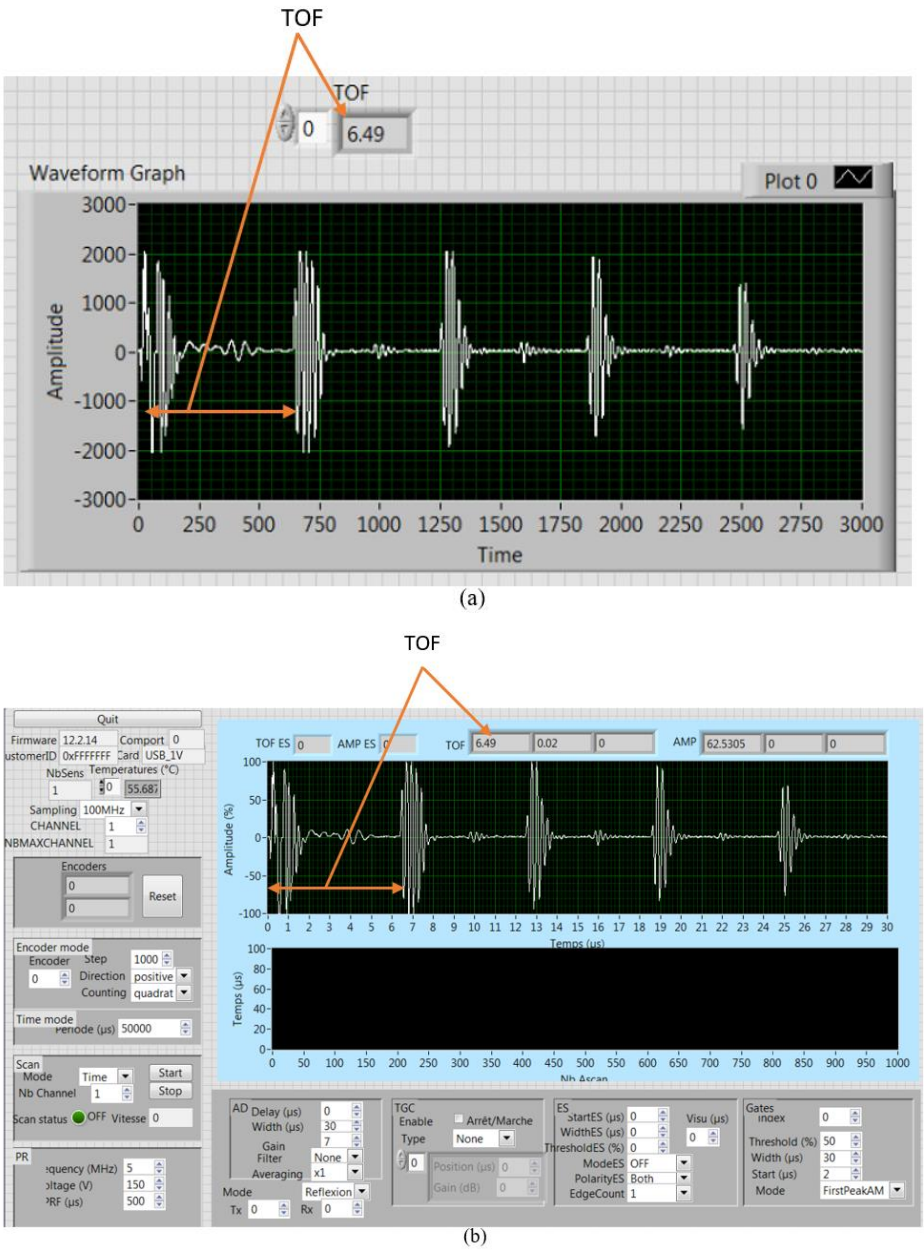

Figure 6. 9: RF transmission air/vegetable oil; vegetable oil/air.

6.2 Chapter summary

This chapter presented experimental validation of radio frequency wireless communication through oil medium and also through oil/steel/air interfaces. Experiments to test data transmission were performed with vegetable oil used as a medium. The signal and data were correctly transmitted and received without loss with RF at 433 MHz using remote control and the low power LoRa611Pro wireless transceiver 433 MHz data transmission module. In this investigation, the RF transceiver module used in the experiment had very low transmitted power compared to ignition power stated earlier for zone 0 environments in British Standard (BSI PD CL/TR 50427:2004). The radio frequency module LoRa611Pro wireless transceiver can be integrated into the NDTBOT for control, system communication and online NDT data transmission in storage tank inspection. This technology will reduce the problem of heavy umbilical cable for mobile robot.

Chapter 7

Conclusion and further recommendations

The chapter summarizes the contributions of this work and proposes potential research avenues that we have identified through investigations.

Storage tank failure from floor leakage is difficult to detect because it is not visible externally until some point in time. Based on API 571, the damage mechanisms on the storage tank floor are usually caused by corrosion damage in the form of general corrosion and pitting corrosion (American Petroleum Institute, 2011). The corrosion damage on the top side of the plate is usually caused by coating breakdown while on the bottom side of the plate are generally caused by the reaction with the soil itself. Furthermore, damage to the tanks can lead to leakage of the contents, resulting in severe economic losses and environmental pollution.

A literature review was carried out to understand the operating environment and the key design requirements for in-service inspection robots. The review identified different techniques of inspection and existing developments focusing on in-service robotic inspection. This review established the limitations of current in-service inspection robots. The main limitations were found in robot locomotion designs as well as the communication systems and the high power required to drive the robots which made then unacceptable for zone 0 environment application. To design an appropriate system, the environment of inspection was studied and led to the design and development of prototype NDTBOTs that aim to avoid any spark that can create an explosion in storage tanks by avoiding any external moving parts in the robot. Also, the designs reduced the NDTBOT maximum voltage used in order to be approved by certification body ATEX for operation in zone 0 and zone 1 environments. The first prototype was designed to test the actively controlled buoyancy system for the NDTBOT, which is the main method of locomotion for the robot. An ultrasonic UT probe was mounted on the side of the NDTBOT to inspect the thickness of steel plates placed in a water tank. The NDTBOT buoyancy system was successfully tested in a water tank, and accurate thickness measurement with the ultrasonic

UT probe was obtained. The final prototype of the NDTBOT was designed to incorporate the buoyancy system tested in the first prototype, and all electronics and ultrasonic flaw detector and on-board power batteries were chosen according to the hazardous environment.

The control user interface was designed to control the NDTBOT, and different types of sensors to monitor the state of the robot. With the final prototype, the encapsulation of the NDTBOT in fire proof epoxy will be more straightforward when deploying in a flammable and explosive environment. Ansys CFX simulation was used to study the NDTBOT motion, determine the drag coefficient from the simulations to obtain the NDTBOT acceleration when applying different input voltages to control the system better.

Moreover, validation experiments with the final version of the NDTBOT were carried out to validate the full system capability to inspect the thickness of the steel plate more accurately. Three types of experiment were set up to measure original thickness of steel plates using Venire calliper, Hand-held thickness measurement with contact ultrasound, and with the NDTBOT submerged in a water tank making measurements with an immersion UT probe.

These results conclude that the NDTBOT thickness measurements with an immersion ultrasound probe obtained more accurate results than manual or hand-held contact NDT. Therefore, the results increase confidence that using NDTBOTS to look for corrosion thinning on the floors of storage tanks can give at least equivalent or better results than standard NDT performed by a human operator.

Finally, the thesis discussed the development of RF wireless communication for in-service inspection robots. Simulation with commercial software CADFEKO using vegetable oil and petroleum products as simulation medium with a set of different RF frequencies of 200 MHz, 300 MHz and 433 MHz, the simulation has shown that a receiver antenna placed inside the medium received the transmitted signal from outside the medium.

The experiment for data transmission was conducted with vegetable oil used as a medium. A remote control 433 MHz wireless communication was successfully used to switch on and off a DC motor through vegetable oil. The final experiment was set up to transmit data from air to vegetable oil, and vice-versa using a low power LoRa611Pro wireless transceiver 433 MHz data transmission module. All data was transmitted to the receiver with no data loss. The frequency of 433 MHz was chosen because early calculations showed that although the attenuation increased at higher frequency, and lower frequenciesare less attenuative, but data transmission length becomes smaller at lower frequencies.

vegetable oil is used for the tests because of safety considerations, its characteristics compared to petroleum products show that RF could propagate better in petroleum products than vegetable oil with less dispersion and path loss. In this investigation, the Radio Frequency transceiver module used in the experiment had very low transmitted power compared to the threshold ignition power stated earlier for zone 0 environments. Therefore, the NDTBOT could use RF modules for communication in the storage tank to reduce or eliminate the problem of heavy umbilical cables and offers a method to localise the robot inside the tank by using an array of receivers placed outside the tank with a transmitter placed on board the NDTBOT.

7.1 Further recommendations

In this thesis, the design and development of NDTBOT prototypes was successfully tested armed with ultrasonic UT probes and a RF communication system. However, there is still room for improvement and more development. Here, some tasks with high potential impact are suggested.

- The promising RF results in this thesis should be utilised to develop a localisation system with arrays of receivers placed outside a tank while a transmitter is placed on board the NDTBOT.
- Investigate strategies to make the NDTBOT perform floor NDT in a fully autonomous mode so that long term integrity management of the tank can be carried out via this inspection and monitoring tool.
- Further research is required to develop a swarm of NDTBOTS that collaborate with each other to speed up inspection of a large tank while ensuring that the NDT is able to find most defects and corrosion on a tank floor. Additionally, the ability of a NDTBOT to float/swim could be utilised to perform NDT of the walls of buried tanks. Localisation of the individual NDTBOTS in a swarm will be important to map defects found by each NDTBOT and to ensure that they remain widely dispersed during an inspection.

References

Abdalla Eltigani Ibrahim, Mohd Noh Karsiti, Irraivan Elamvazuthi, (2015). Experimental Buoyancy Control for a Spherical Underwater Robot Vehicle (URV), vol. 1 (1) 42-52. Available at: http://nebula.wsimg.com/0321a6da9f4d8d0f1f5ae8e4226be8b5?AccessKeyId=638139448EC3C95C7DBE&disposition=0&alloworigin=1 (Accessed: 5 July 2016).

American Petroleum Institute, (2011). API Standard Recommended Practice 571: Damage Mechanisms Affecting Fixed Equipment in the Refining Industry. Washington: American Petroleum Institute

Andres San-Millan, (2015), Design of a teleoperation wall climbing robot for oil tank inspection 2015 23rd Mediterranean Conference on Control and Automation (MED), June 16-19. Torremolinos, Spain, 978-1-4799-9936-1/15 /2015 IEEE, pp 255-261.

Altair, (2017). Available at: https://altairhyperworks.com/product/Feko/New-Features (Accessed: 10 September 2017).

Balanis. A, (2005) 'Antenna theory analysis and design' 3nd ed. New Jersey, USA: John Wiley & Sons, pp.201-215.

Bouhadjera, A. (2006) 'An Ultrasonic Mode Conversion Technique for Characterizing Prism-Shaped Material Samples – Experimental and Numerical Results', ECNDT 2006, 9th European Conference on Non-Destructive Testing, Berlin, DE, Sep 25-29, 2006, pp. 1–16.

British Standards (2002) 'Assessment of inadvertent ignition of flammable atmospheres by radio-frequency radiation - Guide\rBS 6656:2002', 3.

Bradby, R. (2008) 'Practical experience in radio frequency induced ignition risk assessment for COMAH/DSEAR compliance', (154), pp. 760–774. Available at: https://www.scopus.com/inward/record.uri?eid=2-s2.0-56349125236&partnerID=40&md5=cff3d2a67e6ccf43b3332ac04326604c. (Accessed: 03 July 2017).

Caruthers, S., (1996). Here are guidelines for inspecting AST internals. Oil and Gas Journal, 94(28), pp.52-55.

Centelles, D. *et al.* (2015) 'Wireless RF Camera Monitoring for Underwater Cooperative Robotic Archaeological Applications', pp. 100–102.

Castro, J. M. et al. (2005) 'Demonstration of mode conversion using anti-symmetric waveguide Bragg gratings', Optics Express, 13(11), p. 4180. doi: 10.1364/OPEX.13.004180.

Chang, J.I. & Lin, C., 2006. A study of storage tank accidents. Journal of Loss Prevention in

the Process Industries, 19(1), pp.51–59. Available at: http://linkinghub.elsevier.com/retrieve/pii/S0950423005000641. (Accessed: 17 March 2016)

Che, X. et al. (2009) 'A Static Multi-Hop Underwater Wireless Sensor Network Using RF Electromagnetic Communications', Icdcs: 2009 International Conference on Distributed Computing Systems Workshops, pp. 460–463. doi: 10.1109/ICDCSW.2009.36.

Che, X. et al. (2010) 'Re-Evaluation of RF Electromagnetic Communication in Underwater Sensor Networks', (December), pp. 143–151. doi: 10.1109/MCOM.2010.5673085 Publisher: IEEE Sponsored by: IEEE Communications Society.

Choi, H. and Popovics, J. S. (2015) 'NDE application of ultrasonic tomography to a full-scale concrete structure', IEEE Transactions on Ultrasonics, Ferroelectrics, and Frequency Control, 62(6), pp. 1076–1085. doi: 10.1109/TUFFC.2014.006962.

Clement, S. et al., 2012. Underwater Sensor Networks: A New Energy Efficient and Robust Architecture. Sensors, 12(12), pp.704–731. Available at: http://www.mdpi.com/1424-8220/12/1/704/. (Accessed: 20 October 2017).

Cochran, S. (2006) 'Ultrasonics, Part 12. Fundamentals of ultrasonic phased arrays', Insight: Non-Destructive Testing and Condition Monitoring, 48(4), pp. 212–217. doi: 10.1784/insi.2006.48.4.212.

Cornerstone (2018) Camera inspections. Available at: http://www.ccseattle.com/home-sewer-repair/camera-inspection-sewer-pipes-seattle (Accessed: 04 Jun February 2018).

Dario, P. et al. (2010). Distributed Routing Algorithms for Underwater Acoustic Sensor Networks, ed., Auerbach Publications. Available at: http:/www.crcnetbase.com/doi/book/10.1201/9781420067125. (Accessed: 09 Jun 2017).

David K. Cheng, (2006). 'Field and Wave Electromagnetics 2nd Edition Solution.pdf'. Available at: ftp://doc.nit.ac.ir/cee/m.yousefnia/Books/Electromagnetic_Cheng.pdf (Accessed: 17 September 2016).

Du, B. X. and Li, X. L. (2017) 'Dielectric and thermal characteristics of vegetable oil filled with BN nanoparticles', IEEE Transactions on Dielectrics and Electrical Insulation, 24(2), pp. 956–963. doi: 10.1109/TDEI.2017.005758.

Dury, JC. 2005. NDT Fundamentals, Basic principles of sound.

Elleithy, A., Liu, G., & Elrashidi, A. (2012). Underground wireless sensor network communication using electromagnetic waves resonates at 2.5 GHz. Journal of Wireless Networking and Communications, 2(6), 158–167. https://doi.org/10.5923/j.jwnc.20120206.01

ENVIROPRO. (2018) Atmospheric tank inspection. Available at:

https://www.enviropro.co.uk/entry/127485/Inspectahire-Instrument-Company/Atmospheric-tank-inspection/. (Accessed: 10 September 2018).

Feuilly, N., 2009, Etude de l'influence de la microstructure sur la diffusion d'une ondeultrasonore en vue de l'amerioration du controle non destructif des materiaux polycrystallins.P hD T hesis Universite de la Mediterranee

Franconi, N. G. et al. (2014) 'Wireless Communication in Oil and Gas Wells', Energy Technology, 2(12), pp. 996–1005. doi: 10.1002/ente.201402067.

Georgia (2017). Available at: http://www.georgiaoilmens.com/above-ground-storage-tanks (Accessed: 20 May 2017).

Hardt, M., Ruiter, N. V and Gemmeke, H. (2012) 'Analysis of The Influence of Multiple Scattering on The Reconstruction of Ultrasound Tomography Signals using Synthetic Aperture Focussing Technique', Systems, Signals and Image Processing (IWSSIP), 2012 19th International Conference on, (April), pp. 11–13.

Health and safety Executive 2015. Storage of flammable liquids in tanks. Available at: http://www.hse.gov.uk/pUbns/priced/hsg176.pdf. (Accessed: 15 March 2016).

Health and safety Executive 2015. Storage of flammable liquids in tanks. Available at: http://www.hse.gov.uk/pUbns/priced/hsg176.pdf. (Accessed: 15 February 2016)

Hoegh, K. and Khazanovich, L. (2015) 'Extended synthetic aperture focusing technique for ultrasonic imaging of concrete', NDT and E International. Elsevier, 74, pp. 33–42. doi: 10.1016/j.ndteint.2015.05.001

Inacio, S. I. et al. (2016) 'Dipole antenna for underwater radio communications', 3rd Underwater Communications and Networking Conference, Ucomms 2016. doi: 10.1109/UComms.2016.7583457.

Inoue, Y. et al. (2006) 'A study of ultrasonic propagation for flow rate measurement using ultrasonic flowmeter', Proc. 5ISUD, pp. 89–92. Available at: http://www.isud-conference.org/proc/split/ISUD-05_089_Inoue.pdf (Accessed: 12 March 2015).

Inspector Newtonlabs (2017) 'Underwater In-Tank Inspection Robot'. Available at: http://www.newtonlabs.com/pdf/inspector_datasheet010815.pdf. (Accessed: 12 February 2018).

IOlympus, N. (2006) 'Ultrasonic transducers technical notes', *Technical brochure: Olympus NDT, Waltham, MA*, pp. 39–49. Available at: http://scholar.google.com/scholar?hl=en&btnG=Search&q=intitle:Ultrasonic+Transducers+Technical+Notes#0. (Accessed: 05 November 2015).

IOlympus, N. (2006) 'Ultrasonic transducers technical notes', Technical brochure: Olympus NDT, Waltham, MA, pp. 39–49. Available at: http://scholar.google.com/scholar?hl=en&btnG=Search&q=intitle:Ultrasonic+Transducers+Technical+Notes#0. (Accessed: 15 November 2015).

Ireneusz B., Marek N., Gerald L. (2014) The Acoustic Emission Monitoring System of

Aboveground Storage Tanks, 31st Conference of the European Working Group on Acoustic Emission (EWGAE) – Fr.2.B.3. available at: http://www.ewgae2014.com/portals/131/bb/fr2b3.pdf. (Accessed: 15 December 2015).

Kalra P., Weimin S., and Jason G, (2006) A Wall Climbing Robotic System for Non-Destructive Inspection of Above Ground Tank, IEEE CCECE/CCGEL, Ottawa, May 2006.

Kalra P., Jason.G, and Max.M, (2006) A Wall Climbing Robot for Oil Tank Inspection, proceeding of the 2006 IEEE International Conference on Robotics and Biomimetics Dec. 17- 20, 2006, Kunming, China, 1-4244-0571-8/06 /2006 IEEE.

Kumar, S. (2016) 'A Comprehensive Review of Recent Advances and Challenges in Underwater Wireless Optical Communication', pp. 1–2.

Krautkramer, H. and Krautkramer, J. (1990) Ultrasonic Testing of Materials. doi: 10.1007/978-3-662-10680-8.

Liying S., Yibo L. (2010) Review of On-line Defects Detection Technique for Above Ground Storage Tank Floor Monitoring, proceeding of the 8th World Congress on Intelligent Control and Automation July 6- 7 2010, Jinan, China, 978-1-4244-6712-9/10/ 2010 IEEE, pp 4178- 418.

Lloret, J. *et al.* (2012) 'Underwater wireless sensor communications in the 2.4 GHz ISM frequency band.', *Sensors (Basel, Switzerland)*, 12(4), pp. 4237–64. doi: 10.3390/s120404237.

Lucas (2007). Available at: https://en.wikipedia.org/wiki/Prism#/media/File:Light_dispersion_conceptual_waves.gif. (Accessed: 20 October 2015).

Maverick Demonstration "Submarine that goes in Gasoline", Solex Robotics. Avalable at: http://www.solexrobotics.com/Solex6.html. (Accessed: 18 November 2015)

Myers, Philip E. (1997) 'Aboveground Storage Tanks'.The McGraw-Hill companies, United State of America. Pp36-50.

Milligran. T. (2005) 'Modern antenna Design , 2nd ed, Hoboken Jersery: John Wiley & Sons.pp 303-307.

Mohammad M., Mahdi B., Mohammad Z, (2015) A Novel Design of Wall Climbing Robot for Inspection of Storage Steel Tanks, proceeding of the 3rd RSI International Conference on Robotics and Mechatronics, October 7-9, 2015, Tehran, Iran, 978-1-4673-3/15.00 2015 IEEE, pp557-562.

Moore, M., Phares, B. and Washer, G. (2004) 'Guidelines for Ultrasonic Inspection of Hanger Pins', (July), p. No.FHWA-HRT-04-042. Available at: http://trid.trb.org/view.aspx?id=703199%5Cnhttp://www.fhwa.dot.gov/publications/research/infrastructure/structures/04042/04042.pdf. (Accessed: 20 November 2016).

NACE International. (2016) ‘The Impact of Corrosion on Storage Tanks and Piping’. Avalable at: https://archive.epa.gov/emergencies/content/fss/web/pdf/koch_04.pdf. (Accessed: 05 December 2017).

NAVSEA OP 3565/NAVAIR 16-1-529. (2003) ‘Electromagnetic radiation hazards (hazards to personnel, fuel and other flammable material). Available at: https://info.publicintelligence.net/navsearadiationdanger.pdf. (Accessed: 05 January 2017).

NDTPI. (2018) Ultrasonic testing available at: https://www.ndtphils.com/services/non-destructive-testing-ndt/advanced-ndt/magnetic-flux-leakage-testing. (Accessed: 20 Jun 2018).

Oleksandr P. Ivakhnenko (2012). Magnetic Susceptibility of Petroleum Reservoir Crude Oils in Petroleum Engineering, Crude Oil Exploration in the World, Prof. Mohamed Younes (Ed.), ISBN: 978-953-51-0379-0, InTech, Available at: http://www.intechopen.com/books/crude-oil-exploration-in-the-world/magneticsusceptibility-of-petroleum-reservoir-crude-oils-in-petroleum-engineering. (Accessed: 05 April 2017).

Olympus, 2016. Ultrasonic Flaw Detection Tutorial Wave Propagation available at: http://www.olympus-ims.com/en/ndt-tutorials/flaw-detection/wave-propagation/.(Accessed: 15 Jun 2017).

Olympus, 2018. Intro to ultrasonic testing available at: https://www.olympus-ims.com/en/ndt-tutorials/intro/ut/. (Accessed: 05 January 2018).

OTIS, 2002. In Service Robotic Storage Tank Inspection & Cleaning in Saudi Arabia. Available at: http://www.tcr-arabia.com/ndt/In-Service-Robotic-Storage-Tank-Inspection-and-Cleaning-Saudi-Arabia.shtml. (Accessed: 20 November 2015).

Paranjpe, G & Deshpande, P. (1935) ‘Dielectric proprieties of some Vegetable oils’, Proc. Indian Acad. Sci. (Math. Sci.) (1935) 1: 880. Available at: https://doi.org/10.1007/BF03035644. (Accessed: 20 May 2017).

Park, D. et al., 2015. Underwater sensor network using received signal strength of electromagnetic waves. In 2015 IEEE/RSJ International Conference on Intelligent Robots and Systems (IROS). IEEE, pp. 1052–1057. Available at: http://ieeexplore.ieee.org/lpdocs/epic03/wrapper.htm?arnumber=7353500. (Accessed: 05 February 2017).

PETROBOT (2016). Inline Inspection of Storage Tanks – The PETROBOT Solution. Available at: http://petrobotproject.eu/wp-content/uploads/WP2-Inline-Inspection-of-Storage-Tanks-The-PETROBOT-Solution.pdf. (Accessed: 15 May 2017).

Prakash, Ravi. 2015. Non-Destructive Testing Techniques. Kent, GBR: New Academic Science,2012.

Remote and Controller, (2018). Available at: http://www3.emersonprocess.com/Remote/mobile/flipbook/roc800-seriesoverview_d350944x012/files/assets/common/downloads/publication.pdf.

(Accessed: 05 January 2018).

RobTank (2001). Oil tank floor inspecting robot. Available at: http://www1.lsbu.ac.uk/esbe/mrndt/robtank.shtml. (Accessed: 25 October 2015).

Rydl, L. and Simpson, C. (2004) 'Wireless technology uses in the oil and gas industry', V(2), pp. 666–672.

Safety, I. and Saving, E. M. (2018) 'Acoustic Emission Inspection and Monitoring of Petroleum Storage Tanks and Piping Increased Safety with Excellent Money Saving' http://www.idinspections.com/wp-content/uploads/Acoustic-Emission-Inspection-of-Petroleum-Tanks-and-Piping-May-2016.pdf (Accessed: 17 February 2018).

Saunderson, D.H. (1988) 'The MFE tank-floor scanner-a case history,' Non-Destructive Evaluation, IEE Colloquium on. IET, pp. 1–8.

Schempf H. (1994). Neptune-Above-Ground Storage Inspection Robot System, Proceeding of IEEE International Conference on Robotics and Automation, San Diego, Vols 1-4, Part 2. pg. 1403-1408.

Schempf H., Brian C., Nathan E. (1995). Neptune-Above-Ground Storage Inspection Robot System, Proceeding of IEEE Robotics and Automation, Magazine pg. 9-15.

Shi, Y. et al. (2015) 'Theory and Application of Magnetic Flux Leakage Pipeline Detection', Sensors, 15(12), pp. 31036–31055. doi: 10.3390/s151229845.

Siemens (2018). Available at: https://new.siemens.com/global/en/markets/oil-gas/industrial-communications.html. (Accessed: 20 Jun 2018).

Silverwing (2016). Available at: https://www.silverwingndt.com/applications/tank-bottom-integrity/ (Accessed: 02 April 2016).

Solar Environmental (2010) 'Robotics inspection system Industry of the Future. Available at; Petroleum'. http://www.nrel.gov/docs/fy99osti/26044.pdf. (Accessed: 20 November 2015).

Stingray (Diakont, 2017) 'Online Storage Tank Floor Inspection Services' , p. 92123. Available at: http://www.diakont.com/energy_services/18/online-storage-tank-floor-inspection.html. (Accessed: 20 April 2018).

Stuber. (1996) "Principles of Mobile Communication," Klumer Academic Publishers, 1996, 2001Harry T. 2002. A slice little robot. Available at: http://idehkavan-tech.com/articles/2-4.pdf. (Accessed: 04 December 2015).

Sun L., Li Y., (2011) Investigation on Sensor Array in Large Vertical Storage Tank Bottom Inspection using AE Methods, 2011 Chinese Control and Decision Conference (CCDC), 978-4244-7/11/ 2011 IEEE, pp 2838- 2842.

Sylvester, A.H. et al., 2014. Variable Buoyancy Control for a Bottom Skimming Underwater Vehicle. In 2014 Oceans - St. John's.IEEE, pp. 1-6. Available at

http:/ieeexplore.ieee.org/lpdocs/epic03/wrapper.htm?arnumber=7003058. (Accessed: 05 December 2016).

Tariq P. Sattar, Hernando E. Leon-Rodriguez and Salman H., (2012) A Compact Wall-Climbing and Surface Adaptation Robot for Robot for Non-Destructive Testing, 2012 International Conference on Control, Automation and Systems, Oct. 17-21, in ICC, Jeju Island, Korea.

Tariq P. Sattar, Hernando E. Leon-Rodriguez and Jianzhong Shang (2004). Amphibious NDT Robots, Climbing, and Walking Robots: Towards New Applications, Houxiang Zhang (Ed.), ISBN: 978-3-902613-16-5, pp 128-136 (InTech, DOI: 10.5772/5078. Available at: http://www.intechopen.com/books/climbing_and_walking_robots_towards_new_applications/amphibious_ndt_robots. (Accessed: 05 January 2016).

Tariq P. Sattar, Hernando E. Leon-Rodriguez and Jianzhong Shang (2004). Amphibious NDT Robots, Climbing, and Walking Robots: Towards New Applications, Houxiang Zhang (Ed.), ISBN: 978-3-902613-16-5, pp 137-149 (InTech, DOI: 10.5772/5078. Available at: http://www.intechopen.com/books/climbing_and_walking_robots_towards_new_applications/amphibious_ndt_robots. (Accessed: 05 January 2016).

TSC Micropump (2015). Available at: https://micropumps.co.uk/DATA/pdf/DS09%20%20MG2000%20Sheet%20REV%203%20SMALL.pdf. (Accessed: 09 December 2015).

Ultrasound. (2017). Available at: https://www.uscultrasound.com/blog/ultrasound-101/.(Accessed: 25 July 2017).

Victor 2003. International Reference Guide to Hazardous Areas. Available at: http://www.victor-lighting.com/default/off/page/Hazardous_Guide.html. (Accessed: 05 November 2015).

Wood, S.L, Hendricks, A & Corbet, M., 2015. Automated Buoyancy Control System for a Remotely Operated Underwater Crawler. 2015 MTS/ IEEE Oceans – Genova, pp.1-10.

Zhou, Y. *et al.* (2016) 'Research on Fire and Explosion Accidents of Oil Depots', *Chemical Engineering Transactions*, 51, pp. 163–168. doi: 10.3303/CET1651028.

Appendix A

A-1: NDTBOT electrical equipment selection

- **Centrifugal micro-pump description**

The micro-pump has low energy consumption with a variable input voltage from 6 to 12 volts Figure 3. 4; it uses centrifugal force to pressurise and move liquid from the inlet to the outlet. A rotating set vane (called an “impeller”) is spun by the pump shaft. As liquid is forced through the impeller, rotational energy is transferred from the impeller to the liquid, which gains velocity and pressure through the centrifugal force applied and is flung from the impeller. The volute (a spiral-shaped case) funnels the now-pressurised liquid to the outlet.

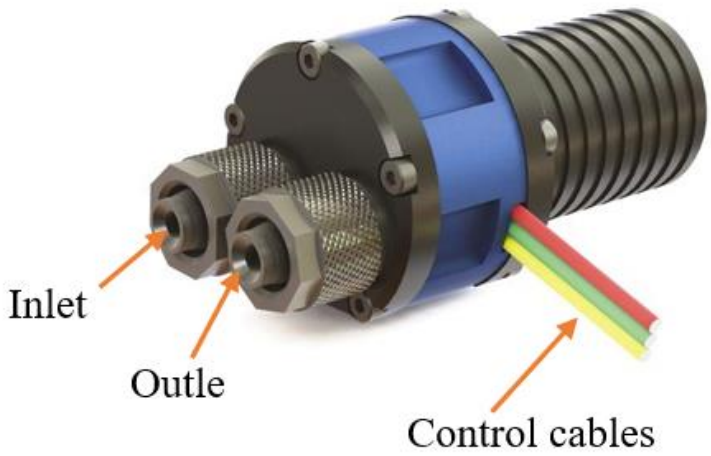

Micro-pump.

The pump delivers a constant flow with high or low pressure; it is suitable for low or high viscosity liquids and self-priming. The pump can be used with all common liquids and resists most chemicals and solvents. The body of the pump is constructed from precision CNC machined aluminium alloy, and the wetted part is stainless steel, peek and polyacetal. The pump has two tubing connectors made with stainless steel for easy and quick connection. It operates with smooth and consistent flow with high performance. Table3.3, shows the characteristics of the micro-pump.

Table: Micro-pump operation characteristics

Size	70x32x30 mm
Weight	109g
Operating temperature	-20 – 100 oC
Input connection (tube)	4 mm
IP Rating	IP67, IP68
Noise levels	15dB
Viscosity up to	0,15 m^2/s
MTBF (Mean Time Between Failures)	10,000hrs

The micro-pump selection complies with European regulation EN 50014 for electrical apparatus for potentially explosive atmospheres Group II. Table 3.4 shows group II flammable material and suitable flammable material for selected micro-pump.

Table: Micro-pump chemical characteristic

Group	**Flammable material (gases and vapours)**	**Select Pump suitable material (gases and vapours)**
IIA	Propane, Acetone, Benzene, Butane, Methane, Petrol, Hexane, Paint solvents.	Acetone, Benzene, Methane, Butane, Hexane, Methane.
IIB	Ethylene, Propylene oxide, Ethylene oxide, Butadiene, Cyclopropane, Ethyl ether.	Butadiene, Ethyl ether, Ethylene oxide, Propylene.
IIC	Hydrogen, Acetylene, Carbone disulphide.	Acetylene, Carbon disulphide, hydrogen.

- **NDTBOT on-board microcomputer**

The selection of the micro-computer was made to reduce the maximum power consumption of the NDTBOT. Latte Panda, Figure 3.5, is a micro-computer with pre-installed Windows 10 with a good processor Atom quad-core 1.84 GHz CPU 500 MHz, 4G RAM DDRL3L and 64 GB EMMC with a low voltage of 5 volts.

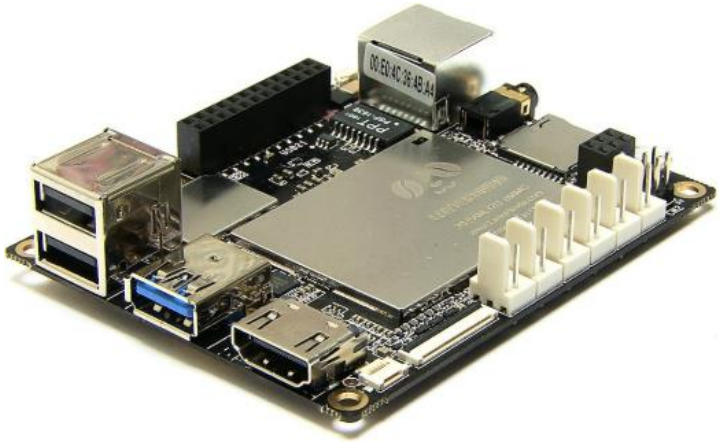

LattePanda.

It is compatible with a wide range of peripheral devices such as a touch connector, sensor connections, LAN, Wi-Fi and Bluetooth, etc. The Lattepanda's Arduino compatibility co-processor with plug and play headers and GPIO pins supports standard 5 Volt sensors and actuators that enable it to interact with the physical world.

- **Microcontroller**

The controller used in this work is the Arduino microcontroller. The microcontroller is an open source physical computing platform based on a simple input/output board and development environment that implements a processing language. It can be used to develop stand-alone interactive objects or can be connected to software via a computer. Many versions of the official Arduino hardware have been commercially produced to date. The Arduino used is programmed with an IDE (Integrated Development Environment).

A-2: The NDTBOT user interface codes

```
Arduino microcontroller
#include <LiquidCrystal.h>
#include <SHT1x.h>
#define dataPin  10
#define clockPin 11
SHT1x sht1x(dataPin, clockPin);
float temp_c;
float humidity;
const int analogInPin = A0;
int sensorValue = 0;
// a string to hold incoming data
String inputString = "";
// whether the string is complete
boolean stringComplete = false;
String commandString = "";
// Pin declaration
int led1Pin = 2;
int led2Pin = 3;
int led3Pin = 4;
int led4Pin = 5;
int led5Pin = 7;
int led6Pin = 6;
int led7Pin = 8;
boolean isConnected = false;
LiquidCrystal lcd(8,9,4,5,6,7);
//Setup message bytes
byte inputByte_0;
byte inputByte_1;
byte inputByte_2;
float tempC;
int reading;
int tempPin = 0;
void setup() {
  Serial.begin(9600);
  pinMode(led1Pin,OUTPUT);
  pinMode(led2Pin,OUTPUT);
  pinMode(led3Pin,OUTPUT);
  pinMode(led4Pin,OUTPUT);
  pinMode(led5Pin,OUTPUT);
  pinMode(led6Pin,OUTPUT);
  pinMode(led7Pin,OUTPUT);
  initDisplay();
}
```

```
void loop() {
if(stringComplete)
{
  stringComplete = false;
  getCommand();
  if(commandString.equals("STAR"))
  {
    lcd.clear();
  }
  if(commandString.equals("STOP"))
  {
    turnLedOff(led1Pin);
    turnLedOff(led2Pin);
    turnLedOff(led3Pin);
    turnLedOff(led4Pin);
    turnLedOff(led5Pin);
    turnLedOff(led6Pin);
    turnLedOff(led7Pin);
    lcd.clear();
    lcd.print("Ready to connect");
  }else if(commandString.equals("TEXT"))
  {
    String text = getTextToPrint();
    printText(text);
  } else if(commandString.equals("LED1") {
    boolean LedState = getLedState();
    if(LedState == true)
    {
      turnLedOn(led1Pin);
    }else{
      turnLedOff(led1Pin);
    }
  }
    else if(commandString.equals("LED2"))
  {
    boolean LedState = getLedState();
    if(LedState == true)
    {
      turnLedOn(led2Pin);
    }else {
      turnLedOff(led2Pin);
    }
  }
```

```
else if(commandString.equals("LED3"))
  {
   boolean LedState = getLedState();
   if(LedState == true){
    turnLedOn(led3Pin);
   }else  {
    turnLedOff(led3Pin);
   }
  }
   else if(commandString.equals("LED4"))
  {
   boolean LedState = getLedState();
   if(LedState == true)
   {
    turnLedOn(led4Pin);
   }else{
    turnLedOff(led4Pin);
   }
  }
   else if(commandString.equals("LED5"))
  {
   boolean LedState = getLedState();
   if(LedState == true)  {
    turnLedOn(led5Pin);
   }else {
    turnLedOff(led5Pin);
   }
  }
else if(commandString.equals("LED6"))
  {
   boolean LedState = getLedState();
   if(LedState == true)
   {
    turnLedOn(led6Pin);
   }else{
    turnLedOff(led6Pin);
   }
  }
else if(commandString.equals("LED7"))
  {
   boolean LedState = getLedState();
   if(LedState == true){
    turnLedOn(led7Pin);
   }else {
  turnLedOff(led7Pin);
   }
```

```
inputString = "";
}
// Read values from the sensor
  sensorValue = analogRead(analogInPin);
   Serial.print("Liquid: ");
  Serial.print(sensorValue);
  //Serial.println("");
  Serial.print("  ");

  temp_c = sht1x.readTemperatureC();
  humidity = sht1x.readHumidity();
  Serial.print("Temp: ");
  Serial.print(temp_c, 2);
   Serial.print("C");
   Serial.print("  ");
  Serial.print("Humid: ");
  Serial.print(humidity);
  Serial.print("F");
  Serial.println("");
  Serial.print(" ");
  delay(10);
}
void initDisplay()
{
  lcd.begin(16, 2);
  lcd.print("Ready to connect");
}
boolean getLedState()
{
  boolean state = false;

if(inputString.substring(5,7).equals("ON"))
  {
    state = true;
  }else{
    state = false;
  }
  return state;
}
void getCommand()
{
  if(inputString.length()>0)  {
     commandString =
inputString.substring(1,5);
  }
}
```

```
 void turnLedOn(int pin)
{
 digitalWrite(pin,HIGH);
}

void turnLedOff(int pin)
{
 digitalWrite(pin,LOW);
}String getTextToPrint()
{
 String value = inputString.substring
(5,inputString.length()-2);
 return value;
}void printText(String text)
{
 lcd.clear();
 lcd.setCursor(0,0);
   if(text.length()<16)
   {
    lcd.print(text);
   }else
   {
    lcd.print(text.substring(0,16));
    lcd.setCursor(0,1);
    lcd.print(text.substring(16,32));
   }
}
void serialEvent() {
 while (Serial.available()) {
   // get the new byte:
   char inChar = (char)Serial.read();
   // add it to the inputString:
   inputString += inChar;
// if the incoming character is
a newline, set a flag
// so the main loop can do
something about it:
   if (inChar == '\n') {
    stringComplete = true;
   }
 }
}
```

Visual C# code

```
using System;
using System.Collections.Generic;
using System.ComponentModel;
using System.Data;
using System.Drawing;
using System.Linq;
using System.Text;
using System.Threading.Tasks;
using System.Windows.Forms;
using System.IO.Ports;
namespace WindowsFormsApplication1
{
   public partial class Form1 : Form
   {
      int h;
      int m;
      int s;
      private string in_data;
      bool isConnected = false;
      String[] ports;
      SerialPort port;
      public Form1() {
         InitializeComponent();
         disableControls();
         getAvailableComPorts();
         this.SetStyle(ControlStyles.FixedWidth,
true);
         foreach (string port in ports)
         {
            comboBox1.Items.Add(port);
            Console.WriteLine(port);
            if (ports[0] != null)
            {
               comboBox1.SelectedItem = ports[0];
            }
         }
      }
      private void button1_Click(object sender,
EventArgs e)
      {
         if (!isConnected)   {
```

```
   connectToArduino();
    }    else
           {
   disconnectFromArduino();
           }
       }
void getAvailableComPorts()
       {
 ports = SerialPort.GetPortNames();
       }
 private void connectToArduino()
       {
   isConnected = true;
string selectedPort = comboBox1.GetItem
Text(comboBox1.SelectedItem);
port = new SerialPort(selectedPort, 9600,
Parity.None, 8, StopBits.One);
port.Open();
port.Write("#STAR\n");
button1.Text = "Disconnect";
 enableControls();
 port.DataReceived +=
 port_DataReceived;
  try
 {
   port.Open();
data_tb.Text = "";
           }
catch (Exception ex)
           {
MessageBox.Show(ex.Message, "Error");
           }
       }
private void checkBox1_CheckedChanged
(object sender, EventArgs e)
       {
     if (isConnected)
           {
   if (checkBox1.Checked)
               {
  port.Write("#LED1ON\n");
               } else{
      port.Write("#LED1OF\n");
               }
           }
       }
       private void
checkBox2_CheckedChanged(object sender,
EventArgs e)
       {
          if (isConnected)
          {
             if (checkBox2.Checked)
             {
                port.Write("#LED2ON\n");
             }
             else {
                port.Write("#LED2OF\n");
             }
          }
       }
       private void
checkBox3_CheckedChanged(object sender,
EventArgs e)
       {
          if (isConnected)
          {
             if (checkBox3.Checked)
             {
                port.Write("#LED3ON\n");
             }
             else{
                port.Write("#LED3OF\n");
             }
          }
       }
       private void
checkBox4_CheckedChanged(object sender,
EventArgs e)
       {
          if (isConnected)
          {
             if (checkBox4.Checked){
                port.Write("#LED4ON\n");
             }  else{
```

```
                port.Write("#LED4OF\n");
            }
        }
    }
private void checkBox5_CheckedChanged
(object sender, EventArgs e)
    {
        if (isConnected)
        {
            if (checkBox5.Checked)
            {
                port.Write("#LED5ON\n");
            }
            else  {
   port.Write("#LED5OF\n");
            }
        }
    }
 private void checkBox6_CheckedChanged
(object sender, EventArgs e)
    {
        if (isConnected) {
            if (checkBox6.Checked)
            {
                port.Write("#LED6ON\n");
            }
            else{
          port.Write("#LED6OF\n");
            }
        }
    }
 private void checkBox7_CheckedChanged
(object sender, EventArgs e)
    {
        if (isConnected) {
            if (checkBox7.Checked)
            {
  port.Write("#LED7ON\n");
 }  else {
                port.Write("#LED7OF\n");
            }
        }
}
```

```
    private void disconnectFromArduino()
    {
        isConnected = false;
        port.Write("#STOP\n");
        port.Close();
        button1.Text = "Connect";
        disableControls();
        resetDefaults();
    }
   // private void button2_Click(object
sender, EventArgs e)
   // {
    // if (isConnected) {
     //       port.Write("#TEXT" +
textBox1.Text + "#\n");
     //  }
   // }
    private void enableControls(){
        checkBox1.Enabled = true;
        checkBox2.Enabled = true;
        checkBox3.Enabled = true;
        checkBox4.Enabled = true;
        checkBox5.Enabled = true;
        checkBox6.Enabled = true;
        checkBox7.Enabled = true;
        // button2.Enabled = true;
        // textBox1.Enabled = true;
        groupBox1.Enabled = true;
       // groupBox3.Enabled = true;
    }
    private void disableControls()
    {
        checkBox1.Enabled = false;
        checkBox2.Enabled = false;
        checkBox3.Enabled = false;
        checkBox4.Enabled = false;
        checkBox5.Enabled = false;
        checkBox6.Enabled = false;
        checkBox7.Enabled = false;
        // button2.Enabled = false;
        // textBox1.Enabled = false;
        groupBox1.Enabled = false;
       // groupBox3.Enabled = false;
    }
    private void resetDefaults()
```

```
        {
            checkBox1.Checked = false;
            checkBox2.Checked = false;
            checkBox3.Checked = false;
            checkBox4.Checked = false;
            checkBox5.Checked = false;
            checkBox6.Checked = false;
            checkBox7.Checked = false;
            //  textBox1.Text = "";
        }
        private void Start_btn_Click
(object sender, EventArgs e)
        {
// string selectedPort =
comboBox1.GetItemText
(comboBox1.SelectedItem);
 //port = new SerialPort(selectedPort, 9600,
Parity.None, 8, StopBits.One);
// port.DataReceived += port_DataReceived;
           // port.Write("#STAR\n");
           // button1.Text = "Connect";
            //button1.Text = "Disconnect";
           // enableControls();
           // try
          //  {
              //  port.Open();
              //  data_tb.Text = "";
           // }
           // catch(Exception ex)
           // {
 // MessageBox.Show(ex.Message, "Error");
          //  }
        }
void port_DataReceived(object sender,
 SerialDataReceivedEventArgs e)
        {
            in_data = port.ReadLine();
  this.Invoke
(new EventHandler(displaydata_event));
        }
        private void displaydata_event
(object sender, EventArgs e)
        {
 data_tb.Text = in_data;
        }
        private void button2_Click_2(object
sender, EventArgs e)
        {
            if (textBox1.Text == "") {
                textBox1.Text = "0";
            }
  if (textBox2.Text == "") {
        textBox2.Text = "0";
            } if (textBox3.Text == "") {
                textBox3.Text = "0";
            }
    h = Convert.ToInt32(textBox1.Text);
    m = Convert.ToInt32(textBox2.Text);
   s = Convert.ToInt32(textBox3.Text);
            timer1.Start();
        }
 private void timer1_Tick(object sender,
EventArgs e){
            s = s - 1;
            if (s == -1){
           m = m - 1;
                s = 59;
            } if (m == -1)
            {
                h = h - 1;
                m = 59;
       }  if (h == 0 && m == 0 && s == 0)
            {
                timer1.Stop();
MessageBox.Show(" Battery Low!",
"Time");
            }
            string hh = Convert.ToString(h);
            string mm = Convert.ToString(m);
            string ss = Convert.ToString(s);
            label1.Text = hh;
            label3.Text = mm;
            label5.Text = ss;
        }
        private void button3_Click(object
sender, EventArgs e){
            timer1.Stop();
        }
    }
}
```

A-3: Reynolds number and kinematic viscosity

- **Reynolds number**

The Reynolds number is the dimensionless quantity in fluid mechanic used to predict flow patterns in different fluid flow situations. At low Reynolds number N_R, the flow tends to be dominated by laminar flow, while at high Reynolds numbers N_R turbulence results from differences in the fluid's speed and direction. With respect to laminar flow which occurs at low Reynolds numbers, where viscosity forces are dominant, and is characterized by smooth, constant fluid motion created by the NDTBOT motion. Turbulent flow occurs at high Reynolds numbers and is dominated by inertial forces. The Reynolds number is expressed as:

$$N_R = \frac{\rho_l v L}{\mu} = \frac{vD}{\vartheta} \qquad \text{(A.1)}$$

Where ρ_l is the density of the fluid, v is the velocity of the moving robot, D is a characteristic linear dimension, μ is the dynamic viscosity of the fluid and ϑ is the kinematic viscosity of the fluid.

- **Kinematic viscosity**

Kinematic viscosity is the ratio of absolute or dynamic viscosity to density; it is expressed as

$$\vartheta = \frac{\mu}{\rho_l} \qquad \textbf{(}\text{A.2)}$$

Where μ is the absolute or dynamic viscosity and ρ_l is the density.

Kinematic viscosity and density of petroleum medium vary with the country of production and the temperature. In this work the temperature of the medium is taken between 30 to 40 degrees Celsius. The kinematic viscosity was calculated with equation (3.9), Reynolds number was calculated with equation (3.8).

A-4: Mech convergence

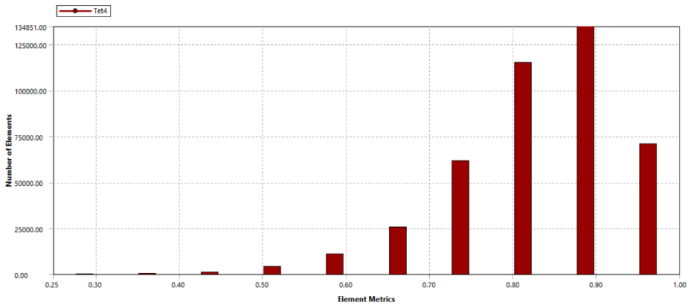

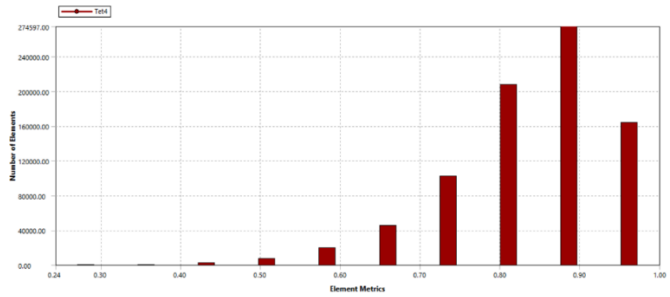
Tet4
274597.00
240000.00
200000.00
160000.00
120000.00
80000.00
40000.00
0.00
Number of Elements
0.24
0.30
0.40
0.50
0.60
0.70
0.80
0.90
1.00
Element Metrics

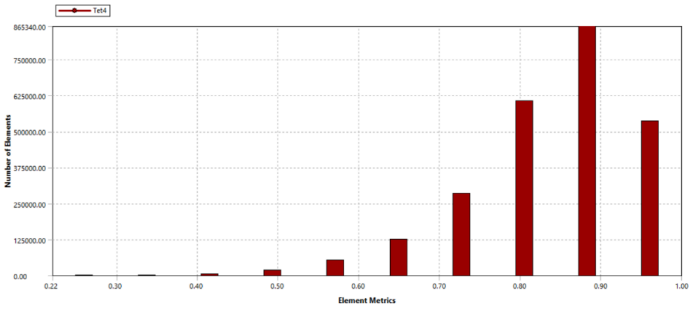
Tet4
865340.00
750000.00
625000.00
500000.00
375000.00
250000.00
125000.00
0.00
Number of Elements
0.22
0.30
0.40
0.50
0.60
0.70
0.80
0.90
1.00
Element Metrics

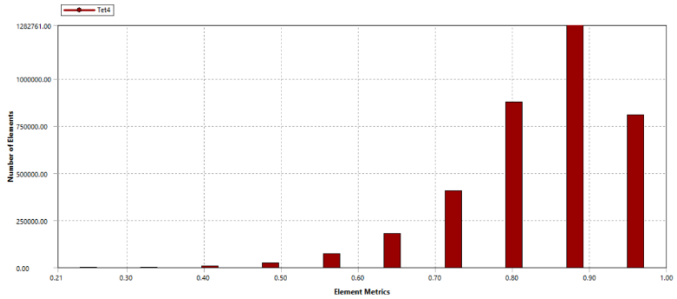
Tet4
1282761.00
1000000.00
750000.00
500000.00
250000.00
0.00
Number of Elements
0.21
0.30
0.40
0.50
0.60
0.70
0.80
0.90
1.00
Element Metrics

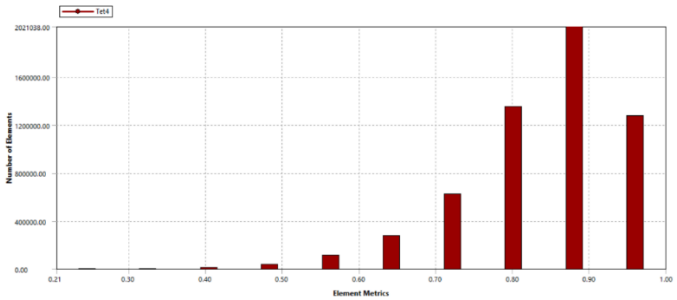
Tet4
2021038.00
1600000.00
1200000.00
800000.00
400000.00
0.00
Number of Elements
0.21
0.30
0.40
0.50
0.60
0.70
0.80
0.90
1.00
Element Metrics

Appendix B

B-1: Derivation of the wave equation

- **Complex permittivity of a medium**

Assuming that no other current flows in a given medium with conductivity σ, the current density $\tilde{j}$ is related to $\tilde{E}$ by $\tilde{j} = \sigma\tilde{E}$ the Ampere's law equation (5.1d) can be written as $\nabla \times \tilde{H} = \tilde{j} + j\omega\varepsilon\tilde{E} \quad = \sigma\tilde{E} + j\omega\varepsilon\tilde{E} = j\omega(\varepsilon + j\frac{\sigma}{\omega})\tilde{E}$ where the complex permittivity ε_c is defined as:

$$\varepsilon_c = (\varepsilon + j\frac{\sigma}{\omega}) \tag{B.1}$$

Then $\nabla \times \tilde{H} = j\omega\varepsilon_c\tilde{E}$.

In simple, nonconducting source in free medium characterised by $\rho_v = 0, j = 0, \quad \sigma = 0$, the above time-harmonic Maxwell's equations, Gauss's law, could be simplified using divergent of curl theorem applied to Ampere's law equation (5.1d); $\nabla.\nabla \times \tilde{H} = 0$, it follows that $\nabla.\left(j\omega\varepsilon_c\tilde{E}\right) = 0$ or $\nabla.\tilde{E} = 0$ which implies that the charge is zero ($\rho_v = 0$) and Maxwell's (David and Cheng, 2006) equations become :

$$\boldsymbol{\nabla}.\tilde{\boldsymbol{E}} = \mathbf{0}. \quad \text{Gauss's law} \quad \text{(B.2a)}$$

$$\boldsymbol{\nabla} \times \tilde{\boldsymbol{E}} = -\boldsymbol{j\omega\mu}\tilde{\boldsymbol{H}}. \quad \text{Faraday's law} \quad \text{(B.2b)}$$

$$\boldsymbol{\nabla}.\ \tilde{\boldsymbol{H}} = \mathbf{0}. \quad \text{Divergence law} \quad \text{(B.2c)}$$

$$\boldsymbol{\nabla} \times \tilde{\boldsymbol{H}} = \boldsymbol{j\omega\varepsilon_c}\tilde{\boldsymbol{E}}. \quad \text{Ampere's law} \quad \text{(B.2d)}$$

- **Waves equation**

The electromagnetic wave equation is a second-order partial differential equation that describes the propagation of EM wave through a medium or in a vacuum. The wave equation is derived from Maxwell's equations and is three-dimensional. Thus, the homogeneous form of the equation, written regarding either the electric field $\tilde{\mathrm{E}}$ alternatively, the magnetic field $\tilde{\mathrm{B}}$, by taking the curl of both side of Faraday's (David and Cheng, 2006) equation to get

$$\nabla \times \left(\nabla \times \tilde{E}\right) = -j\omega\mu\left(\nabla \times \tilde{H}\right). \tag{B.3}$$

By substituting equations (5.2d) into (5.4), we obtain

$$\nabla \times \left(\nabla \times \tilde{E}\right) = -j\omega\mu\left(j\omega\varepsilon_c\tilde{E}\right) = \omega^2\mu\varepsilon_c\tilde{E}. \tag{B.4}$$

curl of $\tilde{E}$ is

$$\nabla \times (\nabla \times \tilde{E}) = \nabla(\nabla . \tilde{E}) - \nabla^2 \tilde{E}. \quad \text{(B.5)}$$

Where $\nabla^2 \tilde{E}$ is the Laplacian of $\tilde{E}$, which in Cartesian coordinate is given by

$$\nabla^2 \tilde{E} = (\frac{\partial^2}{\partial x^2} + \frac{\partial^2}{\partial y^2} + \frac{\partial^2}{\partial z^2})\tilde{E}. \quad \text{(B.6)}$$

Given equation (5.3a), the use of equation (5.6) gives

$$\nabla^2 \tilde{E} + \omega^2 \mu \varepsilon_c \tilde{E} = 0. \quad \text{(B.7)}$$

Which is known as the homogeneous wave equation for electric $\tilde{E}$. By defining the propagation constant γ as

$$\gamma^2 = -\omega^2 \mu \varepsilon_c \quad \text{(B.8)}$$

- **Plane-wave propagation in a medium**

Electromagnetic propagation in any medium is described by the homogeneous wave equation where the attenuation constant (α) and the phase velocity (β) are obtain by replacing the equations 5.2 Complex permittivity into (5.9) gives

$$\gamma^2 = -\omega^2 \mu (\varepsilon - j\frac{\sigma}{\omega})$$

$$\gamma^2 = -\omega^2 \mu \varepsilon + j\omega^2 \mu \frac{\sigma}{\omega}$$

$$\gamma^2 = j\omega\mu(\sigma + j\omega\varepsilon)$$

$\gamma = \sqrt{j\omega\mu(\sigma + j\omega\varepsilon)}$ since γ is a complex then $\gamma = \alpha + j\beta$ therefore

$$\gamma = \sqrt{j\omega\mu(j\omega\varepsilon + \sigma)} = \alpha + j\beta \quad \text{(B.9)}$$

Where ω is the angular frequency (rad/s), μ is the magnetic permeability, which is equal to the free space permeability, ε is the dielectric permittivity in media. In equation (5.10) the real part, alpha (α) Np/m is the attenuation constant while beta (β) rad/s the imaginary part is the phase constant. The attenuation constant defines the rate at which the fields of the wave are attenuated as the wave propagates.

Appendix C

C-1: Radio frequency user interface codes

```
using System;
using System.Collections.Generic;
using System.ComponentModel;
using System.Data;
using System.Drawing;
using System.Linq;
using System.Text;
using System.Threading.Tasks;
using System.Windows.Forms;
using System.IO.Ports;

namespace RFsender
{
   public partial class Form1 : Form
   {
      private DateTime datetime;
      private string in_data;
      // create global variable string data
      string dataOUT;  //
      string sendWith;  // create global
       variable string data
      string dataIN;
      public Form1()  {
         InitializeComponent();
      }private void Form1_Load
(object sender, EventArgs e)
      {
string[] ports = SerialPort.GetPortNames();
 cBoxCOMPORT.Items.AddRange(ports);

btnOpen.Enabled = true; //intial condition
btnClose.Enabled = false; //intial condition

chBoxDtrEnable.Checked = false;
// for intial condition
 serialPort1.DtrEnable = false;
chBoxRTSEnable.Checked = false; //for initi

     serialPort1.RtsEnable = false;

btnSendData.Enabled = false;

// initial condition
```

```
 chBoxWriteLine.Checked = false;
chBoxWrite.Checked = true;
sendWith = "Write";
 chBoxAlwaysUpdate.Checked = false;
chBoxAddToOldData.Checked = true;  }
  private void btnOpen_Click(object sender,
EventArgs e) {
    try  {
   serialPort1.PortName = cBoxCOMPORT.Text;
serialPort1.BaudRate =
Convert.ToInt32(cBoxBaudRate.Text);
serialPort1.DataBits =
Convert.ToInt32(cBoxDataBits.Text);
serialPort1.StopBits =
(StopBits)Enum.Parse(typeof(StopBits),
cBoxStopBits.Text);
           serialPort1.Parity =
(Parity)Enum.Parse(typeof(Parity),
cBoxParityBits.Text);
serialPort1.Open();
 progressBar1.Value = 100;
  // this to for prevent "open" button cliked when
serial port already active
btnOpen.Enabled = false;
 btnClose.Enabled = true;
 lblStatusCom.Text = "ON";
        } catch(Exception err)  {

           MessageBox.Show(err.Message,"Error",
MessageBoxButtons.OK, MessageBoxIcon.Error);
           btnOpen.Enabled = true;
           btnClose.Enabled = false;
           lblStatusCom.Text = " OFF";
   }
    }
    private void btnClose_Click(object sender,
EventArgs e)
    {
       if (serialPort1.IsOpen)
       {

          serialPort1.Close();

          progressBar1.Value = 0;
```

```
btnOpen.Enabled = true;
    btnClose.Enabled = false;
   lblStatusCom.Text = " OFF";
        }
       }
private void btnSendData_Click
(object sender, EventArgs e){
          if (serialPort1.IsOpen)
          {
dataOUT = tBoxDataOut.Text;
 if (sendWith == "WriteLine") {
serialPort1.WriteLine(dataOUT);
datetime = DateTime.Now;
string time = datetime.Hour + ":" +
datetime.Minute + ":" + datetime.Second;
tBoxDataOut.AppendText(time +
 "\t\t" + in_data + "\n");
  }
  // serialPort1.WriteLine(dataOUT);
else if (sendWith == "Write") {
serialPort1.Write(dataOUT);
datetime = DateTime.Now;
string time = datetime.Hour + ":"
+ datetime.Minute + ":" + datetime.Second;
 tBoxDataOut.AppendText(time +

"\t\t" + in_data + "\n");
   }
   // serialPort1.Write(dataOUT);
     }
    }
 private void
 chBoxDtrEnable_CheckedChanged
(object sender, EventArgs e)
   {
if (chBoxDtrEnable.Checked)
     {
   serialPort1.DtrEnable = true;
// activate DTR for serial port1
MessageBox.Show("DTR Enable", "
Warming", MessageBoxButtons.OK,
MessageBoxIcon.Warning);
```

```
  }          else { serialPort1.DtrEnable = false; }
//deactivate DTR for serial port1
      }
 private void chBoxRTSEnable_CheckedChanged
(object sender, EventArgs e)
      {
MessageBox.Show("RTS Enable", "Warming",
MessageBoxButtons.OK,
MessageBoxIcon.Warning);
          if (chBoxRTSEnable.Checked)
          {
 serialPort1.RtsEnable = true; // activate RTS
       }
   else { serialPort1.RtsEnable = false; } //deactivate
      }
private void btnClearDataOut_Click(object sender,
EventArgs e)
      {
  if (tBoxDataOut.Text != "") //if TextBox Not Empty
          {
    tBoxDataOut.Text = ""; // Erase TextBox Content
          }
      }
 private void tBoxDataOut_TextChanged(object
sender, EventArgs e)
      {
Int dataOUTLength = tBoxDataOut.TextLength;
  //this code for keep the string format for two digit
//  lblDataOutLength.Text = string.Format("{0:00}",
dataOUTLength);

 // this is for prevent enter key to create new line

          if (chBoxUsingEnter.Checked)

          {

             tBoxDataOut.Text =
tBoxDataOut.Text.Replace(Environment.NewLine,
"");

     }

  }
```

```
private void chBoxUsingButton_Checked
Changed(object sender, EventArgs e)
 {
  if (chBoxUsingButton.Checked)
 {
 btnSendData.Enabled = true;
// when enchecked  transmission
    }
  else { btnSendData.Enabled = false; }
      }
 //this is for send the serial data
when you press enter in the textbox
  private void tBoxDataOut_KeyDown
(object sender, KeyEventArgs e)
      {
  if (chBoxUsingEnter.Checked)
        {
if (e.KeyCode == Keys.Enter)
 //if Enter key pressed
           {
 if (serialPort1.IsOpen)  // port open
               {
dataOUT = tBoxDataOut.Text;
  if (sendWith == "WriteLine")
       {
 serialPort1.WriteLine(dataOUT);
                }
   // serialPort1.WriteLine(dataOUT);
     else if (sendWith == "Write")
          {
   serialPort1.Write(dataOUT);
     }
    // serialPort1.WriteLine(dataOUT);
serialPort1.Write(dataOUT);
//send serial data
               } }}  }
 private void chBoxWriteLine_Checked

Changed(object sender, EventArgs e)

     {

    if (chBoxWriteLine.Checked)

        {
           sendWith = "WriteLine";
           chBoxWrite.Checked = false;
           chBoxWriteLine.Checked = true;
        }
     }

     private                                  void
chBoxWrite_CheckedChanged(object          sender,
EventArgs e)
     {
        if (chBoxWrite.Checked)
        {
           sendWith = "Write";
           chBoxWrite.Checked = true;
           chBoxWriteLine.Checked = false;
        }
     }

     private  void  serialPort1_DataReceived(object
sender, SerialDataReceivedEventArgs e)
     {

        dataIN = serialPort1.ReadLine();
        //dataIN = serialPort1.ReadExisting();
        this.Invoke(new EventHandler(ShowData));
       //  datetime = DateTime.Now;

       //  string time = datetime.Hour + ":" +
datetime.Minute + ":" + datetime.Second;

     //     tBoxDataIN.AppendText(time  +  "\t\t"  +
in_data + "\n");
 }
 private void ShowData(object sender, EventArgs e)
     {
       // tBoxDataIN.Text = dataIN;

        int dataINLength = dataIN.Length;
        ///lblDataInLength.Text                    =
string.Format("{0:00}", dataINLength);
        //

        datetime = DateTime.Now;
        string  time  =  datetime.Hour  +  ":"  +
datetime.Minute + ":" + datetime.Second;
```

```
tBoxDataIN.AppendText
(time + "\t\t" + in_data + "\n");
 if (chBoxAlwaysUpdate.Checked)
         {
       tBoxDataIN.Text = dataIN;
         }
     else if (chBoxAddToOldData.Checked)
         {
            tBoxDataIN.Text += dataIN;
         }
      }
 private void chBoxAlwaysUpdate_Checked
Changed(object sender, EventArgs e)
      {
         if (chBoxAlwaysUpdate.Checked)
         {
   chBoxAlwaysUpdate.Checked = true;
chBoxAddToOldData.Checked = false;
 //this is for toggle  condition
         }
else { chBoxAddToOldData.Checked =
true; }
      }
private void chBoxAddToOldData_Checked
Changed(object sender, EventArgs e)
      {
         if (chBoxAddToOldData.Checked){
chBoxAddToOldData.Checked = true;
chBoxAlwaysUpdate.Checked = false;
         }
else { chBoxAlwaysUpdate.Checked =
true; } }
private void btnClearDataIN_Click
(object sender, EventArgs e) {
         if (tBoxDataIN.Text != "")
         {
            tBoxDataIN.Text = "";
         } }
      private void save_btn_Click

(object sender, EventArgs e)    {

 try

 {
         try

         {


            string pathfile =
@"C:\Users\RICHARD\Desktop\RF_SAVE\Tx\";

            string filename = "light_data.txt";

            System.IO.File.WriteAllText(pathfile +
filename, tBoxDataOut.Text);

            MessageBox.Show("Data has been saved
to" + pathfile, "save File");

         }

         catch (Exception ex2)

         {

            MessageBox.Show(ex2.Message, "Error");

         }

      }


   }


}
```